FULL VEHICLE DYNAMICS MODEL OF A

FORMULA SAE RACECAR USING ADAMS/CAR

A Thesis

by

RUSSELL LEE MUELLER

Submitted to the Office of Graduate Studies of
Texas A&M University
in partial fulfillment of the requirements for the degree of

MASTER OF SCIENCE

August 2005

Major Subject: Mechanical Engineering

FULL VEHICLE DYNAMICS MODEL OF A

FORMULA SAE RACECAR USING ADAMS/CAR

A Thesis

by

RUSSELL LEE MUELLER

Submitted to the Office of Graduate Studies of
Texas A&M University
in partial fulfillment of the requirements for the degree of

MASTER OF SCIENCE

Approved by:

Chair of Committee,	Make McDermott
Committee Members,	Arun R. Srinivasa
	Glen N. Williams
Head of Department,	Dennis L. O'Neal

August 2005

Major Subject: Mechanical Engineering

ABSTRACT

Full Vehicle Dynamics Model of a Formula SAE
Racecar Using ADAMS/Car. (August 2005)
Russell Lee Mueller, B.S. Texas A&M University
Chair of Advisory Committee: Dr. Make McDermott

The Texas A&M University Formula SAE program currently has no rigorous method for analyzing or predicting the overall dynamic behavior of the student-designed racecars. The objective of this study is to fulfill this need by creating a full vehicle ADAMS/Car model incorporating an empirical tire-road force model and validating the longitudinal performance of the model by using vehicle responses recorded at the track. Creating the model requires measuring mass and inertia properties for each part, measuring the locations of all the kinematic joints, testing the Risse Racing Jupiter-5 shocks to characterize damping and stiffness, measuring engine torque, and modeling the tire behavior. Measuring the vehicle performance requires installation of the Pi Research DataBuddy data acquisition system and appropriate sensors. The 2002 Texas A&M University Formula SAE racecar, the subject vehicle, was selected because it already included some accommodations for sensors and is almost identical in layout to the available ADAMS/Car model Formula SAE templates. The tire-road interface is described by the Pacejka '94 handling force model within ADAMS/Car that is based on a set of Goodyear coefficients. The majority of the error in the model originated from the Goodyear tire model and the 2004 engine torque map. The testing used Hoosier tires and the 2002 engine intake and exhaust configuration. The deliverable is a full vehicle model of the 2002 racecar with a 2004 engine torque map and a tire model correlated to longitudinal performance recorded at the track using the installed data acquisition system. The results of the correlation process, confirmed by driver impressions and performance of the 2004 racecar, show that the 2004 engine torque map predicts higher performance than the measured response with the 2002 engine. The Hoosier tire on the Texas A&M University Riverside Campus track surface produces 75±3% of peak longitudinal tire performance predicted by the Goodyear tire model combined with a road surface friction coefficient of 1.0. The ADAMS/Car model can now support the design process as an analysis tool for full vehicle dynamics and with continued refinement, will be able to accurately predict behavior throughout a complete autocross course.

NOMENCLATURE

ACAR	ADAMS/Car Software
ARB	Anti-Roll Bar
B	Pacejka '94 Handling Force Model – Stiffness Factor
BCD	Pacejka '94 Handling Force Model – Stiffness
BCD_{LON} or $_{LAT}$	Pacejka '94 Handling Force Model – Stiffness Adjustment
b_0-b_{13}	Pacejka '94 Handling Force Model – Longitudinal Tire Coefficients
BUS	Bushing
C	Pacejka '94 Handling Force Model – Shape Factor
CAD	Computer Aided Drafting or Design
CEA	Pi Research Club Expert Analysis Software
CG	Center of Gravity
CNV	Kinematic Joint – Constant Velocity
CYL	Kinematic Joint – Cylindrical
D	Pacejka '94 Handling Force Model – Peak Factor
DAQ	Data Acquisition
D_{LON} or $_{LAT}$	Pacejka '94 Handling Force Model – Peak Factor Adjustment
DOF	Degree(s) of Freedom
E	Pacejka '94 Handling Force Model – Curvature Factor
ECU	Engine Control Unit
FIX	Kinematic Joint – Fixed
FSAE	Formula SAE
HOK	Kinematic Joint – Hooke
INL	Kinematic Joint – Inline
INP	Kinematic Joint – Inplane
κ	Pacejka '94 Handling Force Model – Longitudinal Slip Ratio
MAP	Intake Manifold (plenum) Air Pressure Sensor
MKS	ADAMS/Car Units – Meters, Kilograms, Seconds
MMKS	ADAMS/Car Units – Millimeters, Kilograms, Seconds
ORI	Kinematic Joint – Orientation
PAX	Kinematic Joint – Parallel_axes
PER	Kinematic Joint – Perpendicular
PiDB	Pi Research DataBuddy Logger
PLA	Kinematic Joint – Planar
REV	Kinematic Joint – Revolute

SAE	Society of Automotive Engineers
S_H	Pacejka '94 Handling Force Model – Horizontal Shift
SI	International System of Units
SLA	Short-Long Arm Suspension
SPH	Kinematic Joint – Spherical
S_V	Pacejka '94 Handling Force Model – Vertical Shift
TAMU	Texas A&M University
TEES	Texas Engineering Experiment Station
TPS	Throttle Position Sensor
TRA	Kinematic Joint – Translational
V6	Pi Research Version 6 Software
X	Pacejka '94 Handling Force Model – Composite Slip Ratio

TABLE OF CONTENTS

Page

LIST OF FIGURES

Page

Page

LIST OF TABLES

INTRODUCTION

OBJECTIVE

The objective of this study is to develop an accurate detailed computer-aided rigid body model of a FSAE [1] racecar for the purpose of simulating overall vehicle dynamics. The level of detail, defined throughout the subsequent sections, allows the model to predict the position, velocity, acceleration, and resulting loads for each rigid body (predominantly suspension components) throughout the entire simulation when provided with the required driver inputs. The model of the vehicle's dynamics enables iterated simulation of system designs to test concepts early in the design process as well as to predict the response to changes in vehicle parameters. The FSAE racecar used for this study was designed and manufactured by senior level undergraduate mechanical engineering students at TAMU. The model uses measured geometry and mass properties from the as-manufactured racecar with a portion of the data obtained from SolidWorks CAD solid models and drawings created during the design process. Sub-models of the shocks and engine use results obtained from component testing. The simulation results are validated by comparing to actual vehicle response recorded by a data acquisition system installed on the racecar. The critical task in achieving these overall deliverables was correlating the empirical tire model to the measured available traction between the actual tire and track surface.

BACKGROUND

The current design process for the TAMU FSAE racecar has limited feedback, operating in nearly open-loop format. Feedback on previous racecar development is limited. Documentation in design and manufacturing reports contains various levels of quantity and quality. Another source of feedback depends on underclassmen volunteering time and effort before serving on the design team as a senior gathering valuable experience each year. Seniors typically graduate soon after participating in the design course series, taking the knowledge and experience they have gained from the intense process with them. Only a few of the engine sensors are recorded via the ECU data logging capabilities. Currently, no data regarding the overall system dynamics except for lap time using a stopwatch and driver comments are acquired. Any data that are received from the ECU, stopwatch, or driver is not systematically archived for later reference. Technical design reviews at both the conceptual

---

This thesis follows the style of the *International Journal of Vehicle Design*.

and detail level from outside reviewers with various levels of experience, knowledge, and understanding of the design provide feedback based on the students' presentations of the design. Presentations are severely limited in detail due to time constraints. The outside participation is from volunteers who donate their time and expertise while undergraduate mechanical engineering seniors usually have a full schedule of coursework in addition to FSAE. Design, manufacturing, and testing all occur at an accelerated pace throughout the entire process which proceeds from a clean sheet of paper design to fully functional and endurance-tested vehicle ready for competition in less than nine months.

Possibly because of the lack of feedback or the fast-paced densely-packed schedule, analysis tools for overall vehicle dynamics are not utilized. Instead, analysis of steady-steady state behavior, driver impressions, lap times, and past designs determine the envelope for future suspension design parameters. Steady-state vehicle behavior and suspension geometry is evaluated using fundamental analysis methods derived by Gillespie [2]. The suspension subsystem design is iterated to achieve desired values of computed parameters per Milliken [3]. The desired parameter values are based on "rules of thumb", not performance criteria. Multiple iterations of overall system design are limited because of time and funding constraints in the current process. A single iteration evolves through the design, manufacture, and competition of an entirely new racecar with nearly all-new team members, producing one significant test datum with limited information or documentation per year. The results of this study attempt to reduce the time between iterations and increase the rate of development both during the initial design stages and the actual testing prior to competition. The installed data acquisition system will not only validate the results of the model but also provide output data for closing the development feedback loop.

PROCEDURE

The plan for creating the correlated vehicle dynamics model in this study is outlined below:

1. Perform the necessary repairs and maintenance on the 2002 TAMU FSAE racecar, the most important of which is to return the engine to running condition.
2. Collect Sub-Model and Subsystem Data.
    a. Mass, inertia, CG locations.
    b. Kinematic joint locations.
    c. Sub-model data.
        i. Shock dynamometer testing.
        ii. Engine dynamometer testing.
3. Measure vehicle response.
    a. Determine variables to be measured and resolution for each.
    b. Equip vehicle with required sensing and recording capabilities.
    c. Measure system response to the test input.
4. Correlate the model.
    a. Adjust tire model to match measured response.
    b. Verify other parameters and adjust if error is significant (e.g. engine output).
    c. Validate model through testing.
        i. Vary vehicle input and/or parameters to generate a range of responses.
        ii. Incorporate same changes to model and generate simulated responses.
        iii. Compare vehicle and simulated responses.
    d. Repeat steps (a) through (c) as required.

The following sections provide detail discussion on how each step of the procedure was accomplished beginning with further defining the scope of the desired objective.

MODEL DESCRIPTION

MODEL SCOPE

MSC Software's ADAMS/Car program and the FSAE templates[1] are utilized in this study to create the complete vehicle dynamics model of the 2002 TAMU FSAE racecar. The reasons for selecting ACAR are:

1. Capability is more than adequate for the TAMU FSAE program's needs.
2. Available to TAMU at a reasonable cost.
3. Writer's past experience in the automotive industry using ACAR.

The FSAE templates are the first and probably most important boundary applied to the scope of the study because they define the level of complexity for the model and sub-models. Building a custom template from scratch or drastically modifying the available templates is outside the scope of this project and the TAMU FSAE program at this time.

The 2002 racecar was selected for graduate research because it was still a completely assembled vehicle, was not used for driver practice because the engine had not run since the 2002 FSAE competition, and was designed to accommodate data acquisition. The major obstacle was getting the engine to run properly. However, the 2002 racecar design did not require major modifications to the ACAR templates. This benefit more than compensates for having to repair the engine since it reduces the opportunity for the model to generate problems or errors, resulting in more time spent on model correlation and less time spent on debugging the model.

The ACAR model is capable of much more than the present data acquisition system can measure for validation, which brings up the next major limit on the scope of this study – tire data. In a road vehicle, the overall response of the vehicle is highly sensitive to the tire-road interface. Obtaining an accurate model for the tire-road interface is a common problem for full vehicle dynamics model as tire forces depend on several variables: temperatures of the tire surface and carcass, pressure, wear, age, prior use, manufacturing variability, and of course the

[1] ADAMS/Car Formula SAE Templates originally developed by the University of Michigan Formula SAE Racing Team and are available from MSC Software at http://university.adams.com/student_competitions/templates/templates_main.htm [accessed June 2005].

condition of the road surface to name a few. The tire model, discussed later in detail, receives tire contact patch conditions such as slip magnitude, slip direction, applied normal force, and wheel camber as input and returns the corresponding tire handling forces, or “grip” level. Accurately measuring the slip or the resulting forces at the tire-road interface is difficult, expensive, and usually approximated. With the available funding, sensor capabilities limit measured tire data to the longitudinal slip direction, **x**. The section on data acquisition covers how the longitudinal slip is measured and the associated approximation. The normal force applied to the tire is not measured directly but instead is calculated using the measured acceleration and the measured vehicle mass and geometry.

Working within these constraints, the study results in a complete ACAR vehicle dynamics model correlated in the longitudinal direction, ready for further improvements from increased capabilities in data acquisition or research funding in the future. The following sections describe the ACAR model as defined by the FSAE templates, which determines the necessary measurements required in the procedure.

COORDINATE SYSTEMS

Two coordinate systems will be used. The fixed *ground* Cartesian coordinate system is defined by unit vectors **X, Y,** and **Z**. The *vehicle* Cartesian coordinate system has unit vectors **x, y,** and **z** and is initially at time **t** = 0s coincident with the ground coordinate system (Figure 1). The **x** unit vector is aligned along the vehicle longitudinal centerline with the positive direction pointing towards the rear. The **z** unit vector is nominally vertical with the positive direction pointing towards the top of the vehicle. Using a right-hand system, the **y** unit vector positive direction must point towards the driver’s right side. Typically, the location of the origin of vehicle coordinate system is chosen for convenience in measuring vehicle geometry. The **x**-**y** plane is placed slightly below the tires and the **y**-**z** plane some distance in front of the racecar, but these are not critical. ACAR determines the ride height during initial setup of the simulation. The **x**-**z** plane is the plane of symmetry for vehicles with identical left and right geometry but this is not always true. ACAR and the FSAE templates can accommodate an asymmetric vehicle if necessary.

KINEMATIC JOINTS

Kinematic joints are named to describe the mathematical constraint equations they create on the kinematics of the attached rigid bodies [4, p128]. An example found frequently throughout this

model is a *spherical* joint, a.k.a. “ball-and-socket” joint, which constrains the three translational DOF while allowing the three rotational DOF. Table 1 describes each type of kinematic joint as defined by ACAR[2]. The spherical bearings or “rod ends” used at suspension joints on FSAE racecars behave as SPH joints over the design range of motion. Note the *Hooke* joint is identical to a SPH joint except the rotational DOF corresponding to the spin axis is constrained. The typical application for a HOK joint in the ACAR FSAE template is on a rod with a SPH joint at the other end. In effect, the HOK joint removes a free rotational DOF along the rod’s spin axis if it instead had SPH joints at both ends.

The *bushing* is another type of connection modeled in ACAR which allows all six DOF to occur with resulting forces and moments defined by stiffness and damping parameters. The bushing is not listed as a kinematic joint since it does not apply DOF constraint equations on the attached rigid bodies. The ACAR FSAE template does incorporate bushings at various joints for added freedom when adapting the template to suit the specific subject vehicle. For the 2002 TAMU FSAE racecar and many other racecars, the spherical bearings, as well as the other types of bearings used throughout the entire car, have very high stiffness, low friction, and little or no free-play present. Bushings are more suited to the lower stiffness and higher damping characteristics of production automotive applications in elastomeric engine or suspension mounts. Where bushings have been included in the FSAE template, the stiffness and damping parameters have been adjusted to match the behavior of the FSAE racecar bushing applications.

ACAR can *couple* DOF in cases where the desired motion is not represented by the predefined kinematic joints or a bushing. For example, a rack and pinion is modeled by coupling the rotational DOF of the pinion to the translational DOF of the rack at some gear reduction. The coupled DOF by ACAR will then generate a constraint equation on the relative motion between the two parts at the specified reduction.

[2] ADAMS/Car Help Documentation > Components > Attachments > Joints.

SUBSYSTEMS

ACAR uses a set of templates to create the *full vehicle* model as an *assembly* of *subsystems*. The following sections describe each subsystem in relation to the 2002 TAMU FSAE racecar. Refer to the ACAR help documentation for further detail regarding specifics of how the software utilizes the templates. The discussion here is intended to cover the rigid body dynamics of the full vehicle model. Refer to Tables 2-6 which list the hardpoint definitions, part mass and inertia properties, hardpoint locations, any relevant parameters, and bushing characteristics respectively for each subsystem (unless otherwise noted).

Chassis Subsystem

The *chassis* subsystem contains a single rigid body, or *part*, that defines the location of all the vehicle components that are non-rotating and fixed relative to the vehicle coordinate system, e.g. frame, bodywork, driver, radiator, wiring, ballast, etc. The engine and transmission, included within the *powertrain* subsystem described later, is the one exception to this rule. For visual purposes, a solid model of the 2002 FSAE frame was attached in ACAR to the chassis part (Figure 1). Mass and inertia properties of the chassis part depends on the configuration of the vehicle being tested and is varied to achieve the desired overall vehicle CG location and total mass. The following subsystems build off the chassis part to create the full vehicle assembly:

- front and rear suspension
- steering
- powertrain
- front and rear wheels/tires
- brakes
- front and rear anti-roll bars

Parameters are associated with the chassis subsystem for approximating the aerodynamic drag opposing forward velocity of the vehicle: frontal area, air density, and coefficient of drag. ACAR assumes these parameters are in SI units despite the system of units chosen for the full vehicle model. SI units are referred to by ACAR as the *MKS* system of units for meters, kilograms, and seconds. Based on experiences in this study, it is highly recommended to use either MKS or *MMKS* (for mm, kg, and s) to remain consistent. The user should choose either MKS or MMKS to minimize variation of the matrix entries in the system of equations. ACAR is more efficient at solving the equations if the non-zero matrix values are all of similar orders of magnitude.

Front Suspension Subsystem

The function of the front suspension subsystem is to control the independent motion of each front wheel relative to the chassis. The wheels are allowed to precess (controlled by the steering subsystem) and spin independently (controlled by the braking system). The overall layout and individual part descriptions are shown in Figures 2 and 4 with the wheel/tire subsystem excluded for clarity. The axis of the wheel is nominally aligned with the hub axis. The front suspension subsystem design for this vehicle is symmetric about the **x-z** plane. Part mass and inertia properties or joint locations can be defined asymmetrical in the model to reflect the actual vehicle if necessary.

The front suspension design used on the 2002 TAMU FSAE racecar is described as a fully independent SLA with push rod actuated coil-over shock. Each side of the suspension forms a three-dimensional version of a four-bar linkage in order to control the four DOF (three translations, one rotation) of each front upright with a desired amount of stiffness and damping. The hub allows the spin DOF of the wheel with respect to the upright. The upright and hub then precess as the upright rotates about an axis through the upper and lower control arm joints (ball joints) to accommodate the steering subsystem.

The coil-over shock is a damper and coil spring combination. The shock itself is a multi-component dynamic device that will be approximated by a sub-model described later in further detail. The shock is actuated by a bellcrank, or rocker, that transfers the relative motion of wheel and chassis from the push rod attached to the lower control arm. The final linkage is a steering link attaching the steering subsystem to the suspension.

Hardpoints in ACAR are the parametric locations that define where to place the joints and offer the ability to adjust suspension geometry very quickly and easily. The number of joints and the number of hardpoints are not usually equal because some joints share hardpoint locations or are pre-defined relative to other suspension geometry. The template maintains the overall subsystem layout but adjusts the parts' dimensions to fit the hardpoints. The front suspension template uses parameters to adjust the left and right camber and toe angles without having to relocate the hardpoints.

Rear Suspension Subsystem

Figures 3 and 5 display the rear suspension subsystem, which is quite similar to the front suspension subsystem. In the 2002 TAMU FSAE racecar design, the rear suspension adopts the same SLA with push rod actuated coil-over shock concept as the front suspension with some changes to the geometry. The spin DOF for the rear wheels is no longer free as this is a rear-wheel-driven racecar and has drive shafts transferring the torque between the powertrain subsystem and the wheels. The wheel precession is no longer controlled by a steering subsystem since what was a steering link is now a tie rod that links the upright to the chassis in the ACAR FSAE template. On the 2002 TAMU FSAE racecar, the tie rod links the upright to the lower control arm so the inboard tie rod joint in the model will be coincident with the control arm joint to obtain the desired kinematics. The wheel has all six DOF determined by the rear suspension subsystem linkages and drive shafts.

The driveshaft assembly is composed of three parts: tripod, driveshaft, and spindle. Connected by the appropriate kinematic joints, the outboard end (spindle) moves along with the upright through any suspension travel while the inboard end (tripod) remains constrained relative to the chassis. The spindle is fixed to the wheel subsystem and has a single rotational DOF within the upright. The tripod is fixed to the powertrain subsystem with the axial translation DOF free to allow for axial plunge of the driveshaft. As in the front suspension subsystem, the rear suspension subsystem parameters can redefine camber and toe angles for the left and right wheels independent of the hardpoints.

Anti-Roll Bar Subsystem

The 2002 TAMU FSAE racecar did not include an ARB at either the front or the rear. The ACAR templates for FSAE do incorporate a front and rear ARB option and since the 2002 TAMU FSAE racecar could receive an ARB later or the ACAR model could be adapted for another racecar at TAMU that does have an ARB, it is worthwhile to describe the ARB subsystem.

The function of the ARB is described directly in its name – it attempts to prevent the rolling motion of the chassis. As the chassis rolls in a turn, i.e. rotates about the **x** axis, the outside wheel and suspension travels in +**z** while the inside travels in -**z**. The relative difference in suspension travel is directly transferred, via drop links attached to the bellcranks, to a spring which is a U-shaped bar in this template (Figure 6). The arms are in bending and the main bar is in torsion. Typically, the beams in bending are designed significantly stiffer than the bar in torsion, creating a spring dominated by the torsional deflection in the main bar. The ACAR

template for the FSAE racecar assumes rigid body parts to describe the kinematics of the ARB with a torsion spring/damper element (with zero damping, not shown in figure) included between the left and right sides. This is usually not an accurate approximation for production automotive applications but is appropriate for the FSAE racecar.

ACAR uses left and right parts to describe a continuous U-shaped ARB on the vehicle. The ARB subsystem in the ACAR model consists of 4 parts. The left and right side components are connected via the torsion spring/damper element in the middle. The REV joint is located at the midpoint between the left and right *arb_bend* hardpoints. Note half of the total mass/inertia of the assembly is applied to each ARB part. A single parameter is provided in the template that defines the torsional spring rate of the ARB.

Steering Subsystem

Recalling the description of the front suspension subsystem, a rotational DOF is left free for the wheel to precess and steer the vehicle in the desired heading. The function of the steering subsystem is to link the driver's control input to the orientation of the front wheels via the front suspension subsystem. Input from the driver turns the steering wheel in the desired heading.

The location of the steering wheel usually does not lend itself to using a straight shaft to the rest of the subsystem because of driver ergonomics. The FSAE template (Figure 7) has three shafts connected by two HOK joints to accommodate most configurations. The shafts connect the steering wheel to the rack and pinion assembly transferring the rotation of the shafts and pinion to linear translation of the geared rack. The tie rods, or steering links, discussed earlier in the front suspension subsystem are attached to the ends of the rack. As the rack travels, the steering links push (or pull) on the corresponding upright to steer the front wheels.

ACAR defines the support and rack housing relative to the geometry given for the column and rack respectively while the pinion joints occupy a singe hardpoint in the model. The outer ends of the rack are defined by the inboard locations of the steering links in the front suspension subsystem. The steering subsystem has a single parameter that defines the gear reduction between the pinion rotation and the rack translation.

Wheel and Tire Subsystem

The wheel and tire subsystem includes a left and right pair of rigid body parts for each wheel and tire assembly. The FSAE template treats the wheel and tire as a single rigid body directly attached to each spindle within the suspension subsystems. The tire interacts with the ground via the tire sub-model discussed later. The wheel and tire subsystem needs only the type of tire model being used to generate tire-road forces as well as the mass, inertia, and geometry properties. However, the tire geometry depends on the selected tire model. In the present study, the tire model specifies the unloaded radius along with vertical stiffness and damping coefficients. The radius, and therefore the angular velocity, of the wheel varies according to the applied force. There are no additional joints to define since the wheels are fixed to parts in the suspension subsystems, i.e. the spindles and hubs. No parameters are in the subsystem template since the tire model and suspension subsystems include all of the necessary information.

Brake Subsystem

The brake subsystem functions only as a mathematical actuator providing a driver control in the form of torque opposing the spin of the wheels. The template places a brake rotor and caliper at each of the four wheels. None of the brake subsystem components are defined as parts. The geometry in the ACAR model is for visual purposes only. The amount of torque on the wheel spin axis is determined from driver input and brake subsystem parameters. Note the 2002 racecar has a single rear rotor and caliper attached directly to the differential housing. This does not pose a problem for the model since the brake subsystem does not have any mass or inertia. The mass and inertia properties associated with the all the rotors and calipers are added to the appropriate locations, e.g. rear rotor is a portion of the *diff_output* part.

Powertrain Subsystem

The powertrain subsystem contains only three parts. It does not include each of the moving interior components which would add a significant amount of complexity. The FSAE template uses the *powertrain* part to define the combined rigid body behavior of the engine, clutch, and transmission assembly because, like most FSAE racecars, the 2002 TAMU FSAE racecar is powered by a motorcycle engine with integral transmission. The powertrain part attaches to the chassis via four bushings. As in the suspension subsystems, bushings offer an added flexibility not representative of the 2002 racecar's attachments which rigidly bolts the powertrain to the

chassis. In the model, the stiffness and damping characteristics of the powertrain bushings adopt the same characteristics as the suspension control arm bushings.

The powertrain subsystem references two sub-models (sub-models will be discussed in a subsequent section):

1. Powertrain – defines engine output torque given crankshaft speed and throttle position.
2. Differential – defines an applied torque opposing the given relative shaft speed between left and right drive shafts.

Do not confuse the powertrain sub-model with the powertrain subsystem. The subsystem describes the rigid body properties while the sub-model defines torque output only. The differential sub-model transmits torque from the powertrain sub-model to the left and right differential outputs while accommodating the independent left and right shaft speeds. The two parts called *diff_output* transmit torque from the differential sub-model to each of the drive shafts defined in the rear suspension subsystem. The mass and inertia properties of the differential are divided equally across the left and right parts. Parameters within the powertrain subsystem describe the transmission gear ratios, clutch behavior, engine rotating inertia, etc. As mentioned earlier, no internal engine components are included but the engine rotating inertia parameter applies to engine crankshaft speed, approximating the combined overall inertia of the engine's rotating and reciprocating components. No inertia is applied to the clutch or transmission.

SUB-MODELS

The FSAE racecar contains several devices with a high level of component complexity such as the engine, transmission, tires, etc. The available FSAE templates utilize sub-models in order to simplify the full vehicle model, reduce computational requirements, and still provide an accurate representation of the overall vehicle dynamics. The shock and engine sub-models are validated by measuring the response from the individual components.

Shocks

The shock used on the 2002 TAMU FSAE racecar has a coil spring installed concentric to the damper main chamber (Figure 8). For the purpose of this study, it is sufficient to simplify the shock as the combination of spring stiffness and damping coefficients that determine the force generated for a given relative suspension position and velocity (Figures 9-10).

The coil spring stiffness, determined by the coil diameter, coil wire diameter, number of coils, and material properties, has linear behavior until the coils reach the solid stack-up height. ACAR can use tabular data to describe a variable stiffness as a function of displacement. ACAR uses linear interpolation between any of the data points to estimate the stiffness. The spring stiffness of the shock assembly is nonlinear at the travel limits where the shock has elastomer bump-stops with significantly higher stiffness than the coils. The spring data file, which has the table of spring force versus displacement as well as the installed spring length (or preload), is referenced within the suspension subsystem files. The springs used on the 2002 TAMU FSAE racecar are manufactured at specific stiffness ratings and the manufacturer's rated stiffness is used as the baseline stiffness. The shock stiffness, described next, is added in parallel to the coil spring. At the end of the shock travel, the stiffness transitions to a much higher value to model the bump-stop installed on the shock shaft for limiting bump travel. Note the limit on travel is different between the front and rear suspensions. Negative displacements, or stretching of the spring, are not included since the shock cannot pull on the coil spring.

The shock without the coil spring is predominantly a damper. Without going into great detail on the design, the damper piston contains orifices that allow fluid to flow from one side of the piston to the other. The relations among piston speed, flow, orifice resistance to flow, pressure, and force determine the damper properties. The fluid properties can also vary drastically depending on such characteristics as temperature or gas build-up in the fluid chamber. The damper has an additional chamber filled with gas that is separated from the fluid chamber by a floating piston. The gas allows the piston shaft to displace fluid volume by expanding or contracting according to the piston travel. As a result, the gas imposes an additional stiffness component to the force generated by the shock and also depends on temperature. The damping coefficient can be adjusted by threading tiny needles into or out of fixed orifices to modify the fluid passages within the shock assembly. Depending on the particular shock design, these adjustments have the ability to control the damper coefficient at different piston velocities.

Similar to the spring data file, ACAR can read in a table of data relating a given input velocity to the corresponding output force. The damper curve is approximately the middle setting for both adjustment knobs of the shock and is averaged across the available shock test data. Note the gas in the shocks generates a static force causing the shock to extend to its limits at rest. This force is equivalent to a preload on the spring and is defined within the spring data file since an ACAR damper does not include a static force.

Differential

The differential transmits the torque from the powertrain sub-model to the left and right drive shafts in the rear suspension subsystem. The differential allows the transfer of torque to both shafts despite asymmetrical shaft speeds as the vehicle performs various maneuvers. An additional feature in the 2002 racecar's differential is the ability to oppose the difference in shaft speed. For example, if the left wheel begins to spin freely as if on a patch of ice, the input motion is transmitted to the free spinning left shaft while the right shaft, and therefore the right wheel sits still. A *limited slip* differential includes components for opposing the relative shaft speed with an applied torque to the slower drive shaft. The FSAE powertrain template has the ability to reference a viscous differential data file which defines the opposing torque versus a given difference in shaft speed (Figure 11). The 2002 TAMU FSAE racecar utilizes a torque sensing differential which will not match the ACAR FSAE template but behaves as required for longitudinal vehicle modeling, e.g. when the difference in shaft speed is negligible.

Powertrain

The powertrain sub-model consists of the engine, clutch, and transmission. The engine produces torque at a range of crankshaft speeds between *idle* (minimum) and *rev limit* (maximum), at a range of throttle position (driver input), and subject to the engine rotating inertia parameter. The clutch transmits torque from the engine crankshaft to the transmission given the clutch position (driver input) and subject to *stiffness*, *damping*, and *torque threshold* parameters. The transmission transmits torque from the clutch to the differential via a set of selectable gear ratios (driver input) matching the engine speed to the desired torque and wheel speed.

Beginning with the engine, the FSAE template references a data file similar to the spring or damper files in the coil-over shock sub-model. The major difference here is that the engine requires two inputs in order to define the output torque: engine speed and throttle position. Throttle position, controlled by the driver, determines the amount of air entering the engine for combustion and therefore directly relates to the amount of torque generated at a given engine

speed. The table of engine data must be collected from the TAMU FSAE engine dynamometer, which measures the torque produced at a given speed and throttle position.

The clutch allows the driver to disconnect the transfer of torque between engine and transmission during such events as selecting a transmission gear ratio or starting the engine. In this application, the clutch is a mechanical device that uses friction between rotating discs, similar to the braking system, to transfer torque between the engine crankshaft and the transmission. When the driver presses the clutch pedal or lever, the pressure on the disc is removed, effectively disconnecting the engine from the transmission by no longer transferring torque. To reapply the clutch pressure, the driver releases the clutch pedal or lever, increasing friction and the amount of torque transfer. As the friction is determined by the amount of pressure applied between the clutch discs and the properties of the materials utilized, the amount of torque that can be transferred is limited and the limit is above the peak torque from the engine. The FSAE template models the clutch as a torsion spring/damper in parallel between the engine and transmission. The clutch in this model is approximated as a relatively rigid connection between engine crankshaft and transmission input shaft.

Tires

The tire model incorporated within the wheel and tire subsystem template predicts behavior given certain tire contact patch parameters – slip vector, normal force, and orientation (camber angle). The model developed by Pacejka [5] is referred to by ACAR as the *Pacejka '94 handling force model*. The longitudinal tire force $\mathbf{F_X}$ along with the lateral tire force $\mathbf{F_Y}$ and self-aligning moment $\mathbf{M_Z}$ are the three outputs from the handling force model. The following equations define $\mathbf{F_X}$ as it is used by ACAR[3]:

[3] ADAMS/Tire Help Documentation > Tire Models > 'Using ADAMS/Tire Tire Models' > 'Using Pacejka '94 Handling Force Model' p83.

$$\kappa = -\frac{V_{SX}}{V_X}$$

$$C = b_0$$

$$D = [(b_1 \cdot F_Z + b_2) \cdot F_Z] \cdot D_{LON}$$

$$BCD = [(b_3 \cdot F_Z + b_4) \cdot F_Z \cdot \exp(-b_5 \cdot F_Z)] \cdot BCD_{LON}$$

$$BCD = \left.\frac{dF_Z}{d\kappa}\right|_{\kappa+S_H=0}$$

$$B = \frac{BCD}{C \cdot D}$$

$$S_H = b_9 \cdot F_Z + b_{10}$$

$$S_V = b_{11} \cdot F_Z + b_{12}$$

$$X = \kappa + S_H$$

$$E = ((b_6 \cdot F_Z + b_7) \cdot F_Z + b_8) \cdot (1 - b_{13} \cdot \text{sign}(X))$$

$$F_X = D \cdot \sin\left[C \cdot \tan^{-1}\left(B \cdot X - E \cdot \left(B \cdot X - \tan^{-1}(B \cdot X)\right)\right)\right] + S_V$$

The experimentally determined coefficients b_0-b_{13} for the longitudinal tire force model allow the computation of traction force $\mathbf{F_X}$ for given values of normal force $\mathbf{F_Z}$ and longitudinal slip ratio $\boldsymbol{\kappa}$. These coefficients are obtained from extensive tire testing requiring specialized equipment and several tires in order to apply a complete range of slip and normal force conditions while recording the resulting tire forces. Producing the empirical tire data for the Hoosier racing tires used on the TAMU FSAE racecars is outside the scope of the present study. Complete sets of Pacejka tire coefficients made available to TAMU FSAE correspond to the Goodyear FSAE racing tires used on a 13" diameter wheel rim with 20" unloaded outside diameter (Tables 7-8)[4]. The coefficients are available for either 12psi or 15psi tire pressure and either 6.5" or 8" width but only those for 6.5" width at 12psi pressure are used here. The TAMU FSAE racecars predominantly use 7.0" wide Hoosier racing tires due to its past performance in track testing. As a result, Hoosier is the brand used for the study. The Hoosier tire is 7.0" wide on a 13" diameter wheel at the 12psi pressure but using a slightly harder compound to extend tire life so that all the testing can be performed on a single set of tires, reducing cost and tire variability.

[4]Goodyear tire model Pacejka '94 coefficients provided by Michael J. Stackpole (Sep 2001), Goodyear Tire and Rubber Company, Race Tire Development.

Despite the many potential differences that could exist between Goodyear and Hoosier, the performance and behavior of the two brands of racing tire are similar based on past track testing by TAMU FSAE. However, the Goodyear tire model predicts significantly higher performance than what has been recorded at the TAMU track using either brand of tire. The available Goodyear Pacejka coefficients serve only as a starting point for the correlation process with the expectation that the tire model constitutes the majority of error between the simulation results and the recorded response at the track. Using the longitudinal tire force equations shown previously, the normalized longitudinal tire force predicted by the Goodyear model at positive slip ratios is plotted for three values of normal load in Figure 12. The tire model is adjusted to correlate with the measured tire performance at the track through the linear scaling factors, D_{LON} and BCD_{LON}, which adjust the peak factor, D, or the stiffness, BCD, respectively. The effects of changing these factors are displayed in Figure 13. The scaling for both peak and stiffness are kept equal in each case, i.e. $D_{LON} = BCD_{LON}$.

Driver, Road, and Straight-Line Acceleration Event Setup

Much of the driver's input to the vehicle has already been mentioned in the steering, brake, and powertrain subsystems. The driver mass and inertias are lumped together with the chassis part. The driver inputs to the vehicle are: throttle, clutch, brake, transmission gear, and steering wheel. ACAR has several full vehicle and half vehicle simulations and the capability to develop custom simulations or driver controls based on data measured at the track. The present study used only the *straight-line acceleration* event, which simulates the full vehicle model executing a maneuver similar to a drag race. ACAR controls the throttle position, transmission gear, and steering inputs to simulate straight-line acceleration response with several options to customize the event. The straight-line acceleration event was simulated with the inputs shown in Figure 14. *Output prefix* is a character string added to the beginning of each ACAR file produced by the simulation with "_accel" as the rest of the filename. *End time* refers to the total time for the event and is sufficient to allow the full vehicle model to reach the engine 13,500rpm redline. *Number of steps* determines the rate at which the ACAR solution marches to the given *end time*. The time between each simulation step is kept to 0.01s, i.e. 200 steps for 2.0s, which maintained a good balance of simulation accuracy and solver efficiency for this study. *Initial velocity* is the vehicle's initial speed at **t** = 0s and ACAR maintains this speed up until **t** = *start time*. At **t** = *start time*, ACAR steps the driver's throttle control to *final throttle* at the specified transition time called *duration of step*. *Gear position* is the initial transmission gear for the simulation and the *shift gears* toggle is turned off to prevent ACAR from changing gears throughout the event. *Steering*

input is set to “straight line” which tells ACAR to control steering wheel input as required to maintain the vehicle’s straight line heading.

ACAR uses several road profiles based on the selected simulation or a custom road profile can be used. The present study only requires a flat ground plane and is defined in the ACAR *road data file*. The only parameter is the coefficient of friction, **μ**. The road data file also includes limit geometry to describe the size of the ground plane. The coefficient of friction parameter is equivalent to the adjustment factor, D_{LON}, included in the ACAR Pacejka ’94 handling force model except that **μ** applies to both longitudinal and lateral forces. For example, the product D_{LON} x **μ** is the total adjustment applied to the longitudinal peak factor, D. Since the study does not differentiate between tire and road performance, the coefficient of friction for the road surface remains at 1.0.

SUB-MODEL AND SUBSYSTEM DATA COLLECTION

KINEMATIC JOINTS

The actual car differs from the documented design due to manufacturing tolerances or last-minute design changes that occurred after the drawings were created. In order to improve the accuracy of the model, the actual vehicle was measured rather than using the existing solid model drawings. All of the kinematic joints are located by hardpoints defined in the vehicle coordinate system. Accurately measuring all of the hardpoints on the vehicle is not trivial. The present study used physical measuring devices because scanning with some form of tomography was not available. The first obstacle was creating a reference from which to measure all three Cartesian coordinates. One method considered was a surface plate that would provide an extremely flat and solid device to mount the vehicle while taking measurements in one dimension. A surface plate is a thick cast iron plate with a flat milled top surface, several drilled holes or grooves for mounting measuring devices in various positions, and significant support underneath to create an extremely rigid measuring surface. The advantage is having a large solid surface, assuming a large enough surface plate is available, to mount additional measuring devices or precision blocks to gain access to each joint. The major disadvantage, aside from finding a surface plate large enough for a racecar, is mounting the vehicle in the three orientations in order to use the single reference plane.

The option selected for measuring the hardpoints is a laser level that creates two orthogonal planes, vertical and horizontal, by oscillating a laser beam over a 90deg span. The laser level used is the self-leveling David White Mark 2 LC Mini Laser Cross Level #48-M2LC. The laser level is mounted near the vehicle and measurements can be taken from the joint to the plane created by the laser. Two advantages of using the laser level are that the range of the laser far exceeds the size of any surface plate and two orthographic planes means only having to change position once to measure the third dimension. The major disadvantage is finding the normal to a plane created by a laser since it creates an optical, not physical, measuring plane.

Prior to taking any measurements, the suspension must be locked in place so the geometry does not change throughout the entire process.

1. Prepare the laser level.
    a. Rigidly mount the laser level, preferably to a fixed support such as a wall rather than a tripod which could accidentally get bumped. Use a room with ambient lighting just sufficient to read a tape measure and plenty of clean flat floor space.
    b. Align the level's vertical plane with either the **x-z** or **y-z** plane of the vehicle, assume for this example it is **x-z**. Place a mark far from the level along the laser beam in order to find this position again later.
    c. Rotate exactly 90deg about the **z**-axis and mark, again far from the level, this orientation which corresponds to the **y-z** plane.
2. Prepare the vehicle.
    a. Measure the lengths of the shocks with the empty vehicle at static ride height and replace them with adjustable length rigid links of the same length.
    b. Adjust the link lengths to achieve balanced corner weights using scales placed under each tire.
    c. Set the vehicle on stands directly under a relatively rigid component such as the frame to remove any error from deflection in the tires. Position the vehicle with as many joints within line of sight of the laser as possible – multiple positions of the vehicle are definitely required.
3. Measure the first two coordinates of each accessible hardpoint – one from the horizontal (level) plane and the other from the vertical (plumb) plane, e.g. **z** and **x** respectively (Figure 15). In addition to measuring the hardpoints, three reference points are measured on a solid, fixed portion of the chassis frame. Carefully choose the reference points as they must be accessible to the level's laser planes each time the vehicle is repositioned. The three reference points must be measured in order to facilitate coordination of the multiple vehicle/level orientations.
4. Once all of the hardpoints within sight of the laser level and the reference points in the present vehicle position are measured, rotate the level 90deg about the **z**-axis to measure the remaining coordinate from the vertical plane, e.g. along the **y**-axis (Figure 16), for the same set of points.
5. Repeat steps 3 and 4 until all three coordinates for all the hardpoints have been measured.

Remember that measurements need both a line of sight from the laser to the tape and access to the joint. Also, shorter distances reduce error from both tape and laser.

With all the hardpoints and reference points measured, the results are combined to a single database using SolidWorks CAD software. Three orientations of the racecar were required in order to accurately measure each hardpoint of the 2002 racecar. A tape with 1/32" increments was used for measuring distances. However, the laser beam thickness varies from about 1/16" to 1/8" as distance from the laser increases and therefore the edge of the beam is used. To find the normal from the laser plane, the tape is rocked back and forth, pivoting about the hardpoint, while noting the shortest distance to the laser edge (Figure 17).

Each set of measurements from the three orientations is assembled in SolidWorks by lining up the reference points. The final task is to create and position the origin of the vehicle coordinate system. The unit vectors **x, y,** and **z** are oriented to establish the hardpoints in a coordinate system which is meaningful to ACAR. The goal is to locate a theoretical center **x**-**z** plane given the measured hardpoints. Place the **x**-**y** plane slightly below the tires and the **y**-**z** plane some distance in front of the racecar – these are not critical. Though ACAR does have the ability to input asymmetric geometry, the present study is interested in longitudinal behavior. Plus, the FSAE racecar is intended to be symmetric for mixed left and right turn tracks. Given the cumulative measurement error from the tolerances of the tape and laser and the necessity for multiple orientations, the left and right **y** dimensions will be averaged to produce a symmetric set of hardpoints for the ACAR model. The resulting hardpoint locations, as referred to in earlier sections, are listed in Table 4.

VEHICLE CG

The location of the vehicle center of gravity is necessary for the study as ACAR does not have mass properties for every single item installed on the actual vehicle. In other words, the chassis part mass and location is adjusted to achieve the desired overall vehicle CG location and total mass. The rest of the parts' CG locations are relative to hardpoint geometry and are moving relative to the chassis. The powertrain subsystem parts are constrained to the chassis but have fixed mass, inertia, and locations. The location of the vehicle CG is determined via the procedure and derivation found in ISO 10392 [6], unless specified otherwise:

1. Prepare the vehicle.
    a. Rigid links replaced the shocks to lock the suspension in the same location as in the hardpoint measurements.

b. The oil was not drained from the engine crankcase, coolant was not drained from the cooling system, but the fuel tank was topped off. Therefore, some weight transfer of the oil and the coolant to a smaller degree did occur.
c. Scales are placed on a level floor underneath all four tires with a driver sitting in the racecar. Static level vehicle corner weights were noted.

2. Using a large A-frame structure equipped with a chain hoist capable of lifting the front end of the racecar, the vehicle was raised to inclinations in the range of 40-50deg. The rear end was not lifted because the 2002 racecar's chassis front overhang limits inclination to about 20deg, preventing a significant weight transfer on the scales.
3. A long straight aluminum bar was placed across the tops of a front and rear tire. The inclination of the bar was measured with an angle finder (1deg gradations). The static inclined vehicle corner weights for the rear wheels still on the ground were noted.

The results, presented in Table 9, are generated using the following equations [6].

Horizontal distance between vehicle CG and front axle (mm):

$$X_{CG} = \left(\frac{m_{stat,r}}{m_v} \right) \cdot L$$

Height of vehicle CG above ground (mm):

$$Z_{CG} = \frac{L \cdot (m_{incl,r} - m_{stat,r})}{m_v \cdot \tan\theta} + r_{stat,r}$$

Rear axle load while the vehicle is inclined (kg):

$$L = 0.5 \cdot (L_{left} + L_{right}) = 1900\text{mm}$$

Static loaded rear tire radius (mm):

$$r_{stat,r} = 0.5 \cdot (r_{stat,left} + r_{stat,right}) = 260\text{mm}$$

Static rear axle load (kg):

$$m_{stat,r} = m_{r,left} + m_{r,right}$$

Rear axle load while the vehicle is inclined (kg), $m_{incl,r}$

Vehicle angle of inclination, θ

Total mass of vehicle (kg):

$$m_v = m_{f,left} + m_{f,right} + m_{r,left} + m_{r,right}$$

MASS AND INERTIA

Each of the parts modeled in ACAR require mass and inertia properties. The masses of all the parts except the chassis and powertrain are measured using a scale accurate to approximately 30g (1 ounce). The mass of the engine and transmission assembly including all of the associated intake and exhaust components could not be measured with the scale and is an order of magnitude estimate. The inertias are estimated using one of three methods:

1. Simplified geometry that represents the actual part.
2. ACAR calculates inertias based on the geometry in the model and user-specified density.
3. SolidWorks solid model geometry (either simplified or detailed).

Many inertia values are estimated from simple shapes where applicable, e.g. a push rod is approximated as a hollow cylinder. For more complex shapes such as a control arm or upright, the geometry within the ACAR model is similar to the actual geometry on the racecar. The parts are combinations of several simple shapes to create a single volume, e.g. cylinder, tube, sphere, disc, etc. The density of the part can be adjusted to assign the correct mass and ACAR calculates the inertia properties for the volume. The chassis and driver have geometry that requires SolidWorks to generate inertia properties based on available solid model drawings or simplified geometry (Figure 18). The 5,580kg-mm^2 estimate of the engine rotating inertia for the powertrain subsystem is 150% of the crankshaft inertia. The crankshaft inertia is estimated as 6.35kg with a radius of gyration of 24.8mm giving 3,900kg-mm^2. The mass and inertia properties for each part are listed in Table 3 except the chassis part which is shown for each tested vehicle configuration in Tables 10-13.

ENGINE TORQUE MAP

The engine provides the torque output necessary to accelerate the rear wheels via the powertrain subsystem described in detail in an earlier section. The actual torque is a function of several variables but the ACAR model only considers throttle position demanded by the driver and engine speed. The 2002 TAMU FSAE racecar is powered by a four cylinder motorcycle engine with a

total displacement of 600cm^3. Torque output from the crankshaft with the air intake restricted for FSAE competition rules [1] is typically over 40Nm at engine speeds of 6,500-11,500rev/min. The torque is defined in the model for the entire range of engine operating speed at 0% and 100% throttle positions (Figure 19). Part-throttle behavior is not necessary for a straight-line acceleration event because the driver input during the simulation transitions to 100% in 0.1s. Also, the 500rpm resolution across the range of engine speed provides the minimum level of detail to describe the shape of the torque curve. With an accurate engine dynamometer, improved resolution of 200-300rpm is recommended particularly for sharp transitions in the torque curve, e.g. near 6,000rpm for this engine model.

TAMU FSAE has access to an engine dynamometer capable of measuring the torque levels of this particular engine. The motorcycle engine has an integrated transmission which means the engine dynamometer measures torque from the transmission output shaft, not the engine crankshaft. Also, the torque generated at 0% throttle is not measured. The values shown in Figure 19 for 0% throttle are an order of magnitude estimate since the engine does not spend any significant amount of time during the simulation in this condition. The torque is negative at 0% throttle because of engine braking effects and prevents the crankshaft from experiencing free spin when the clutch is disengaged from the engine. When the clutch is engaged with the engine, the same effects provide a significant amount of braking on the entire car when throttle position is at 0%.

There were three options for obtaining the engine torque curve:

1. 2002 engine setup measured on the dynamometer in 2002.
2. 2002 engine setup measured on the dynamometer in 2004.
3. 2004 engine setup measured on the dynamometer in 2004.

Option #1 is eliminated for two reasons, both of which could introduce significant error. First, although the external components such as intake and exhaust systems have not changed, the engine currently installed in the 2002 racecar is not the original engine from 2002. Several changes to the dynamometer's controller, implemented after 2002, have significantly improved control of load and speed. As a result of the improvements, the fuel and ignition maps developed for the 2002 engine are not optimized as well as those in 2004 and subsequently introduce a penalty on the torque output. Based on driver impressions of the 2002 racecar performance

compared to the newer FSAE cars, the 2002 engine suffers from a lack of torque in the lower end of engine speeds causing somewhat of a delay in acceleration.

The primary use of the engine dynamometer is to develop the fuel and ignition maps and improve engine performance on the current TAMU FSAE racecar being designed and built for the upcoming competition. Option #2 is outside the scope of this study simply due to time constraints on the use of the dynamometer. Therefore, the model uses option #3, the 2004 engine torque curve measured on the dynamometer in 2004. The TAMU FSAE racecars have all used the same make and model of motorcycle engine with very similar intake and exhaust designs.

The torque output at the extreme speeds of the entire operating range is not recorded on the dynamometer. These values have been estimated by extending the nearby slope of the recorded torque data. Torque past about 13,000rpm is reduced even further than the nearby slope suggests since the ECU begins implementing various algorithms to prevent the engine from passing the 13,500rpm redline. Coincidentally, the estimated torque at low speeds does not affect the model since the simulation begins with engine speed at about 5,500-6,000rpm.

SHOCK DAMPING AND STIFFNESS TESTING

The 2002 TAMU FSAE racecar uses shocks originally intended for mountain bike rear suspensions. The shock model is a Jupiter-5 from Risse Racing Technology with a center-to-center extended length of 216mm (8.5in) and total travel of 70mm (2.75in). The Jupiter-5 shocks have two knobs for changing needle positions within the internal fluid passages: one for adjusting low speed bump damping and the other for low speed rebound damping. Since the resulting force at any piston velocity also consists of a stiffness component from the gas, the damping and spring components of the total shock output must be defined separately in order to produce the proper sub-model within ACAR. The damping curve will provide ACAR a direct relationship between an input velocity and output force. The spring curve will provide the relationship between input displacement and output force.

The MTS Model 312.21 hydraulic tensile test machine with dual servo valves at the TEES Testing, Machining, and Repair Facility at TAMU generates the required piston motion while measuring the range of forces produced by the Jupiter-5 shock. Clevis adapters were designed and manufactured to mount the Jupiter-5 shocks in the MTS tensile test machine with additional package space for accommodating future testing of potentially larger shocks. The testing

included all four shocks from the racecar in order to establish a range of shock behavior. Each shock is measured for the effects of the bump and rebound adjustment settings. Details of the test plan are:

1. Record total shock response.
    a. Input – sine wave displacement, 13mm amplitude, 1.6Hz (10.0rad/s).
    b. Data logging – 150 samples per cycle, 0.9N (0.2lb_f) sensor noise, 4-5 cycles.
    c. Output – displacement (in), load (kip = 1000lb_f).
    d. Shock adjustment settings.
        i. MID Bump + MID Rebound.
        ii. MID Bump + HI Rebound.
        iii. MID Bump + LOW Rebound.
        iv. HI Bump + MID Rebound.
        v. LOW Bump + MID Rebound.
    e. Shock operating temperature during data logging – 38-43℃ (100-110℉).
    f. Total tests – 20.
2. Record shock stiffness response.
    a. Input – triangle wave (ramp) displacement, 13mm amplitude, 0.0016Hz (0.01rad/s).
    b. Data logging – 2Hz, 0.9N (0.2lb_f) sensor noise, 1 cycle.
    c. Output – time (s), load (kip = 1000lb_f), displacement (in).
    d. Shock adjustment settings – MID Bump + MID Rebound.
    e. Shock operating temperature during data logging – room ambient, 24℃ (75℉).
    f. Total tests – 4.

The shocks were overhauled by Risse Racing prior to testing or spending any time on the racecar. The testing is performed at ambient room temperature. During each test, an infrared temperature gun is pointed at the external surface of the shock piston chamber to indicate shock operating temperature. The “high” speed sine wave testing produces heat in the shock and the temperature is allowed to reach the desired operating temperature during the first several cycles. Data is collected during the cycles after reaching the desired temperature range. The selected temperature range is representative of TAMU race track temperatures which are most of the time in the neighborhood of 40℃. The “low” speed triangle wave testing does not significantly increase the temperature above ambient of about 24℃ (75℉) and external heat is not applied to

the shock during testing. Error associated with the relative temperature difference between the two test setups is assumed negligible.

The results of the shock testing are shown in Figures 20 through 40. The plots of shock force display the total recorded output from the shock. The damping component is generated by subtracting the stiffness component as a function of position from the total shock force. Note the absence of results from shock #3 which was a casualty from human error. To ease installation, the clevis adapters and shock are at the fully extended length to remove any load on the hardware. The next step is to initially position the shock piston at the center of travel prior to beginning the test. The #3 shock was still fully extended when the input sine wave displacement began, pulling the piston shaft 13mm beyond the limit of shock travel. A new replacement shock from Risse Racing was installed on the racecar post-test and was not tested at a later date.

The bump and rebound adjustment settings are LOW, MID, or HI. The LOW and HI settings refer to the limits of the needle adjustment. The adjustment knobs have several evenly spaced detents allowing the user to quickly find a set amount of damping. The MID setting is half the total number detents between LOW and HI. As shown in all three of the tested shocks, the MID setting does not necessarily correspond to the linear halfway point on the range of damping adjustment. Testing a finer resolution on the bump and rebound adjustment settings would allow a much better model of how damping varies with respect to each detent of the knob at the cost of running many more tests. The results from the three tested shocks provide an indication of the range of available damping at the given operating temperature.

An estimate for the amount of low speed seal drag (Coulomb friction) in the shock is available from the stiffness plots (Figures 26, 33, and 40). Comparing the intercept of the bump stiffness curve to the intercept of the rebound stiffness curve, the average difference is approximately 40N. The recorded load with zero displacement both before and after the test settles about halfway between the two intercepts. Assume equal drag on the piston in both directions of displacement and the estimate of Coulomb friction for the tested speed of 0.13mm/s is about 20N (4.5lb_f). Friction is not separated from the measured shock loads and is not included in the ACAR sub-model of the shock.

VEHICLE RESPONSE

DATA ACQUISITION SYSTEM

TAMU FSAE has a DataBuddy (PiDB) model data logger manufactured by Pi Research and designed specifically for use with motorsport applications. PiDB is capable of accepting signals from a variety of sensors, sampling at rates up to 500Hz, and storing 2MB of data on the internal CompactFlash™ memory card. Logged data is downloaded via the USB port on a computer using the supplied PiDB Logger Management software. The procedure for using PiDB to measure vehicle response in the present study is discussed in the following sections. Consult the Pi Research and MoTec documentation for additional details regarding the proper use of the logger, ECU, sensors, or software [7, 8, 9]. Refer to Table 14 for a list of the recorded channels, type of sensors, resolution, sampling rates, and the source of the sensors if applicable.

Logger

PiDB weighs 364g with an aluminum housing measuring 105 x 102.5 x 38.75mm. Underneath and threaded into the housing are four rubber mounting columns which are required for isolating the logger from vibration. In order to shelter the logger from heat, direct spray from oil or water, track debris, and electrical interference, the logger is mounted to the floor of the chassis, ahead of the steering rack, and behind the pedals (Figure 41). The logger internal accelerometers dictate the alignment of the box relative to the vehicle longitudinal and lateral directions. The error associated with roll or pitch of the chassis and logger accelerometers is within the limits of the sensors. In a straight-line acceleration event, roll is not a concern on the FSAE racecar. The pitch on a FSAE racecar is on the order of 1-2deg (0.02-0.02rad). The PiDB accelerometers can only measure to 0.02-0.03G increments. The amount of load transfer is calculated, neglecting pitch, using the longitudinal accelerometer signal and the following [2]:

Transient rear axle load with negligible aerodynamic drag (kg):

$$m_r = m_{stat,r} + m_v \cdot \left(\frac{a_X}{G}\right) \cdot \left(\frac{Z_{CG}}{L}\right)$$

Acceleration due to gravity (m/s^2): $G = 9.81 \frac{m}{s^2}$

Longitudinal acceleration of vehicle CG (m/s^2), a_X

Nearby structural panels in the frame provide adequate protection from the environment. Since the majority of testing at the TAMU track is performed without bodywork installed, the open space-frame tubing above and ahead of the pedals maintains turbulent airflow near the logger. The engine's ignition coils and spark plug wires, mounted behind the driver, are at least 1m from the logger to minimize electrical interference. The MoTec M4 ECU and its wiring harness are mounted behind the steering rack beneath the driver seat. Repositioning the ECU and wiring harness to maximize the distance to the logger is recommended for future racecar designs but was not feasible for the 2002 racecar. Accommodating the DAQ and ECU systems, both needing shelter from electrical interference, is a challenge given the limited real estate on the relatively small FSAE racecar.

Wheel Speed

Tire slip in the longitudinal direction can be calculated by measuring the difference in angular speed between the driven and non-driven wheels if one assumes the non-driven wheels are in a state of near-zero slip. The non-driven wheels therefore determine the speed of the vehicle with respect to ground if the heading is kept along the longitudinal axis of the vehicle, i.e. lateral slip is minimized. The ratio between the speed of the tire contact patch at the driven wheels and the vehicle's ground speed allows calculation of the longitudinal tire slip ratio [5] using the following equations:

Longitudinal slip ratio: $\kappa = -\frac{V_{SX}}{V_X}$

Rear tires longitudinal slip speed (m/s): $V_{SX} = V_X - \omega_r \cdot r_{stat,r}$

Rear tires longitudinal component of the speed of the wheel center approximated by using the front wheel speed and assuming near zero slip at the front tires (m/s):
$V_X = \omega_f \cdot r_{stat,f}$

Static loaded rear tire radius (mm): $r_{stat,r} = r_{stat,f} = 260\text{mm}$

Front and rear wheel speeds, respectively (rad/s): ω_f, ω_r

The only sensors required for making this measurement are a wheel speed sensor at both a driven and a non-driven wheel. The longitudinal tire performance is now fully defined by recording the longitudinal slip ratio and acceleration, i.e. these three sensors constitute the minimum requirement. The subsequent sections discuss additional channels for describing driver behavior, providing additional confidence in model correlation, or a requirement for the logger to function properly.

To measure front wheel speed, a single Hall-effect sensor is mounted to a suspension upright perpendicular to the plane of the rotor and aimed at the outer diameter of the brake rotor (Figure 42). The brake rotor design includes several teeth evenly spaced around the circumference providing the sensor with ferrous metal triggers. The rotor is attached to the hub and spins at the same speed as the wheel and tire. A single front wheel speed is recorded at either the left or right side. The rear wheel speed is also measured at the brake rotor (Figure 43). However, the 2002 racecar uses a common FSAE design with a single rear brake rotor attached to the differential housing. The brake torque applied to the left and right drive shafts is distributed via the differential in the same manner as engine torque. As a result, the rear wheel speed sensor records an average of the left and right wheel speeds. This is an approximate measure of the actual wheel speeds with the assumption that left and right tire slip is equal. The Hall-effect sensor is mounted to the differential support structure perpendicular to the plane of the rotor and aligned with the passing brake rotor mounting hardware providing only three ferrous metal triggers per revolution. In retrospect, the resolution of the wheel speed signal should be maximized when the longitudinal slip ratio is desired. The 2002 racecar design already incorporated these mounting locations for the wheel speed sensors but for future designs, the number of triggers per revolution should be maximized based on available package space and sensor capabilities.

Suspension Travel

The suspension travel at each of the four corners of the racecar is measured using linear potentiometers. The front suspension travel is measured between the bellcrank and chassis frame (Figure 44). The 2002 racecar front bellcranks include a mounting location for the potentiometer rod end. Brackets were fabricated to mount the opposite end to the chassis frame. At the rear, the potentiometer measures relative displacement of the lower control arm, mounted at the pushrod outer rod end, with respect to the chassis frame using fabricated brackets (Figure 45). The rear bellcranks also include a mounting location for either potentiometers or anti-roll bar drop links but the total travel at this location is relatively small. The front setup requires most of

the potentiometers' 100mm of travel while the rear setup requires the overall length to span the distance from frame to pushrod outer rod end.

Steering Wheel Angle

Though not necessary for the present study, steering wheel angle is measured using the rotary potentiometer that came with the PiDB kit. The potentiometer is mounted to the steering column support using a fabricated bracket which orients the axis of rotation parallel to the steering column (Figure 46). The provided plastic pulley and rubber O-ring transfer the rotation of the steering column to the potentiometer with a certain amount of reduction. The steering column is wrapped with electrical tape to reduce slip but during testing, the O-ring still slipped relative to the steering column. The PiDB Hardware documentation [7] suggests using sand paper wrapped around the column to minimize slip. For future designs, consider higher tension in the O-ring and/or changing to a rubber belt with more contact area with the pulley and column.

Beacon and Lap Layout

The beacon transmitter sits on a tripod at the track which determines the height of the receiver on the racecar. The receiver is attached to the chassis frame structural panel behind the driver's head via the industrial Velcro™ provided with the PiDB kit (Figure 47). The Velco™ attachment along with some slack in the harness allows the receiver to be positioned for passing a transmitter on either the left or right side of the racecar. The beacon is necessary for PiDB to generate laps as it records data and is required for the software. Therefore, an arbitrary oval lap is the setup used for testing: two straight sections connected by two 180deg turns. Dimensions are not known since the lap is defined by the space required for the driver to perform the necessary maneuvers instead of the reverse. The beacon is placed inside the oval, pointed outward, near the beginning of the first straight section as a start/finish line, and surrounded by cones for good visibility.

Engine Speed

The PiDB records engine speed from the tachometer signal from the MoTec M4 ECU. Engine speed is used to automatically begin and stop recording data. Do not connect the laptop to the PiDB while the engine is running. The laptop will lock up and must be shut down to unlock and restart the operating system. The cause for the problem is not known despite support from Pi Research, but electrical interference is suspect. This reinforces the need for future designs to

carefully consider placement of the ECU and DAQ systems as far from the engine as possible on such a small racecar.

Throttle Position

The MoTec M4 ECU requires a TPS in order to determine control input to the engine. Since the racecar already has a TPS installed, the PiDB borrows the signal from the MoTec wiring harness. However, the 5V signal must be calibrated within the logger to relate position to voltage. The calibration is generated using the output shown by MoTec relative to the TPS signal measured with a voltmeter. The physical position of the throttle plate relative to sensor voltage was not used because it could generate a difference between the recorded signals of the ECU and DAQ system, particularly at part-throttle.

Sampling Rate

The sampling rates of all but the beacon receiver were set to 100Hz which provided a good balance between signal representation and the limits of the logger 2MB memory card. PiDB averages the wheel speed signal across several triggers from the Hall-effect sensor. The front wheel speed sensor pointed at a 30-tooth trigger wheel (notches in the brake rotor) and produced excellent resolution. However, the rear wheel speed sensor only had three triggers per revolution forcing PiDB to wait longer between updates of the wheel speed signal. The effective update rate for the rear wheel speed is about 10-15Hz as shown in Figure 48 using configuration 1 data as an example. The rear wheel speed holds while the front wheel speed continues to increase. As the front signal “catches up” with the rear signal, the calculated longitudinal slip ratio, also shown in Figure 48, decreases rapidly between updates of the rear signal. The MoTec M4 tachometer signal logged by PiDB resulted in only 20Hz suggesting PiDB is performing an average of tachometer signals as well. The acceleration, engine speed, and rear wheel speed channels, particularly during a straight-line acceleration event of a FSAE racecar, rapidly change at the beginning of the event and the 100Hz rate should be considered a minimum. For critical channels, use higher sampling rates when the balance of memory card limit and track time allows. Non-critical channels may be compromised if memory is a factor by reducing the sampling rate on the lateral acceleration for example.

Miscellaneous DAQ System Suggestions

The PiDB kit purchased by TAMU FSAE contains the Pi DataBuddy MiniDash (Pi Research Part No. 01K-163055-1) for displaying up to eight channels. The logger setup determines which

channels are available to the driver while on the track. During testing, the drivers had to estimate the initial speed prior to beginning the straight-line acceleration event. In retrospect, the drivers could improve consistency in initial speed if the MiniDash had been installed to display the current wheel speed.

Potentiometers, speed sensors, thermocouples, or even strain gauges are all relatively inexpensive when compared to the optical sensing equipment required for measuring tire slip. Corrsys-Datron manufactures a series of non-contact optical sensors for this purpose. For example, the CORREVIT® S-CE[1] can measure the velocity vector with respect to ground, providing an accurate representation of the longitudinal and lateral slip occurring at the tire contact patch. The price is about two to three orders of magnitude above the Hall-effect sensors and significantly outside the limit of funding for this study.

VEHICLE RESPONSE TESTING

The racecar is tested at the TAMU Riverside Campus which has a series of long runways. A majority of the runway surface is cleared for racecar use but weeds growing between the seams in the concrete mixed with a variety of debris create a wide range of grip. Several laps on the same track setup helps clean the surface.

System Configurations

Recall, one of the objectives of the study is to validate the longitudinal performance of the full vehicle model against the actual vehicle response recorded at the TAMU test track. Since the rigid body model of the racecar's kinematics is accurately characterized, the majority of error in the simulated response is expected to arise from the Goodyear tire model representing the Hoosier tire on the actual track surface. The dynamic inputs that affect the performance output from the tire model, i.e. the longitudinal force, are normal load and slip ratio. Using two drivers and the option of adding ballast, the resulting array of four configurations varies the static normal load by 15% and the CG height, i.e. the longitudinal load transfer, by 2% (Table 9). The quantity of ballast chosen is approximately equal to the difference in driver mass. As a result, two configurations – light driver plus ballast and heavy driver without ballast – have nearly equal total mass and only the overall CG location is changed.

[1]CORREVIT® Non-Contact Optical Sensors are manufactured by Corrsys-Datron of Wetzlar, Germany. Sensor specifications available at http://www.corrsys-datron.com/optical_sensors.htm, [accessed June 2005].

The other two configurations – light driver without ballast and heavy driver with ballast – provide a range of static load in addition to the change in CG location. The ballast mounts to the main roll hoop support tubes directly over the rear suspension track width. The CG of the ballast is located along the centerline of the vehicle at a height approximately equal to the top of the tire, about 520mm above the ground.

Procedure

The following procedure outlines the general steps taken to measure the response of the 2002 TAMU FSAE racecar for each configuration:

1. Prior to arriving at the track.
    a. DAQ system and laptop:
        i. Calibrate sensors, set sampling rates, and configure logger as desired.
        ii. Verify channel output in logger display.
        iii. Memory card – clear and/or download any previous sessions from the logger.
        iv. Charge laptop battery if necessary.
    b. Vehicle:
        i. Check fluid levels.
        ii. Check tire pressures and set to 12psi.
        iii. Check lug nut torque.
        iv. Top off fuel tank if necessary.
        v. Verify engine and MoTec are working properly.
        vi. Adjust suspension for static corner weight, camber, and toe settings. For the present study, the settings at static ride height with driver are: front and rear camber angles vary from 0deg to -1deg, front toe overall 1.5mm out, rear toe varies from 5 to 6mm in, and corner weights are equal within 1.4kg from left to right.
2. Prepare track, vehicle, and DAQ system while driver gets ready and belted in the seat.
    a. Track:
        i. Position beacon transmitter at the start of the first straight section of track, pointing from inside the oval out so the beacon only crosses one portion of the track. The driver should pass the beacon while still at a steady initial speed for the straight-line acceleration event.
        ii. Place cones at either end of the two straight sections of track to help the driver return to the same locations for each lap.
    b. DAQ system:

i. Turn logger on.
ii. Confirm logger setup, update driver name and/or track information, and provide a description of the session.
iii. Turn logger off until ready to log a session of laps.
iv. Position beacon receiver on the racecar to match the beacon transmitter location.

c. Vehicle:
i. If applicable, remove or mount the ballast.
ii. Check tire pressures and set to 12psi.
iii. Check lug nut torque.
iv. Top off fuel tank if necessary.
v. Start engine (logger should be off at this point).
vi. Drive vehicle away from pit to starting position on track.

3. Measure response.
a. With engine running and vehicle staged to begin lap, driver turns on the logger. The logger should automatically begin logging (depending on setup) once the front wheel speed becomes nonzero. Use the first lap to clean the tires off and prepare for the straight-line acceleration event as follows.
b. Driver instructions for one complete lap:
i. Accelerate/brake as required to reach a speed of 35kph, shift to second gear, and release clutch lever.
ii. Hold 35kph in second gear while steering straight ahead for a couple seconds.
iii. Go directly to 100% throttle, accelerate while steering straight ahead, shifting at engine redline until fourth gear.
iv. Apply brakes, initiate 180deg turn, and approach opposite straight section of track.
v. Accelerate/brake as required to reach a speed of 35kph, shift to second gear, and keep clutch lever depressed.
vi. Hold 35kph in second gear while steering straight ahead for a few seconds. At the last moment, increase throttle to bring engine speed to near redline.
vii. Simultaneously release clutch lever and increase to 100% throttle, accelerate while steering straight ahead, shifting at engine redline until fourth gear.
viii. Apply brakes, initiate 180deg turn, and approach opposite straight section of track.
ix. Repeat beginning at step (i.) for at least five laps.
x. Return to pit and turn engine off.
c. With engine off, connect laptop to download the session. Return to step (2.b.) and repeat until all four configurations are tested.

The lap contains two types of straight-line acceleration event. Both initially start in a rolling condition at 35kph but one event begins with the clutch already engaged with the engine and the other event begins as the driver releases the clutch pedal. The latter condition is closer to the actual method in which the racecar is accelerated. However, the first case is appropriate for correlating the model as it removes most if not all of the clutch effects in the overall response. Plus, the racecar is not equipped with a tachometer and the drivers could not consistently start the event at the same engine speed. This is possible if the PiDB MiniDash is utilized such as was suggested for displaying wheel speed.

Running the event in second gear is selected to maximize use of the engine. The event begins at around 5900rpm and concludes at engine redline, 13,500rpm. The drivers are instructed to continue shifting and accelerating up to fourth gear to capture shift times. The model is capable of shifting but the default settings are not typical of a sequentially shifted motorcycle engine, i.e. the standard ACAR clutch and shifter inputs are about 2.0s while FSAE shifts require only 0.2s. ADAMS/Driver, another software package working with ACAR, can control the full vehicle simulation in a custom manner but is outside the scope of this study. Creating custom ADAMS/Driver-controlled simulations is the next step towards predicting the racecar response based on the recorded driver inputs at the track.

The track direction was not noted but was kept the same for all configurations. The testing was performed in the following order:

1. 75kg driver – no ballast.
2. 75kg driver – with ballast.
3. 88kg driver – with ballast.
4. 88kg driver – no ballast.

Post-Processing

The data must be downloaded from the logger using the PiDB Logger Management software [8]. The PiDB Logger Management software is strictly for communicating with the logger and does not offer any post-processing of the data. Once the data is on the laptop, the next step was using the Pi Club Expert Analysis (CEA) software [10] supplied with the PiDB kit to view the data. However, CEA does not offer the ability to export time history files for further analysis. It offers the ability to view the data in histograms or with respect to a track map. The track map is generated from the wheel speed channel ideally during an “easy” lap with very little tire slip. For

the present study, time history of the recorded responses is required to perform the necessary analyses and plots. The Pi Version 6 software [11, 12] is able to view the files generated by the PiDB Logger Management software and perform many more tasks than CEA. The most important ability of V6 is exporting the data to a *comma separated value* file which can be used by spreadsheet software, in this case Microsoft Excel.

Once the data is imported to a spreadsheet, the lap data is divided according to the two straight-line acceleration events and the 180deg turn portions are removed. The events with the clutch engaged prior to applying 100% throttle are extracted for further analysis. The lap time for each event is adjusted such that **t** = 0s at the moment the longitudinal acceleration channel rapidly increases. The suspension travel potentiometers were calibrated according to the travel measured at the Risse Racing Jupiter-5 shock. To display the suspension travel as displacement instead of position, the steady state shock position for each corner is used to vertically shift the entire curve to zero. The same procedure is used with the ACAR simulated response discussed later.

MODEL CORRELATION

The only parameter used in this study for adjusting the model to match the simulation results with the measured system response is the scaling of the longitudinal tire model, i.e. $D_{LON} = BCD_{LON}$. The scaling is equal to the ratio of peak recorded normalized longitudinal tire force $\mathbf{F_X/F_Z}$ to the Goodyear tire model prediction of peak $\mathbf{F_X/F_Z}$. Recall, the road coefficient of friction parameter in the road data file is set to 1.0.

COMPARISON OF SIMULATED AND MEASURED RESPONSES

The following discussion refers to Figures 49-76, which show the results of both the ACAR and measured responses for each configuration. The data presented are:

1. Longitudinal Acceleration vs. Time
   a. Measured Response – longitudinal accelerometer channel from PiDB.
   b. ACAR Response – chassis part longitudinal acceleration.
2. Engine Speed vs. Time
   a. Measured Response – tachometer signal from MoTec M4 ECU; channel logged by PiDB, filtered.
   b. ACAR Response – powertrain subsystem engine speed.
3. Longitudinal Chassis Speed vs. Time
   a. Measured Response – front wheel speed channel from PiDB; assumes constant tire radius of 260mm.
   b. ACAR Response – chassis part longitudinal speed.
4. Longitudinal Slip Ratio vs. Time
   a. Measured Response – calculated with front and rear wheel speeds from PiDB; assumes constant tire radius of 260mm, filtered.
   b. ACAR Response – calculated slip between rear tire and road surface; tire radius based on Goodyear tire model vertical stiffness and applied normal load.
5. Normalized Tire Force vs. Longitudinal Slip Ratio
   a. Measured Response – calculated with longitudinal accelerometer from PiDB, vehicle CG location, and vehicle geometry; assumes constant tire radius of 260mm.
   b. ACAR Response – calculated using longitudinal and normal loads on tire; tire radius based on Goodyear tire model vertical stiffness and applied normal load.
6. Throttle Position
   a. Measured Response – throttle positions channel from PiDB.

   b. ACAR Response – driver input to powertrain subsystem.
7. Damper Travel
   a. Measured Response – damper position channels from PiDB; vertical shift places steady state position at zero.
   b. ACAR Response – damper length; vertical shift places steady state length at zero.

For all but the normalized longitudinal tire force, the measured response data is from a single straight-line acceleration event that the driver obtained the most precise initial vehicle speed. The plots of tire force as a function of slip ratio present all the available measured response data for each particular configuration.

Configuration 1

Figures 49-55 show the measured vehicle responses and the ACAR simulated responses for configuration 1, light driver without ballast. The Goodyear tire model scaled to 78% (D_{LON} = BCD_{LON} = 0.78) results in the upper limit, for this configuration, of the recorded normalized longitudinal tire force $\mathbf{F_X/F_Z}$ (Figure 53).

Configuration 2

Figures 56-62 show the measured vehicle responses and the ACAR simulated responses for configuration 2, heavy driver without ballast. Note the initial speed is only 32kph for this configuration (Figure 58). The ACAR model in this instance was simulated with a 32kph initial speed to match the recorded data, which did not include an event with 35kph initial speed. The Goodyear tire model is scaled to both 78% and 75% for this configuration. The 78% curve appears beyond the upper limit for this set of events and the 75% curve represents grip near the recorded tire performance as shown by the peak slip (Figures 59-60).

Configuration 3

Figures 63-69 show the measured vehicle responses and the ACAR simulated responses for configuration 3, light driver with ballast. The Goodyear tire model is scaled to 78% for this configuration to provide good correlation overall.

Configuration 4

Figures 70-76 show the measured vehicle responses and the ACAR simulated responses for configuration 4, heavy driver with ballast. The Goodyear tire model is scaled to 72% for this

configuration to provide good correlation with the recorded tire performance (Figures 73-74). The slip ratio predicted by ACAR at D_{LON} = 72% remains above the recorded slip ratio at **t** = 0.5-1.0s indicating the level of grip is changing (Figure 73). The road surface at different locations along the track or heat building up in the tire are two examples of why grip would change during the event.

Overall Observations

Predicted longitudinal acceleration during about the first 0.3s of all the simulations is consistently high compared to the measured response. Recall the engine torque map in the model is based on dynamometer measurements of the 2004 engine. The difference between the 2004 and 2002 racecars both in track performance and driver impressions confirm a significant lack of initial torque in the 2002 engine. This difference in torque is apparent in the transient response of the dampers where the model consistently predicts larger displacements.

The measured longitudinal acceleration lags the throttle control input by about 0.05-0.10s. The predicted response from ACAR shows longitudinal acceleration of the chassis part tracking TPS with virtually no lag indicating there is some inertia not modeled in the templates. One explanation involves the transport inertia within the engine intake system. The intake system uses a single inlet providing air to a plenum that distributes air to the four combustion chambers via runners to each cylinder. The combustion chamber does not respond to TPS input until pressure within the intake plenum increases and the required restriction [1] on the inlet limits this fill rate. The engine speed at the beginning of the straight-line acceleration event is about 6,000rpm (100Hz), i.e. each revolution of the crankshaft requires 0.01s. It is entirely possible the plenum could take about 5 revolutions of the crankshaft in order to respond to a 100% TPS input from a near-idle condition. Also, the response time would be compounded by the transient performance of the ECU such as poor tuning of the acceleration enrichment.

Before modifying the model to include the inertia, minimize the response time in the 2002 engine. Tune the ECU with the 2002 engine on the dynamometer while addressing transient control parameters in addition to the baseline fuel and ignition maps. The objective is to match the 2002 engine performance with recent FSAE engines and accurately measure the torque output. Several combinations of TPS and speed are required for tuning the fuel and ignition maps. Recording torque output with the dynamometer at each TPS/speed position will add significant detail to the engine model improving prediction of part-throttle behavior in future simulations. Validate the changes using PiDB, which can log the MAP signal from the MoTec M4 ECU, and

quantify the time required to fill the plenum. If the measured response time continues to differ significantly from the simulation, the powertrain subsystem would need an additional DOF describing the transport inertia behavior.

CONCLUSIONS

The results of the study indicate the range of on-track longitudinal tire behavior for the Hoosier tire is about 75±3% of the Goodyear tire model. Though the correlation procedure fixed the road surface coefficient of friction while varying the tire model parameters, the reverse would result in the same longitudinal vehicle response. The peak available grip between tire and road is determined by the product of $\mu \times D_{LON}$. Therefore, the study does not differentiate between tire performance and road surface performance – the results instead describe the interface between tire and road. If subsequent use of the model assumes the interface applies to both longitudinal and lateral behavior, then the next logical step is to evaluate the model accuracy in predicting lateral or combined lateral/longitudinal behavior. This is achieved by one of two configurations:

- $D_{LAT} = D_{LON} = 75\pm3\%$ with $\mu = 100\%$.
- $D_{LAT} = D_{LON} = 100\%$ with $\mu = 75\pm3\%$.

Recall, the scaling of the tire "stiffness" factor, BCD_{LON}, does not affect peak tire performance. Though BCD_{LON} was scaled the same as D_{LON} throughout this study, comparison of initial slope in Figures 13, 53, 60, 67, and 74 supports the claim that the overall vehicle response is significantly less sensitive to changes in the stiffness factor, BCD, than changes in the peak factor, D. In turn, the configuration with the tire parameters kept at 100% and the road surface reduced to 75±3% is a fair assumption given the results of this study. However, confidence in this assumption requires significantly more data describing the vehicle response with lateral slip maneuvers, e.g. constant radius acceleration event (a.k.a. skid pad), slalom, or complete autocross course.

RECOMMENDED NEXT STEPS

Using the results and suggestions of this study, the full vehicle ACAR model has potential as a valuable analysis tool for the FSAE racecar design process. Next steps, in order of recommended priority, include:

1. Improve 2002 engine performance and ACAR model powertrain subsystem correlation using the dynamometer to tune the ECU and record an accurate torque map. Measure the MAP signal during a straight-line acceleration event to quantify the intake plenum fill rate.
2. Apply tire model scaling instead to the road surface coefficient of friction and validate overall vehicle dynamics against maneuvers with lateral slip, e.g. constant radius acceleration event.
3. Add refinement to powertrain subsystem:
    a. Expanding the engine torque map to cover part-throttle conditions.
    b. Modify the templates to include a DOF between the driver input, TPS, and the engine model to describe transport behavior in the intake system.
4. Expand use of ACAR's simulation capabilities:
    a. Utilize the many other standard simulation events (note – braking parameters need to be defined at this stage if braking events will be simulated).
    b. Develop custom *driver control files* (.dcf) or use ADAMS/Driver to apply the same controls measured at the track to the model.

SUMMARY

The objective of the study was to create a full vehicle dynamics model of the 2002 TAMU FSAE racecar using ACAR and validate the model's longitudinal performance against recorded vehicle responses using a DAQ system. The process of achieving this objective involved:

1. Repairing the 2002 racecar.
2. Measuring the vehicle mass, estimating inertias, and measuring geometry in order to populate the ACAR model database.
3. Testing the Risse Racing Jupiter-5 shocks to define the sub-model stiffness and damping properties.
4. Installing the Pi DataBuddy data acquisition system on the 2002 racecar.
5. Testing the racecar and recording the response in a longitudinal acceleration event at the TAMU Riverside Campus.
6. Correlate the ACAR simulation results to match the measured response via scaling the Goodyear tire model to represent the Hoosier tire on-track performance.

The most significant deliverable from this study is a working full vehicle ACAR model which allows future vehicle dynamic analysis. In a close second, the installed and working PiDB DAQ system helps provide the detailed feedback from the track which is missing from the present FSAE design process.

The results of the correlation process have shown that the dynamometer results for the 2004 engine predict higher performance than the measured response of the 2002 engine. This observation from the data is confirmed by driver impressions and comparison to the 2004 racecar performance. An engine torque map generated from the dynamometer measurements for the as-installed 2002 engine setup is necessary for eliminating this error.

The Hoosier tire on the TAMU Riverside Campus track surface is 75±3% of the predicted peak longitudinal tire performance by the Goodyear tire model combined with a road surface friction coefficient of 1.0.

REFERENCES

1. Society of Automotive Engineers (SAE) (2005) *2005 Formula SAE Rules*, SAE, Warrendale, PA.
2. Gillespie, T. D. (1992) *Fundamentals of Vehicle Dynamics*, SAE, Warrendale, PA.
3. Milliken, W. F. and Milliken, D. L. (1995) *Race Car Vehicle Dynamics*, SAE, Warrendale, PA.
4. Ginsberg, J. H. (1998) *Advanced Engineering Dynamics*, 2nd edition, Cambridge University Press, New York, NY.
5. Pacejka, H. B. (2002) *Tire and Vehicle Dynamics*, SAE, Warrendale, PA.
6. International Organization for Standardization (ISO) (1992) 'Road Vehicles with two axles – Determination of centre of gravity', *International Standard*, ISO Reference Number 10392:1992(E).
7. Pi Research (PR) (2002) *PiXpress DataBuddy System Hardware Reference*, PR, Indianapolis, IN.
8. PR (2002) *PiXpress DataBuddy Logger Management Software User Guide*, PR, Indianapolis, IN.
9. MoTec Systems USA (MoTec) (1996) *Motec M4, M48 & M8 User's Manual*. MoTec, Huntington Beach, CA.
10. PR (2001) *PiXpress Club Expert Analysis User Guide*, PR, Indianapolis, IN.
11. PR (1998) *Pi Version 6 PC Software Guide 1998 Edition*, PR, Indianapolis, IN.
12. PR (1999) *Pi Version 6 PC Software Guide 1999 Addendum to 1998 Edition*, PR, Indianapolis, IN.

APPENDIX A

FIGURES

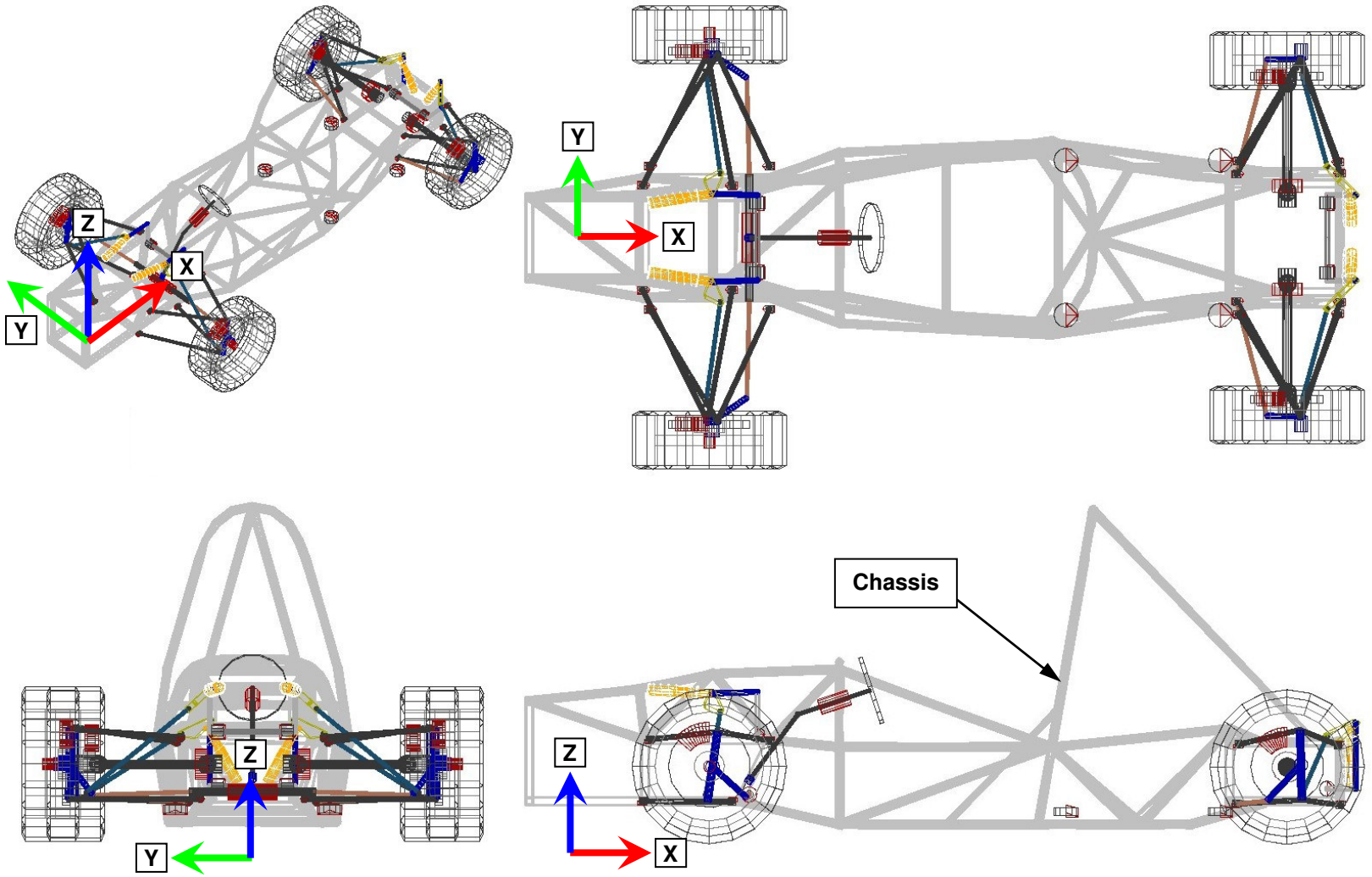

Figure 1: Coordinate System Orientation

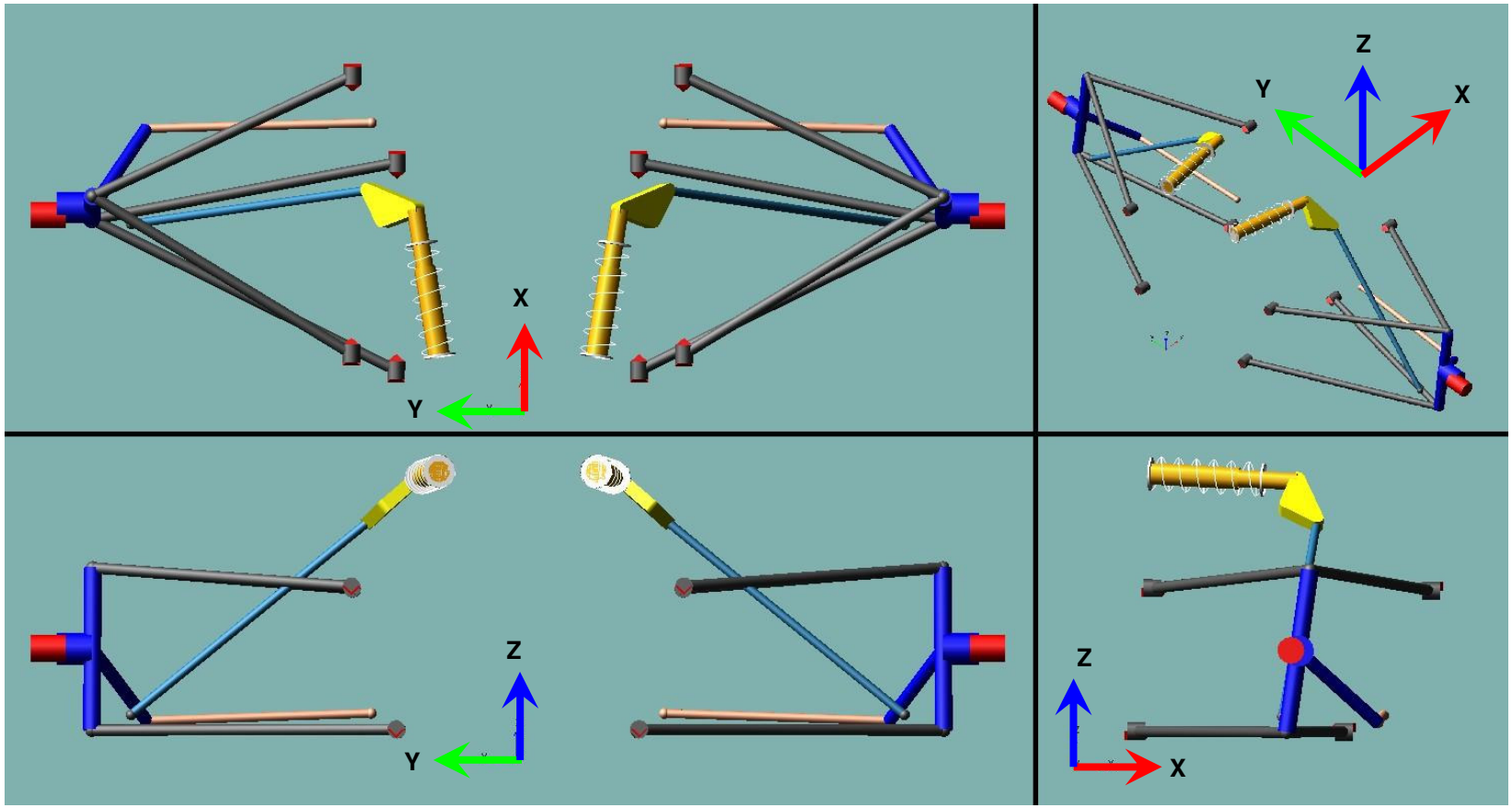

Figure 2: Front Suspension Subsystem

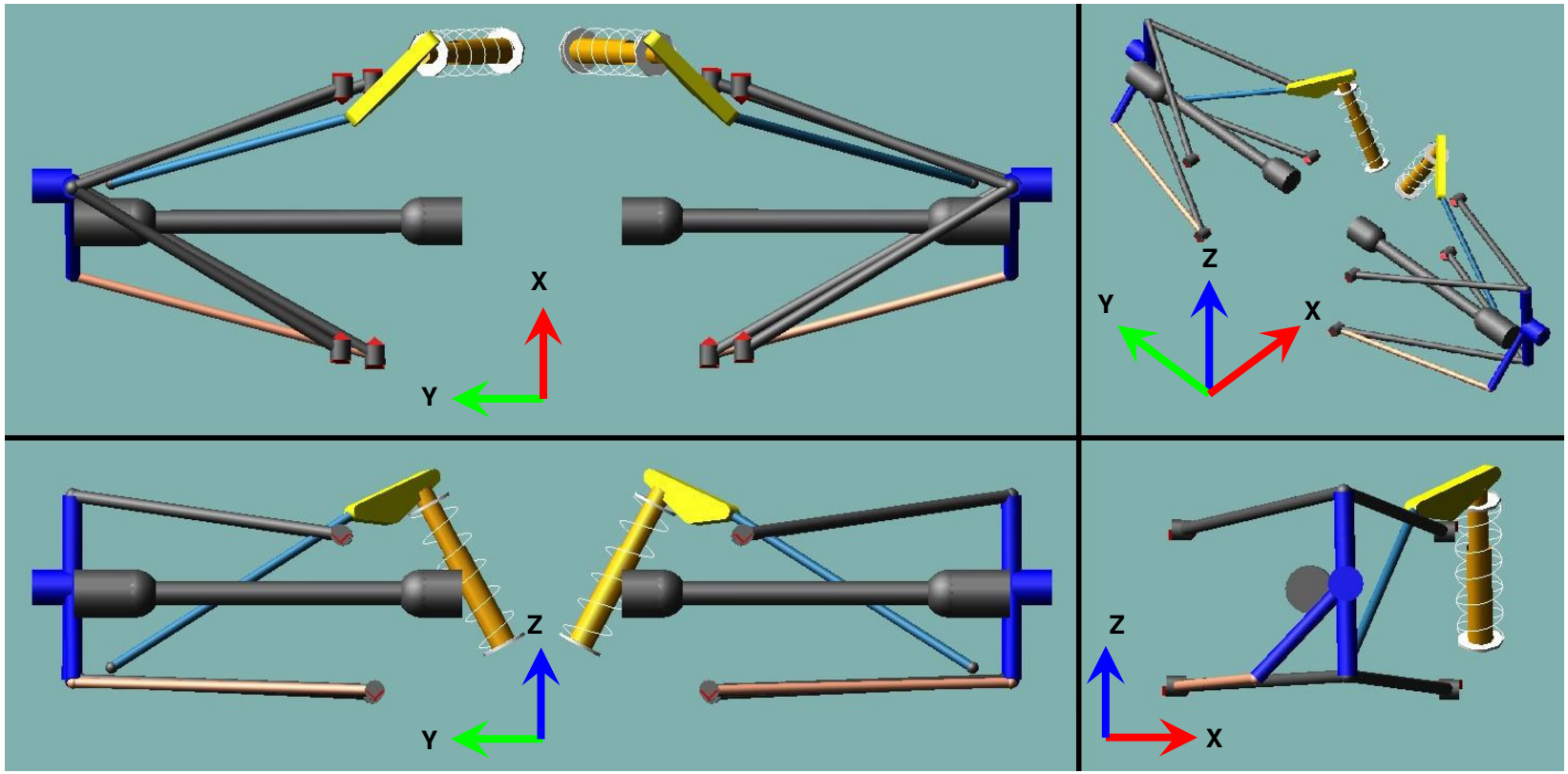

Figure 3: Rear Suspension Subsystem

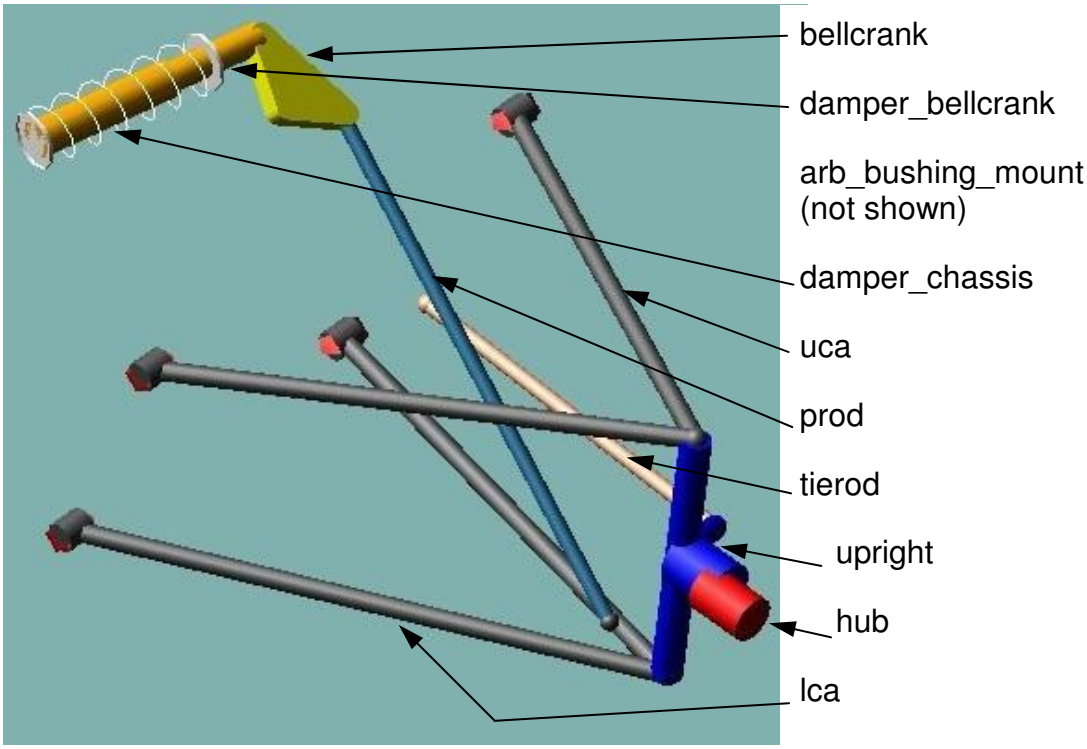

Figure 4: Front Suspension Subsystem Parts

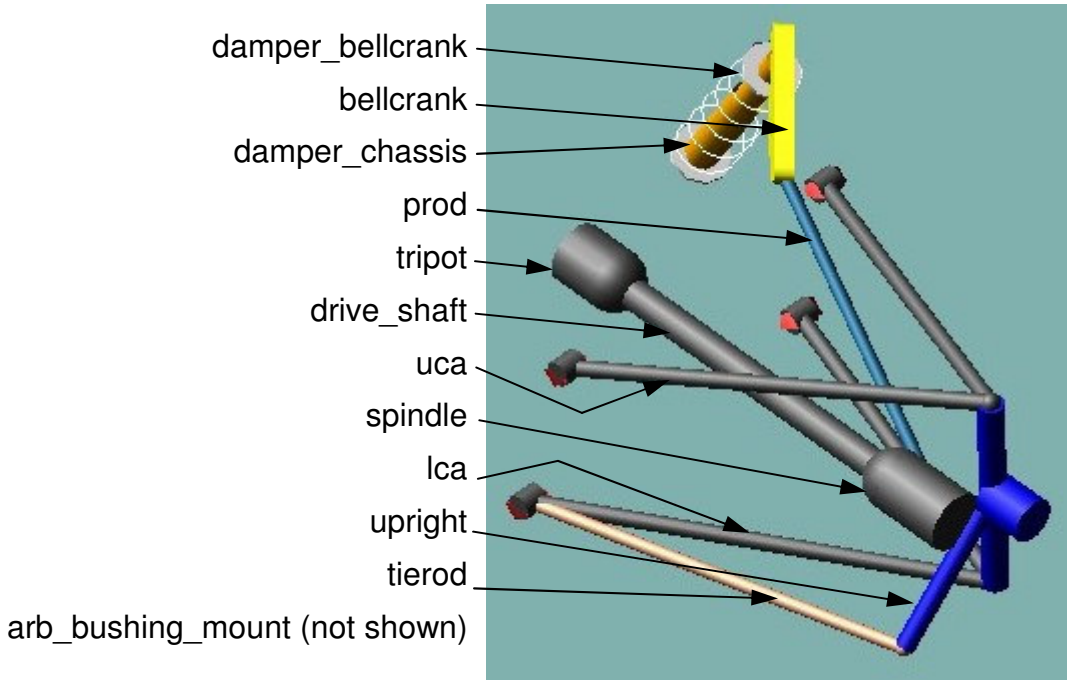

Figure 5: Rear Suspension Subsystem Parts

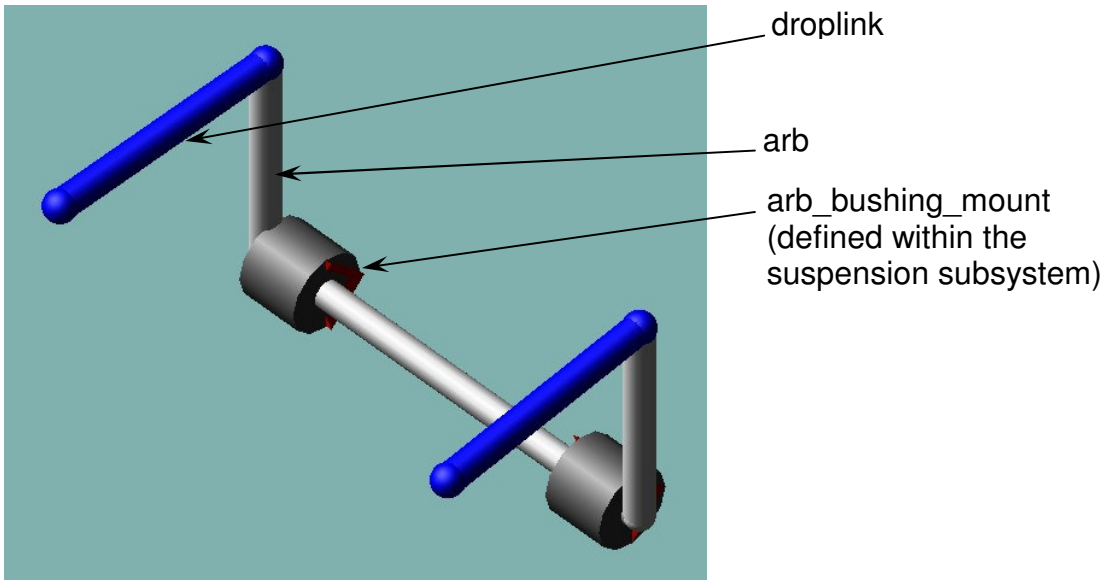

Figure 6: Anti-Roll Bar Subsystem Parts

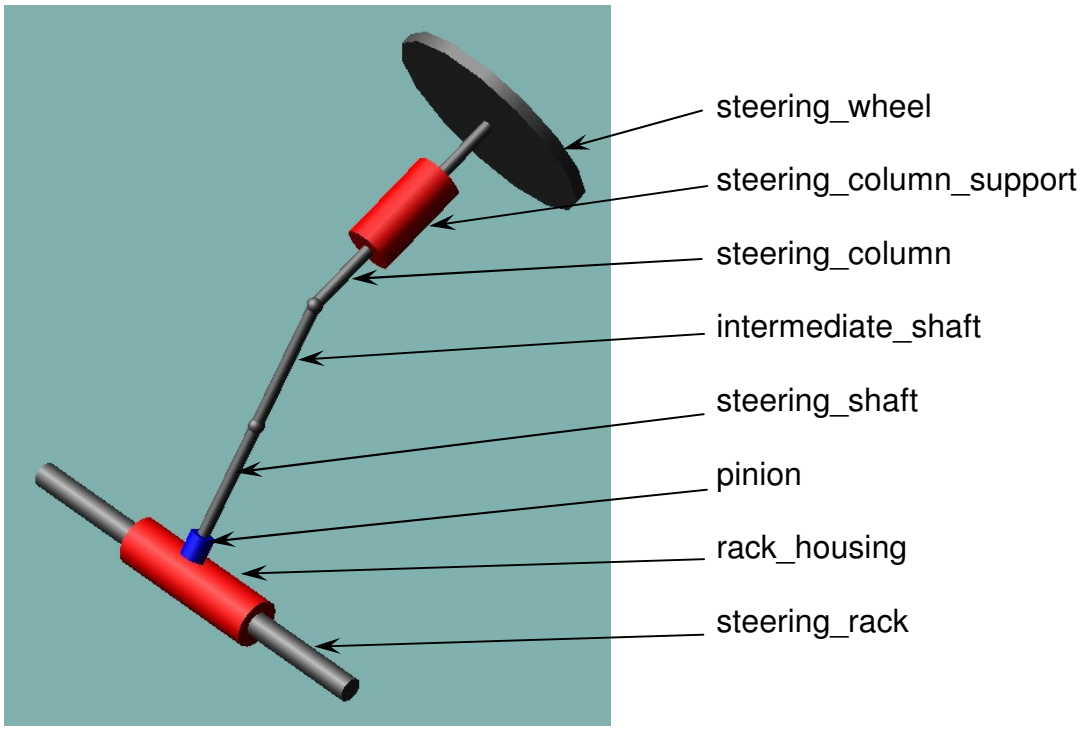

Figure 7: Steering Subsystem Parts

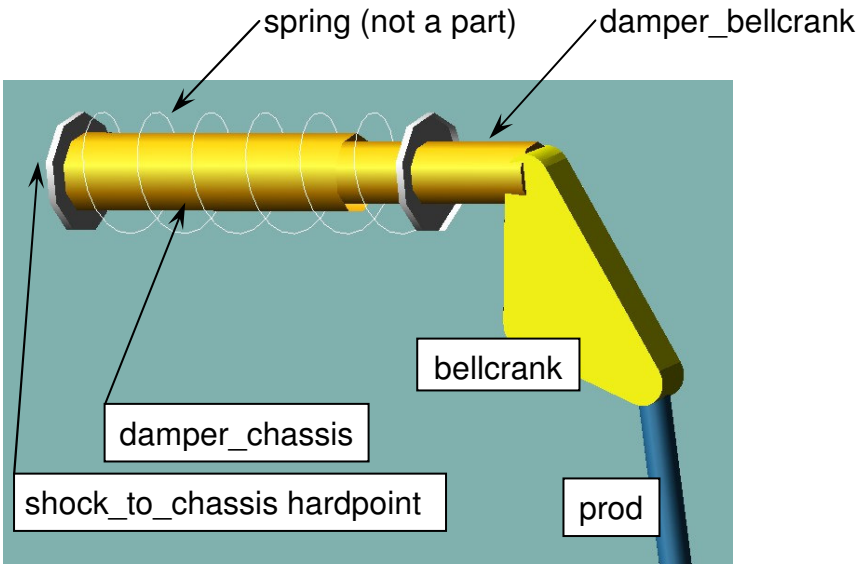

Figure 8: Coil-Over Shock Sub-Model

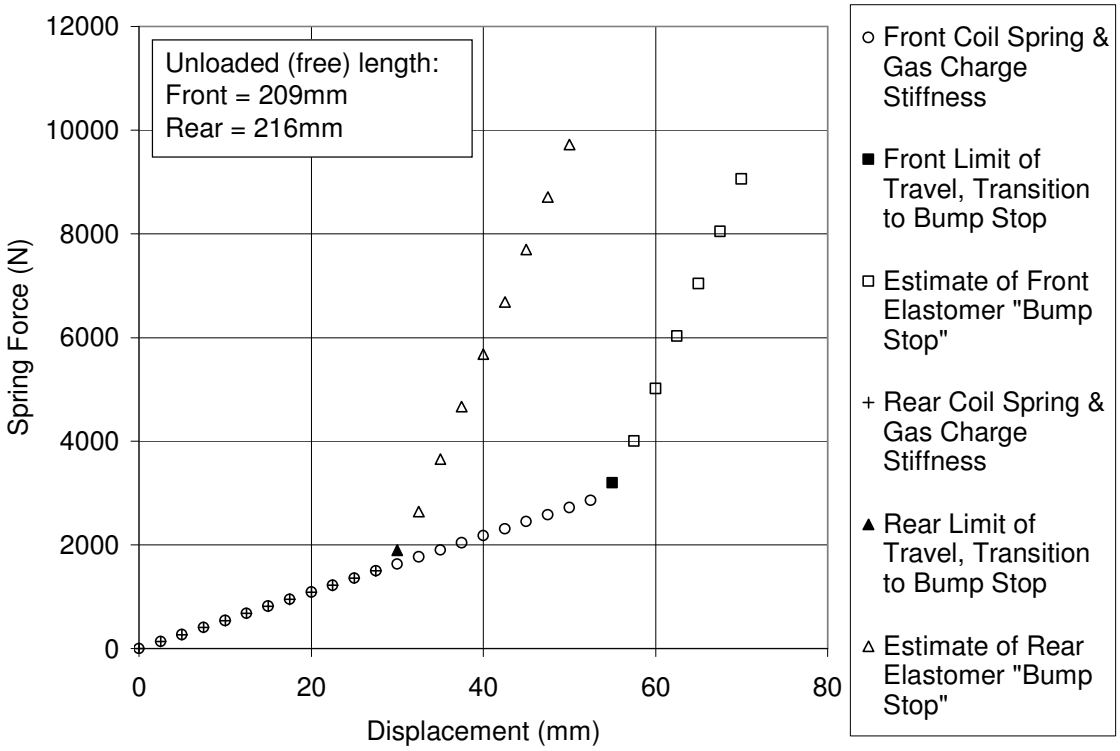

Figure 9: Suspension Springs

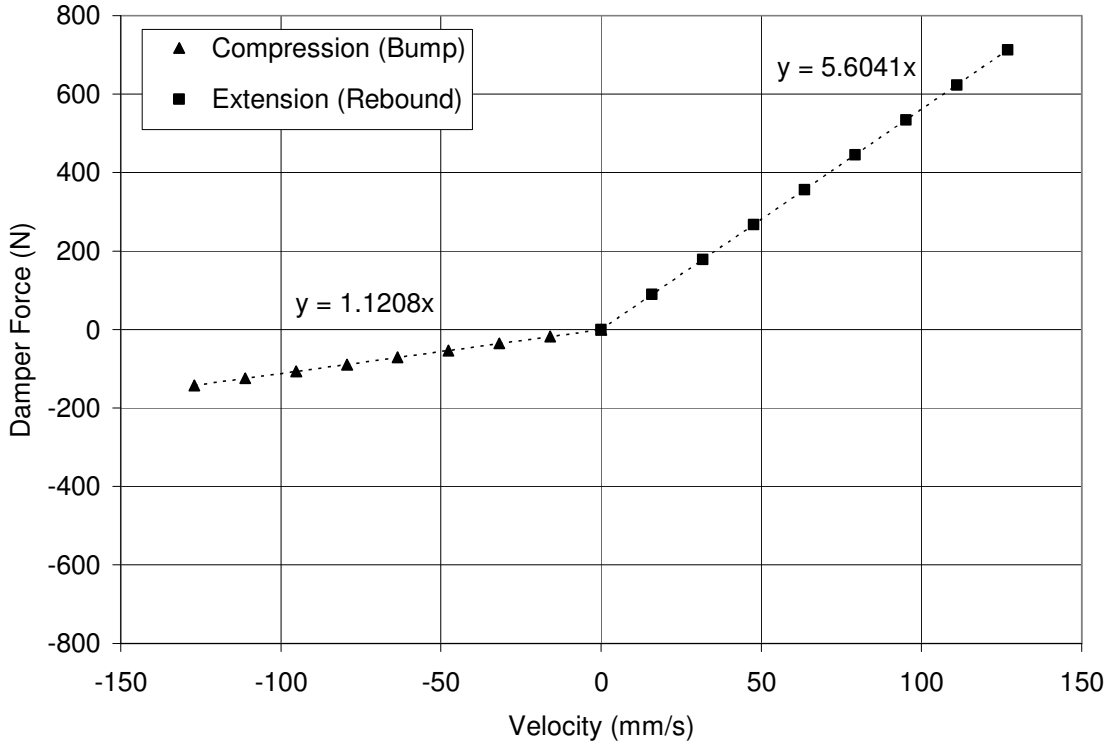

Figure 10: Suspension Dampers

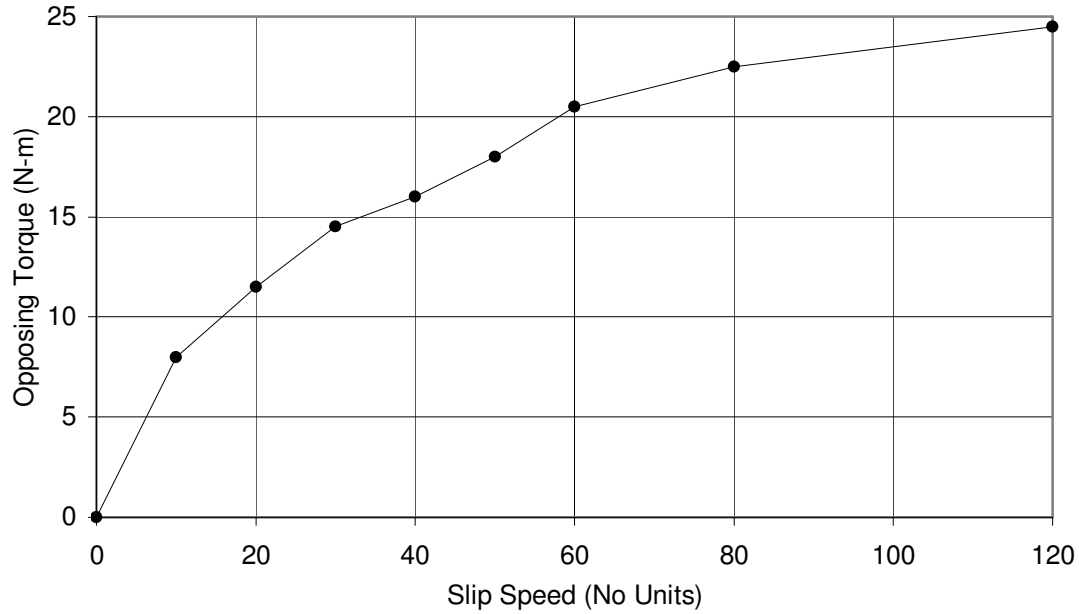

Figure 11: Viscous Differential

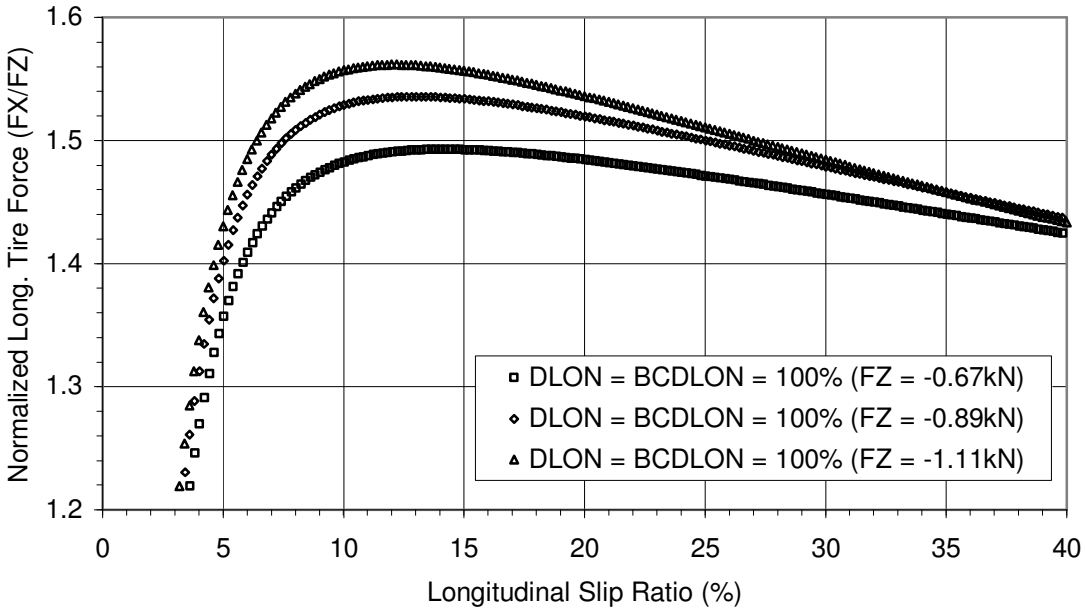

Figure 12: Normal Load Effects on Normalized Longitudinal Tire Force
(Goodyear FSAE Tire Model, 20in outside diameter, 6.5in width, 13in diameter rim, 12psi inflation pressure)

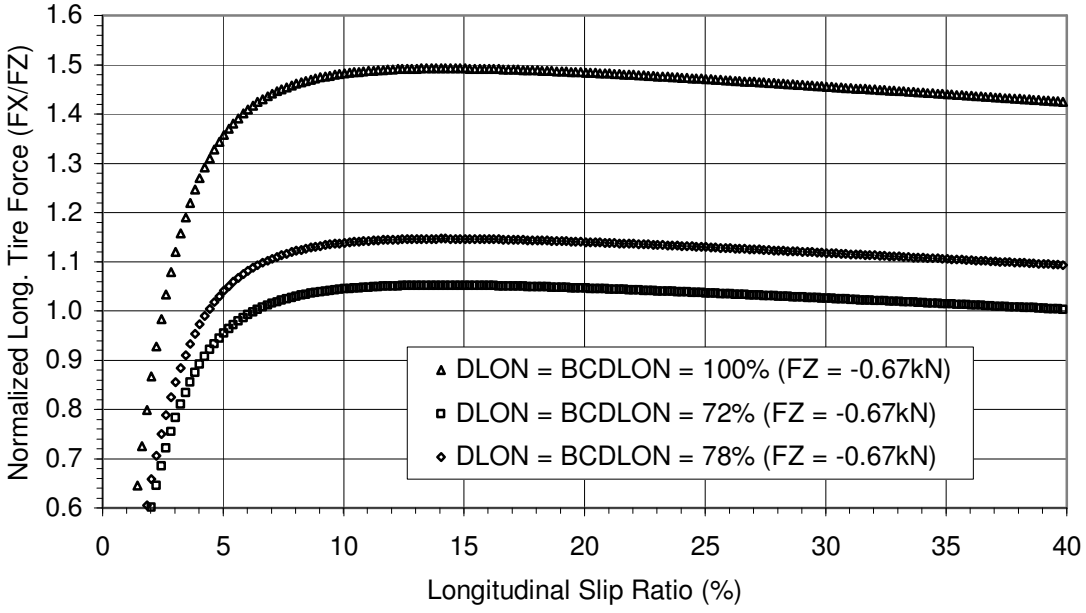

Figure 13: Scaling Effects on Normalized Longitudinal Tire Force
(Goodyear FSAE Tire Model, 20in outside diameter, 6.5in width, 13in diameter rim, 12psi inflation pressure)

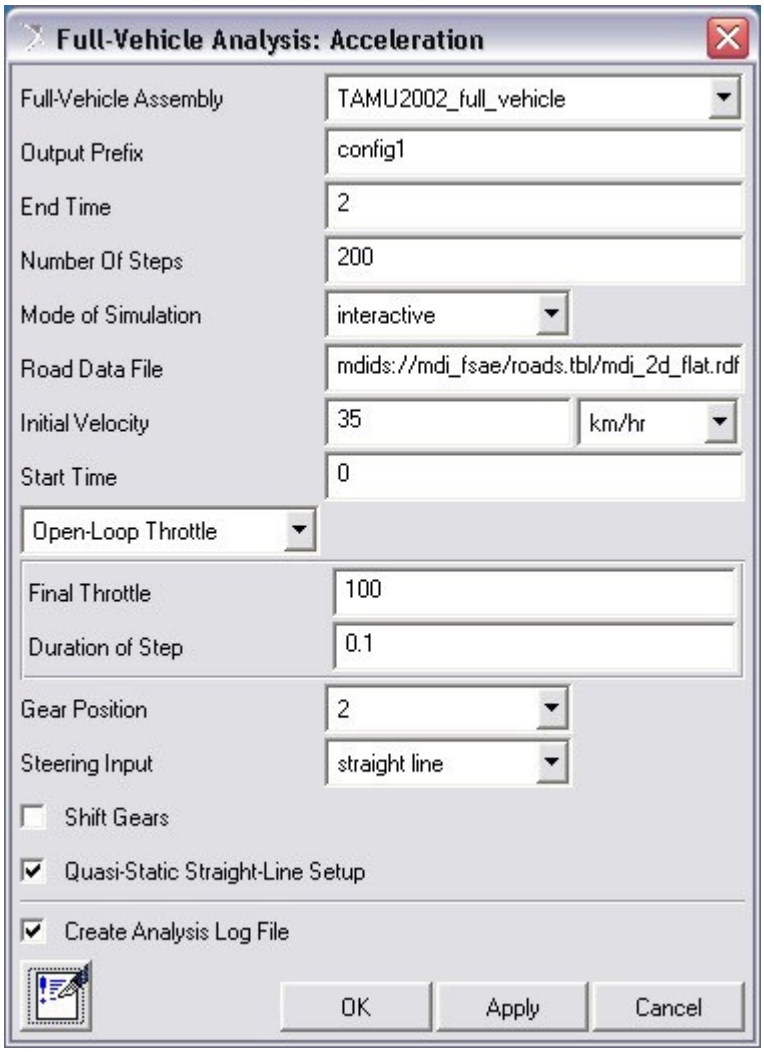

Figure 14: Simulation Setup – Full-Vehicle Analysis Straight-Line Acceleration

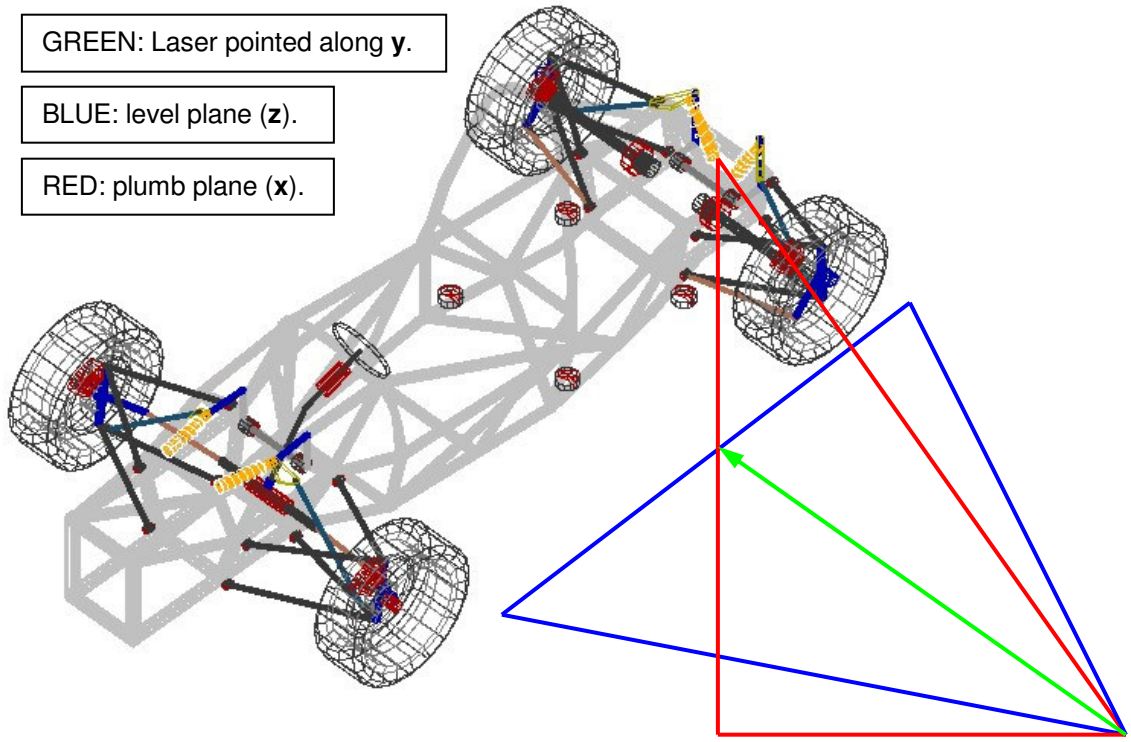

Figure 15: Kinematic Joint Locations – First Laser Level Orientation (**y** direction)

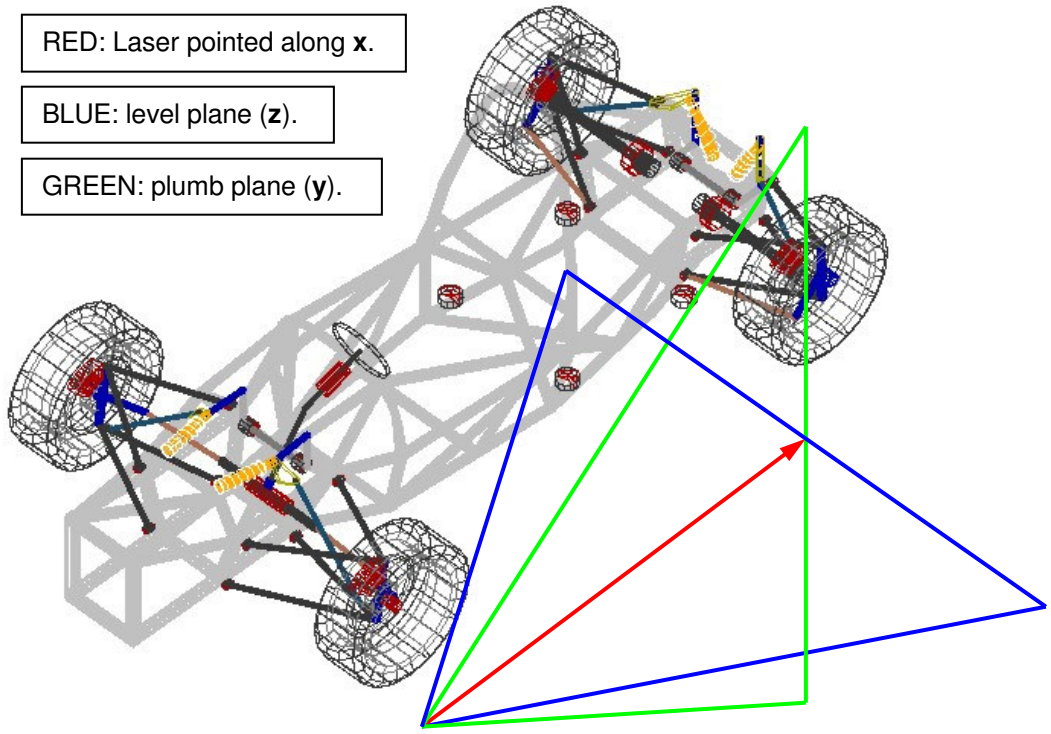

Figure 16: Kinematic Joint Locations – Second Laser Level Orientation (**x** direction)

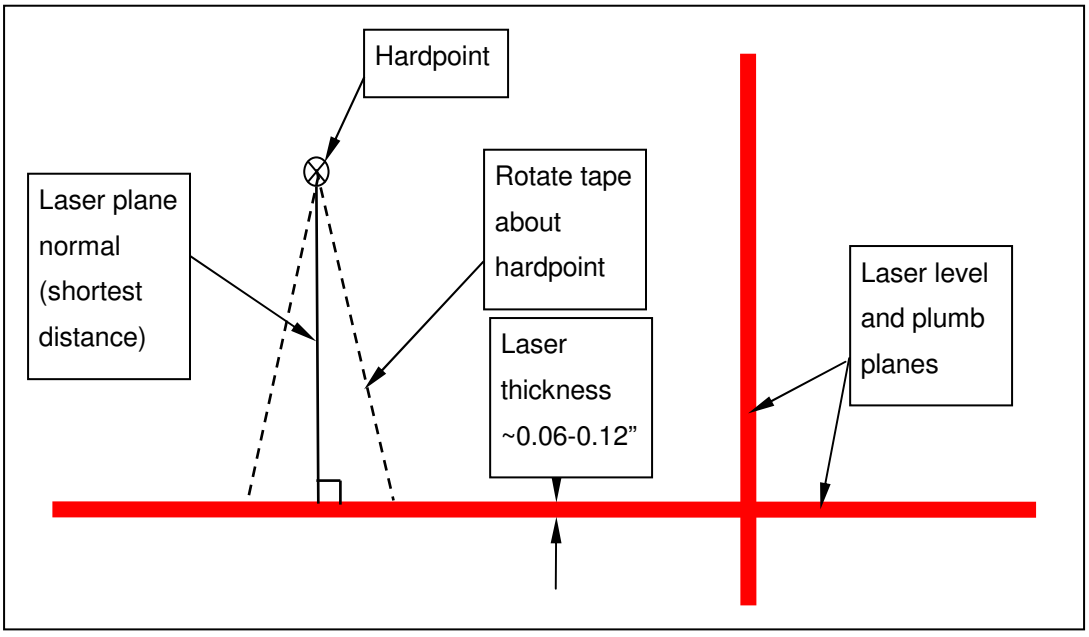

Figure 17: Hardpoint Measurement Using a Laser Level

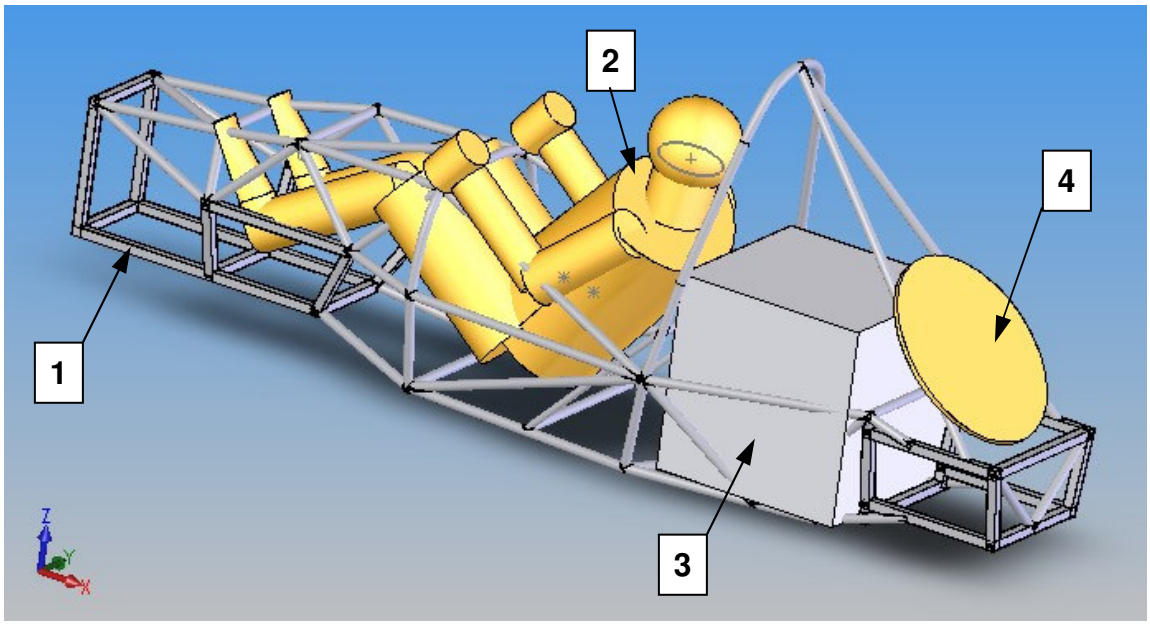

1. Solid model drawing of 2002 frame.
2. Simplified geometry of driver.
3. Simplified geometry of powertrain part.
4. Simplified geometry of ballast.

Figure 18: SolidWorks Model for Estimating Inertia

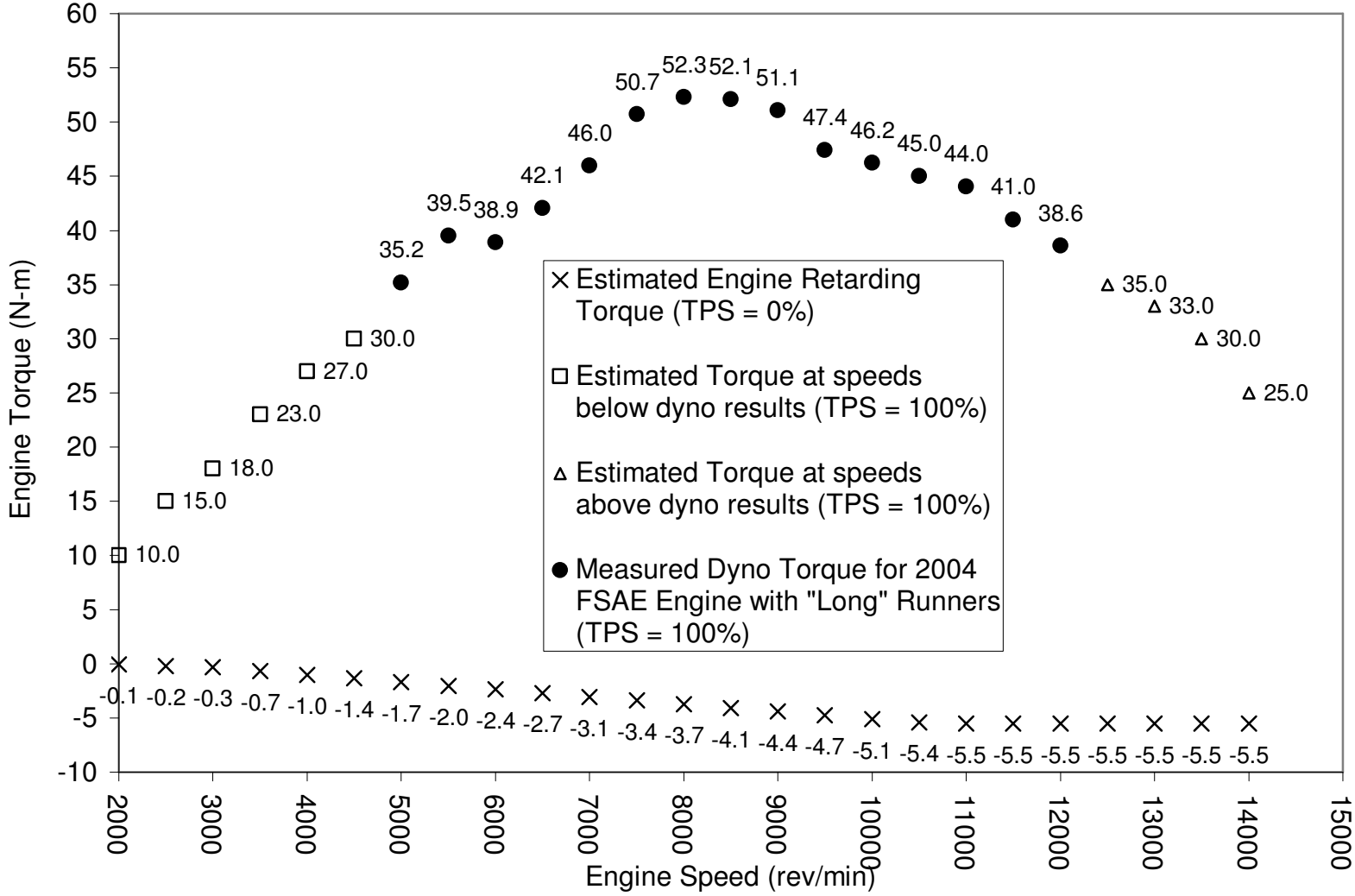

Figure 19: Powertrain Subsystem Engine Torque Map

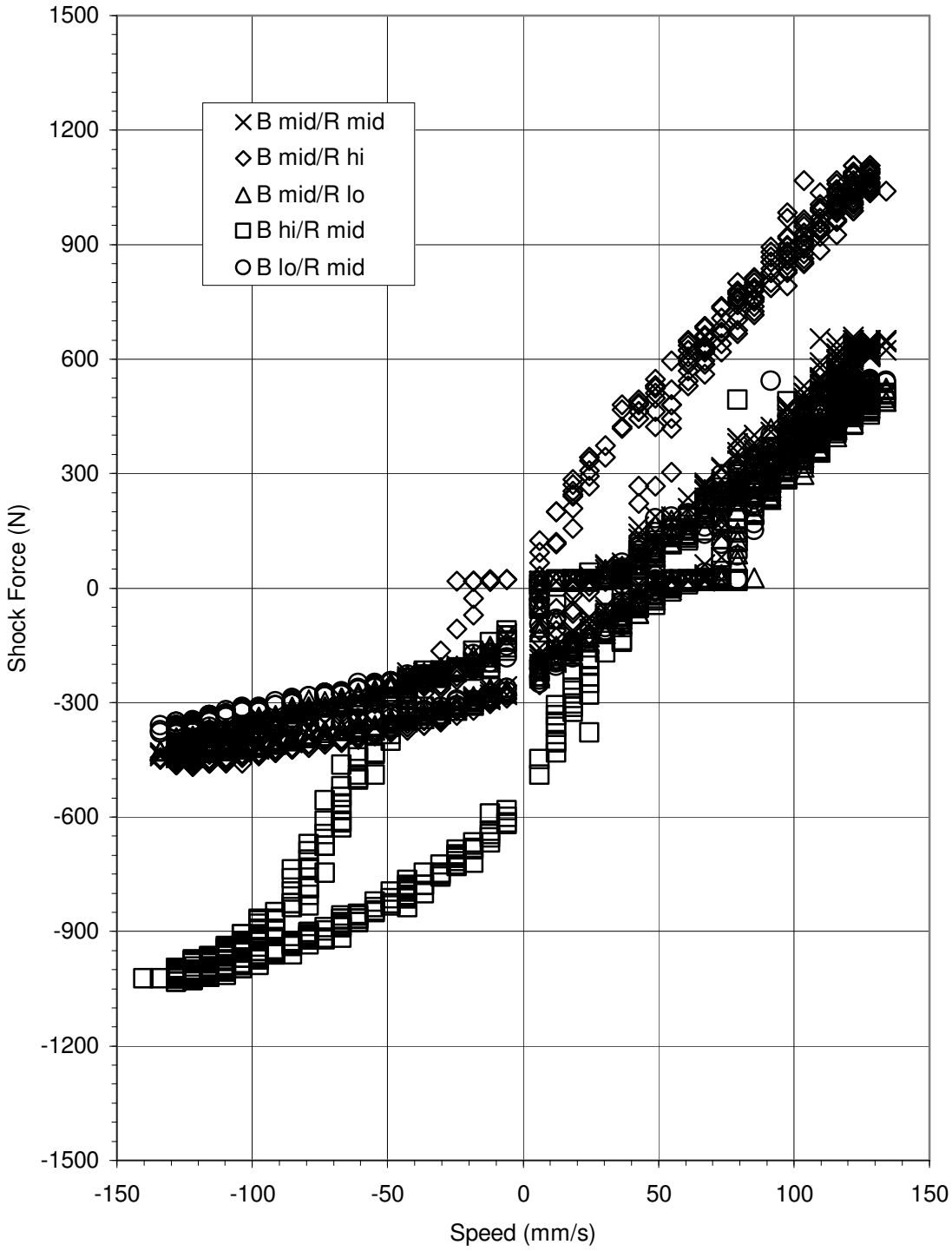

Figure 20: Risse Racing Jupiter-5 Shock #1 – Total Force, All 5 Tested Settings

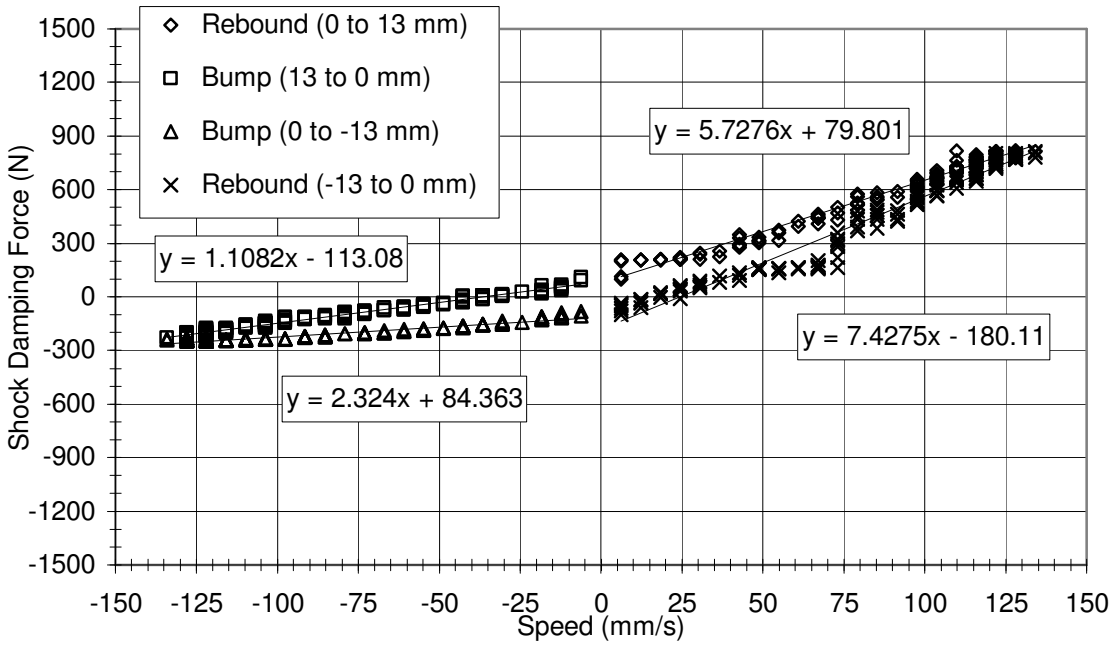

Figure 21: Risse Racing Jupiter-5 Shock #1 – Damping, MID Bump + MID Rebound

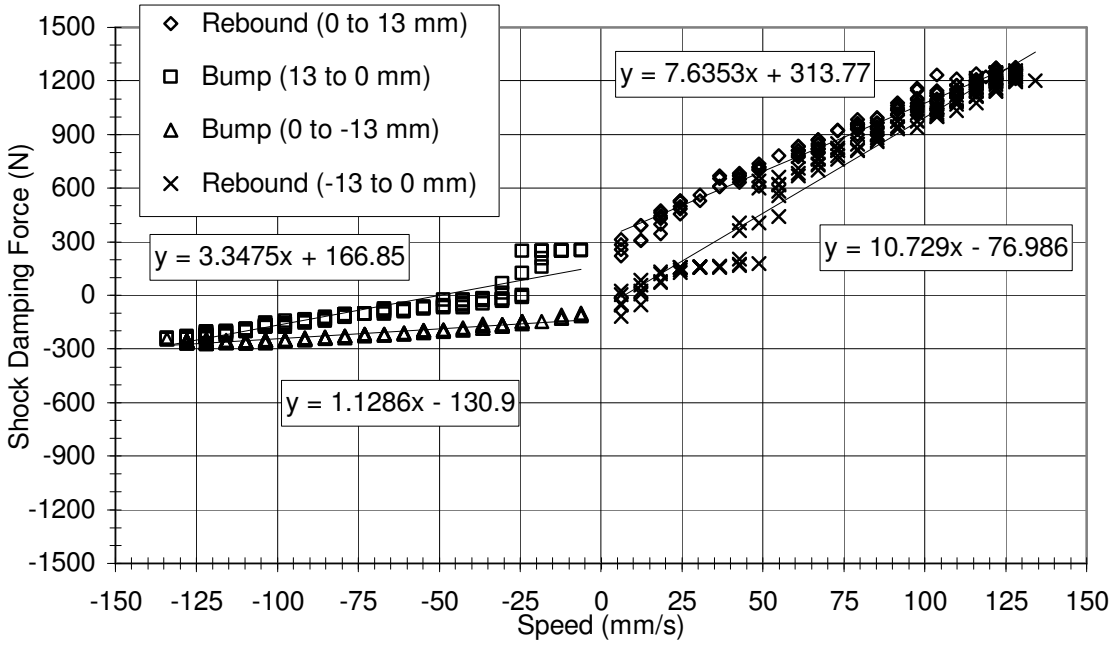

Figure 22: Risse Racing Jupiter-5 Shock #1 – Damping, MID Bump + HI Rebound

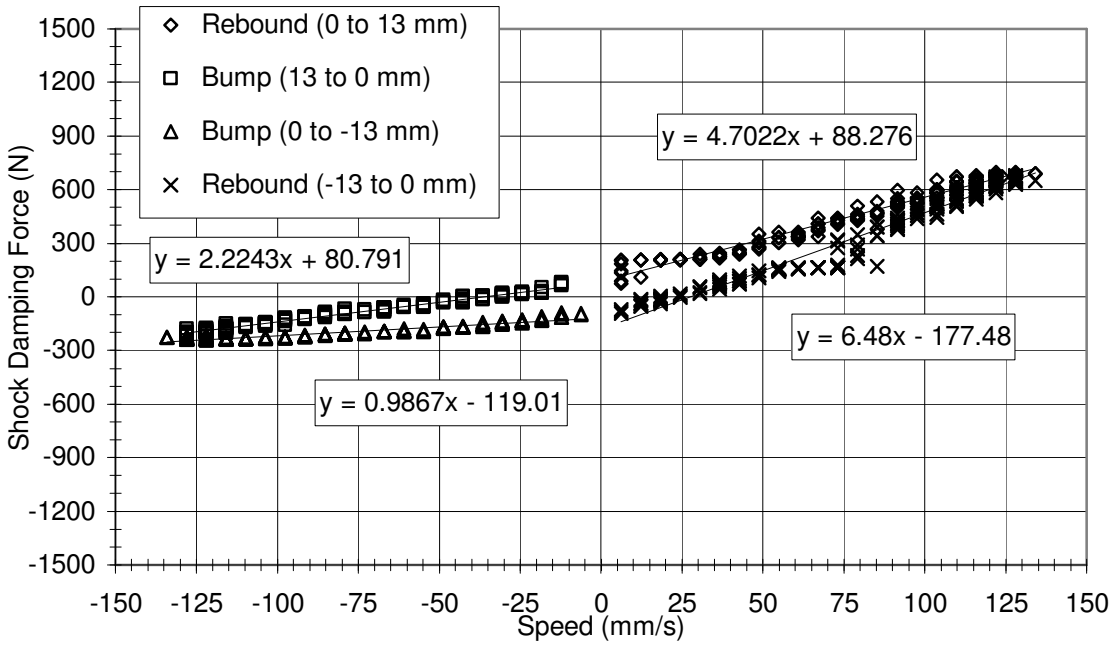

Figure 23: Risse Racing Jupiter-5 Shock #1 – Damping, MID Bump + LOW Rebound

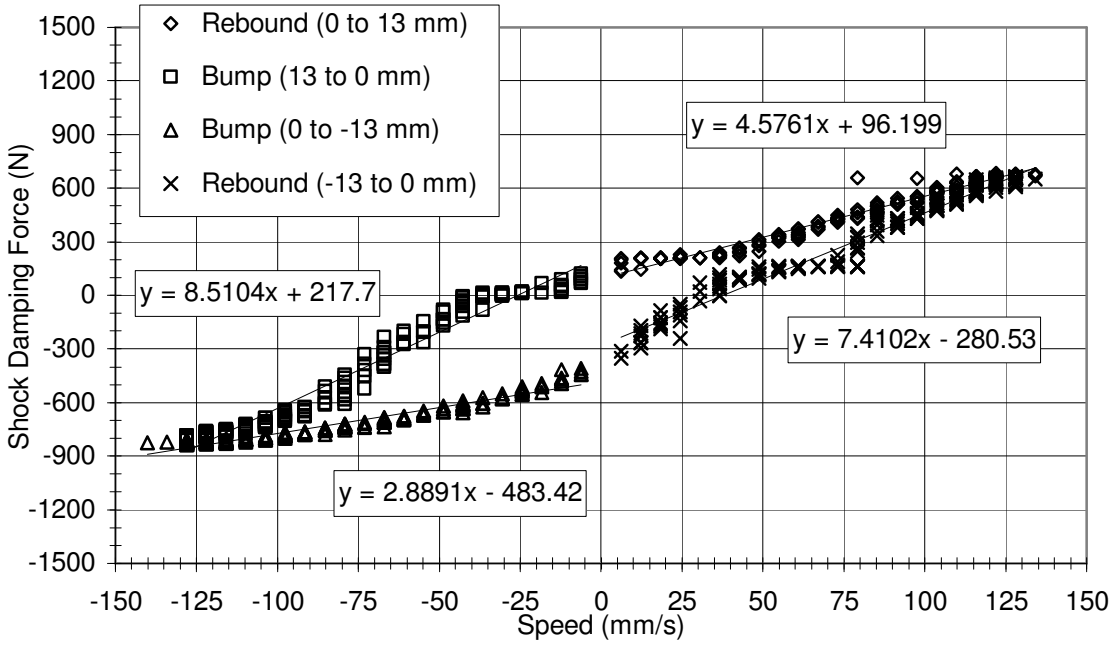

Figure 24: Risse Racing Jupiter-5 Shock #1 – Damping, HI Bump + MID Rebound

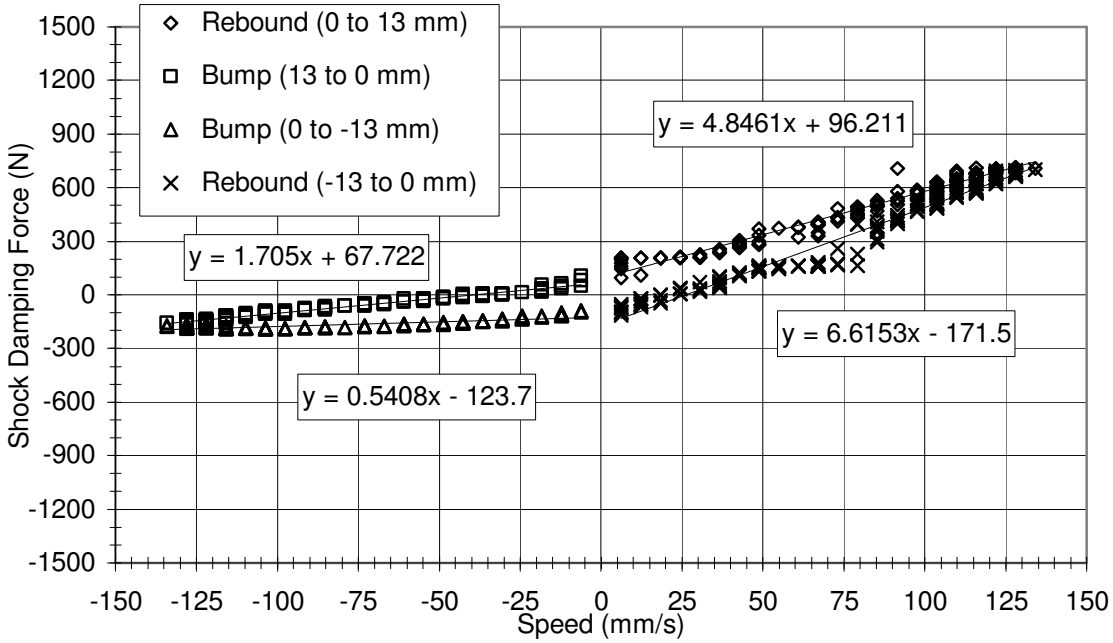

Figure 25: Risse Racing Jupiter-5 Shock #1 – Damping, LOW Bump + MID Rebound

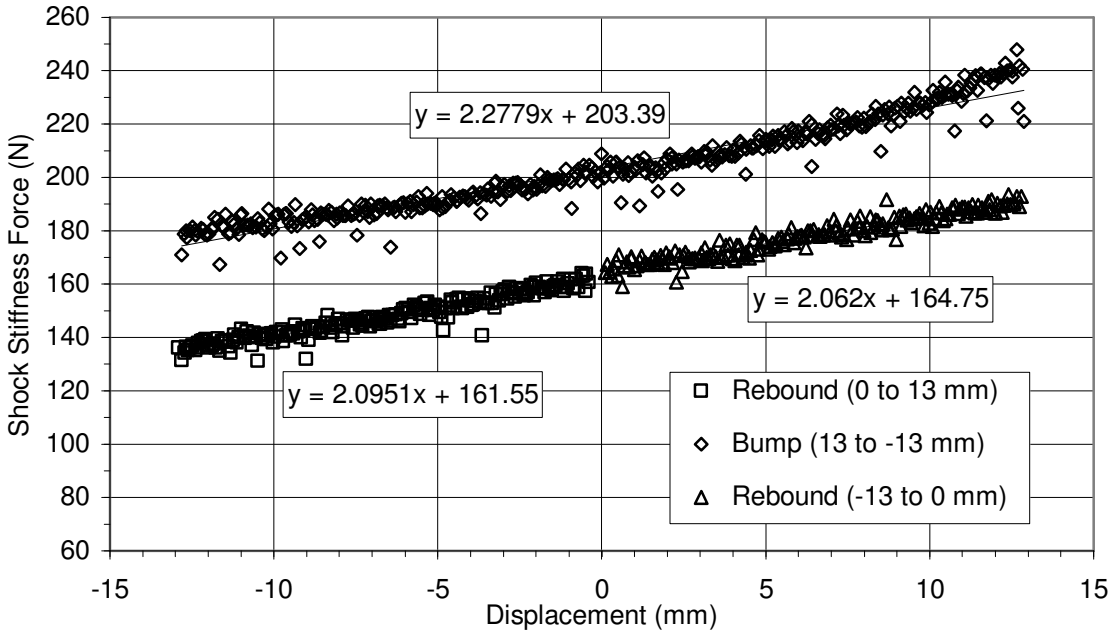

Figure 26: Risse Racing Jupiter-5 Shock #1 – Stiffness (Speed = 0.13 mm/s)

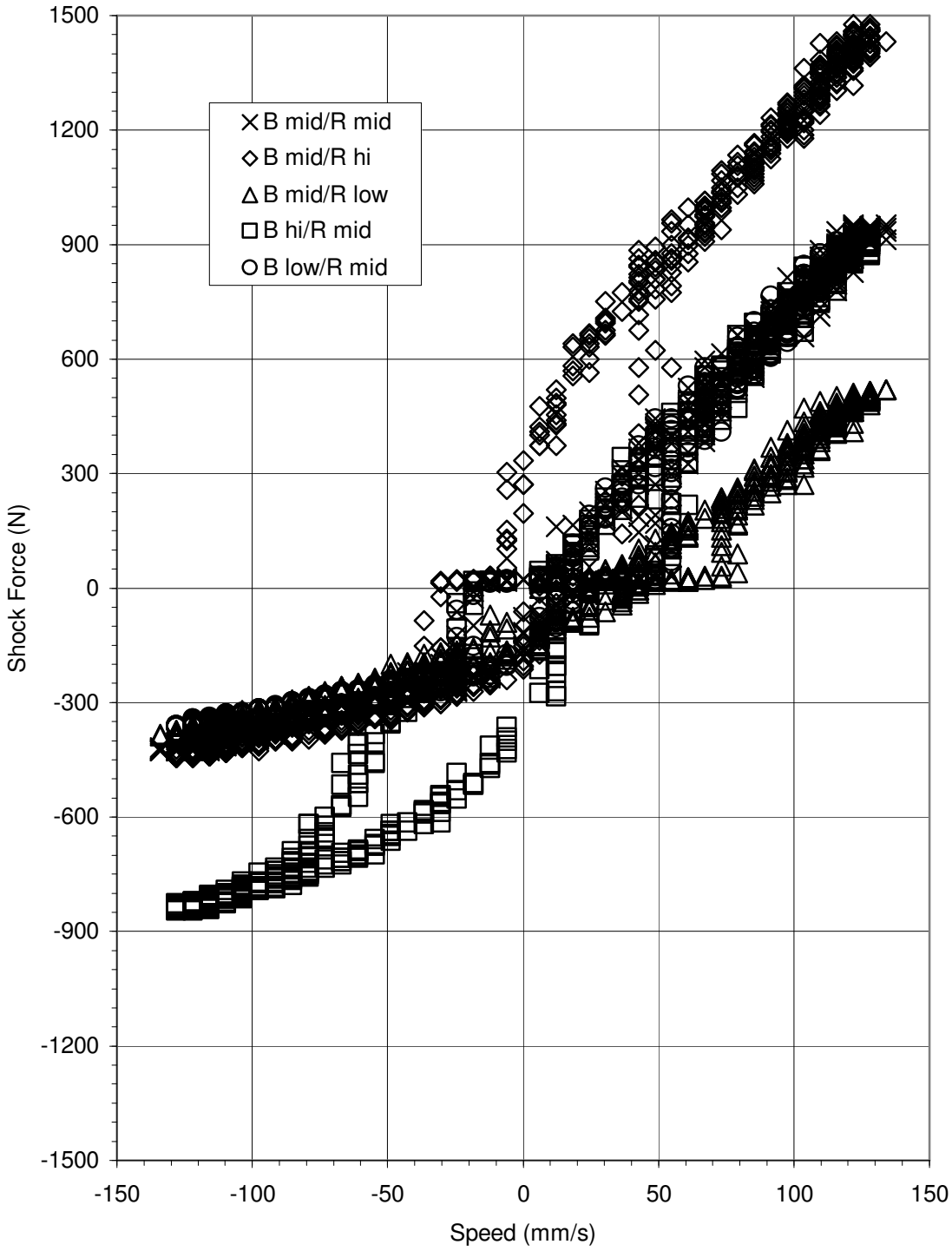

Figure 27: Risse Racing Jupiter-5 Shock #2 – Total Force, All 5 Tested Settings

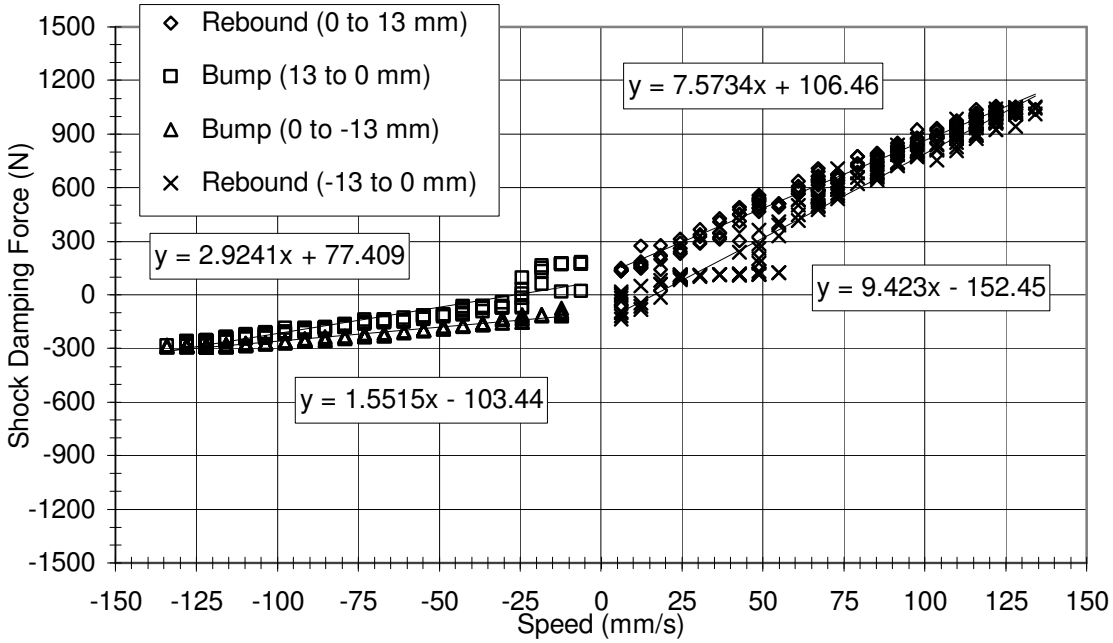

Figure 28: Risse Racing Jupiter-5 Shock #2 – Damping, MID Bump + MID Rebound

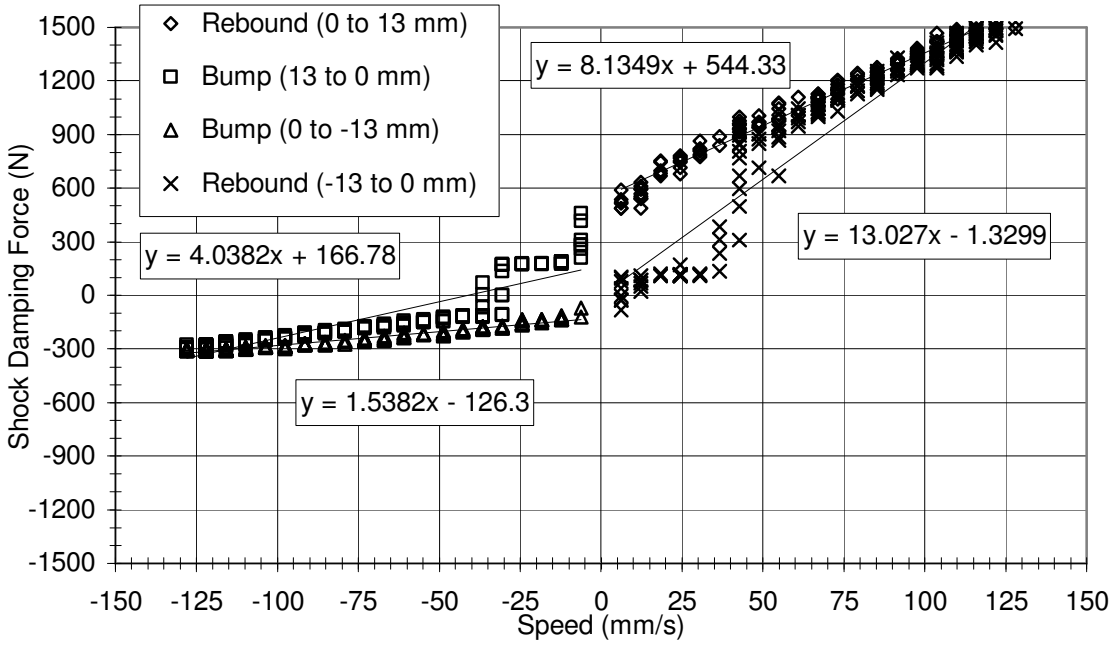

Figure 29: Risse Racing Jupiter-5 Shock #2 – Damping, MID Bump + HI Rebound

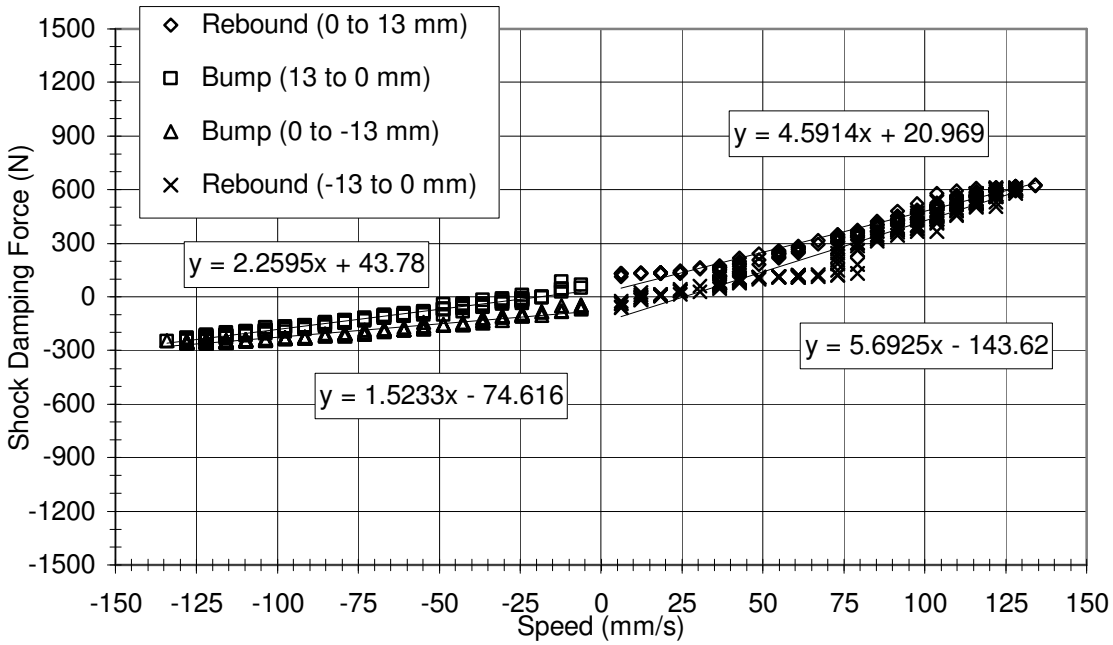

Figure 30: Risse Racing Jupiter-5 Shock #2 – Damping, MID Bump + LOW Rebound

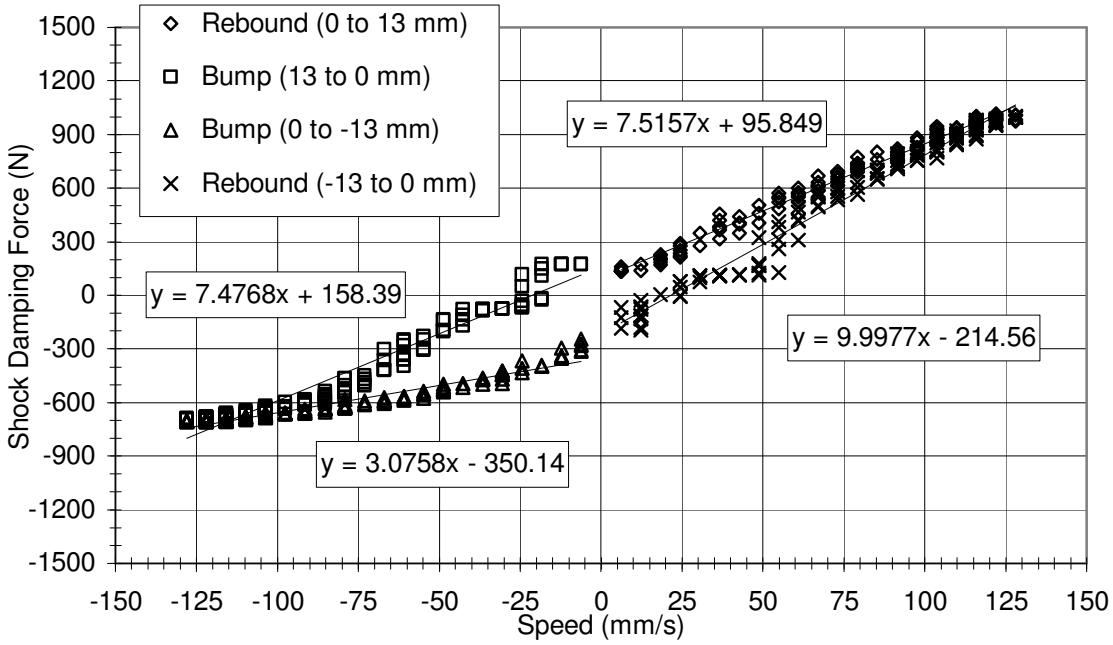

Figure 31: Risse Racing Jupiter-5 Shock #2 – Damping, HI Bump + MID Rebound

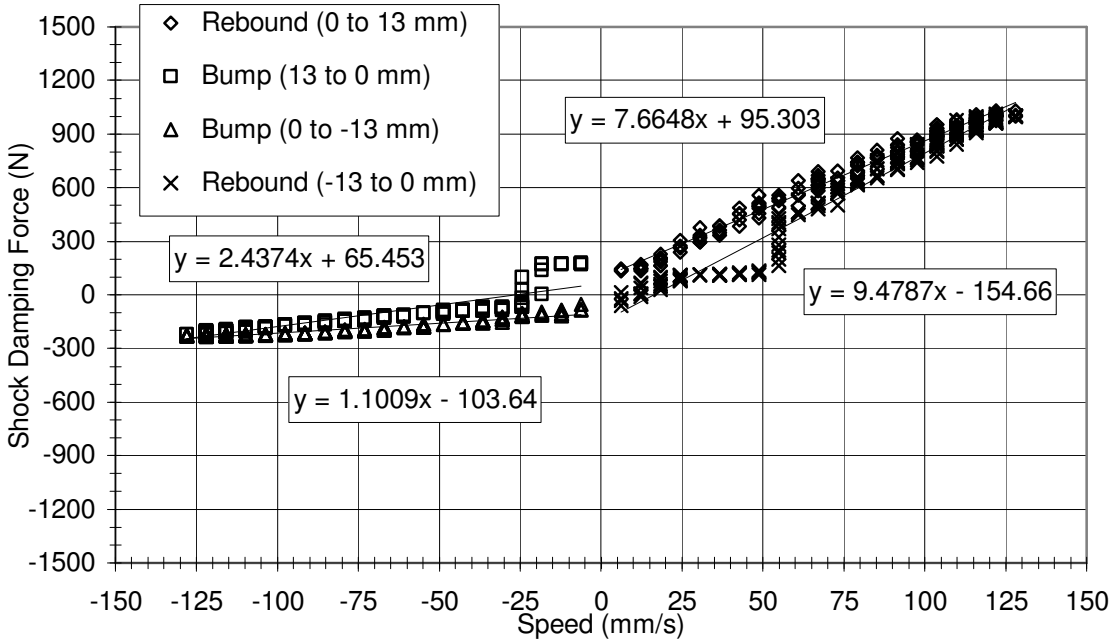

Figure 32: Risse Racing Jupiter-5 Shock #2 – Damping, LOW Bump + MID Rebound

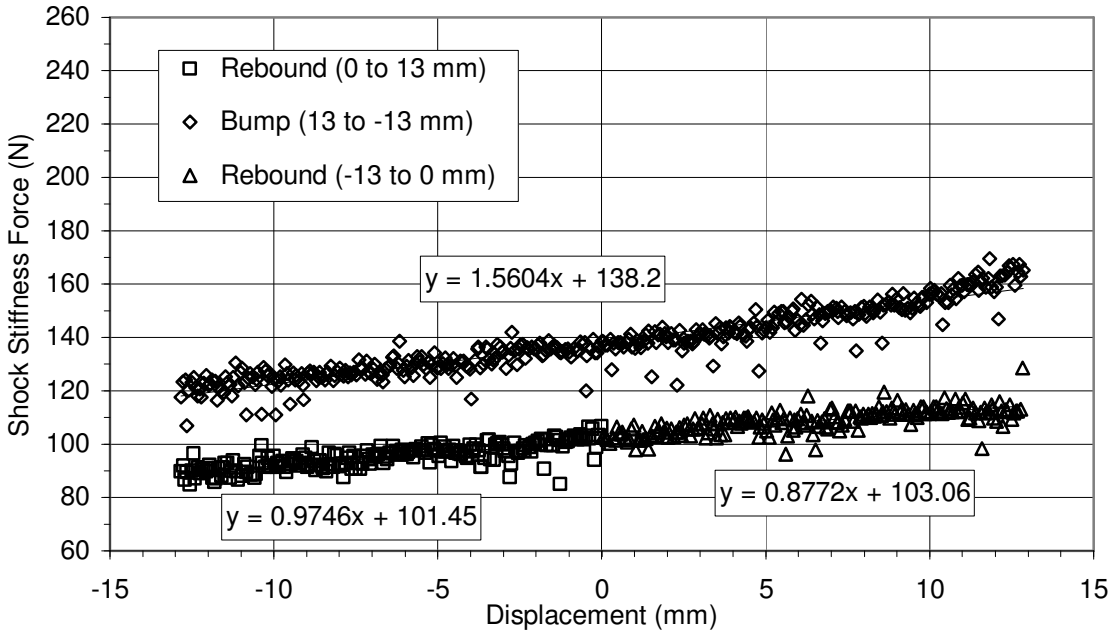

Figure 33: Risse Racing Jupiter-5 Shock #2 – Stiffness (Speed = 0.13 mm/s)

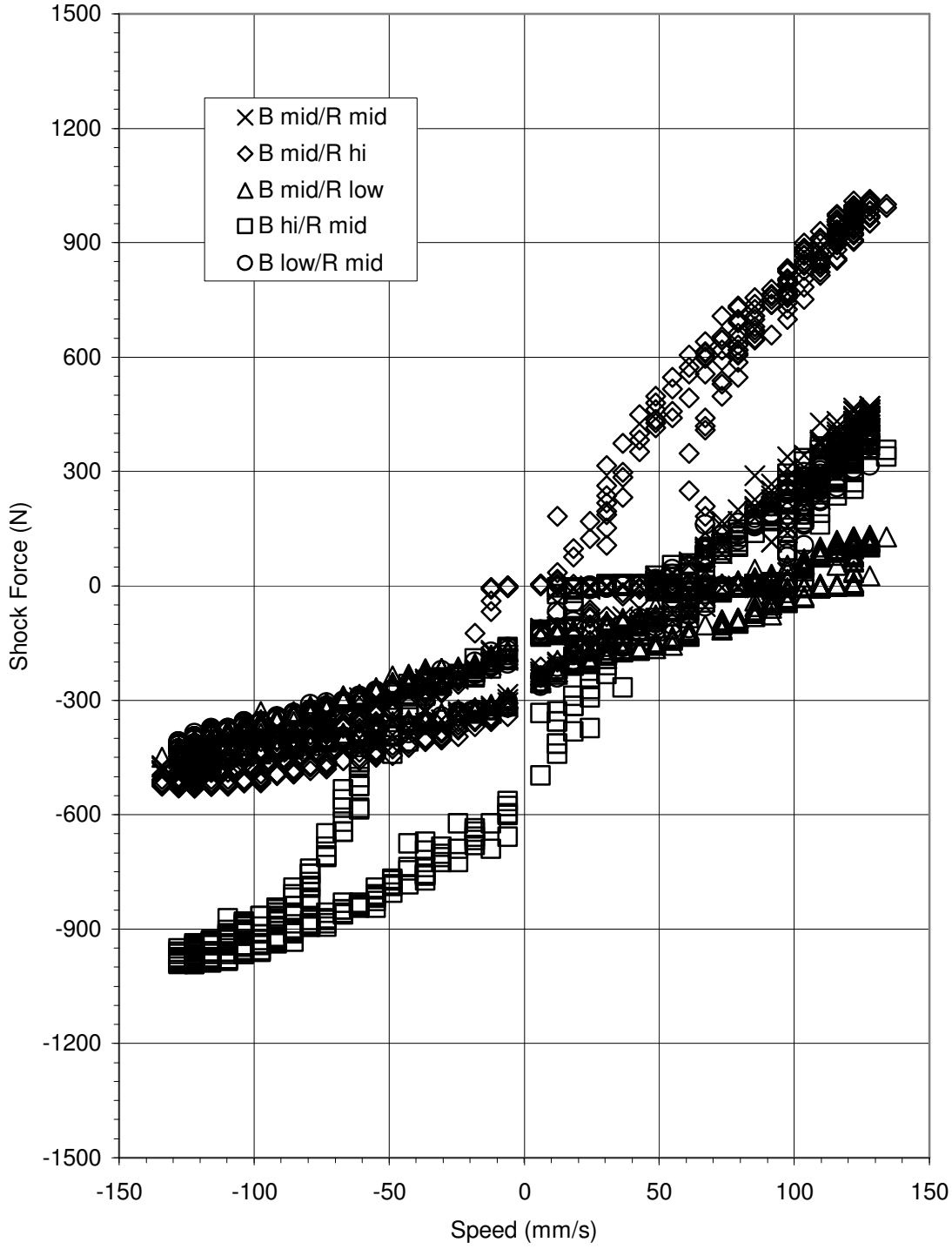

Figure 34: Risse Racing Jupiter-5 Shock #4 – Total Force, All 5 Tested Settings

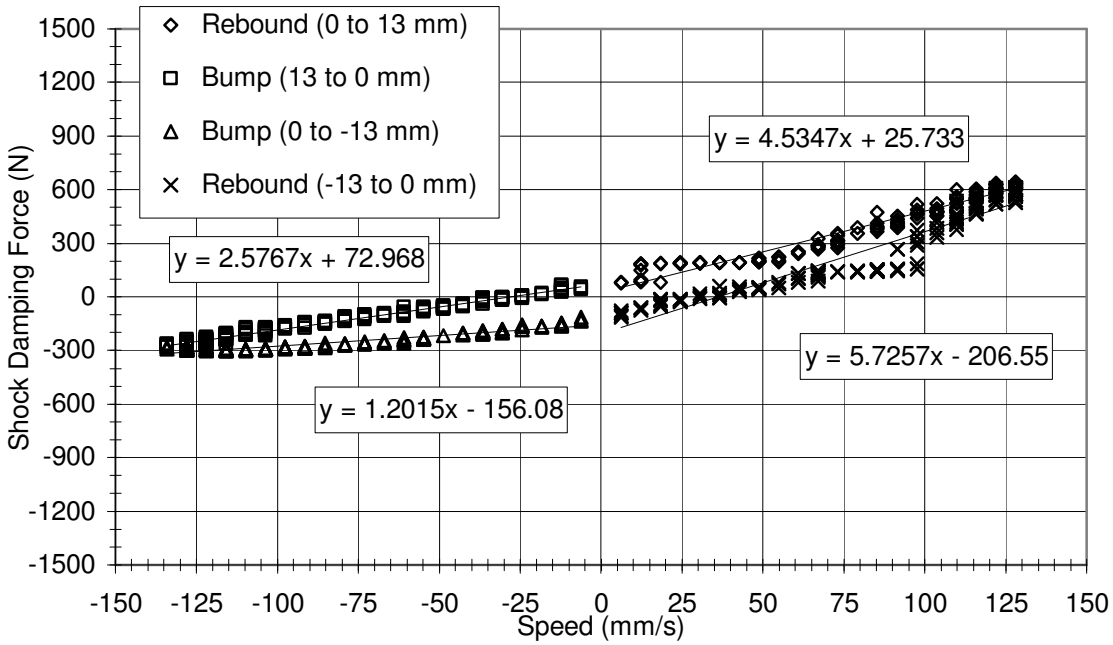

Figure 35: Risse Racing Jupiter-5 Shock #4 – Damping, MID Bump + MID Rebound

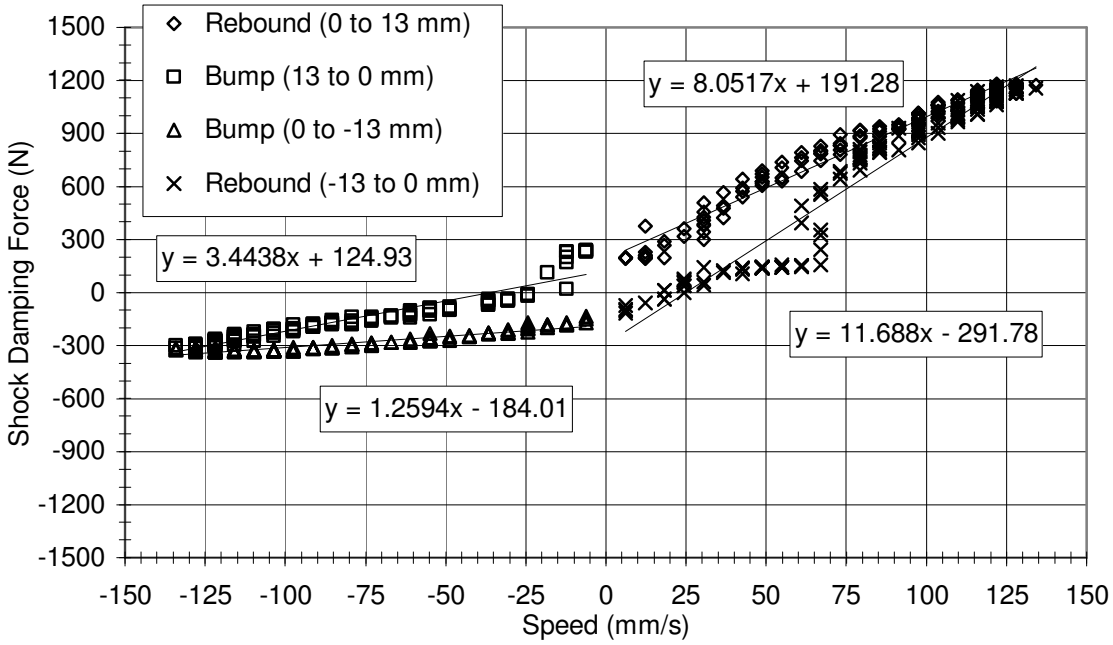

Figure 36: Risse Racing Jupiter-5 Shock #4 – Damping, MID Bump + HI Rebound

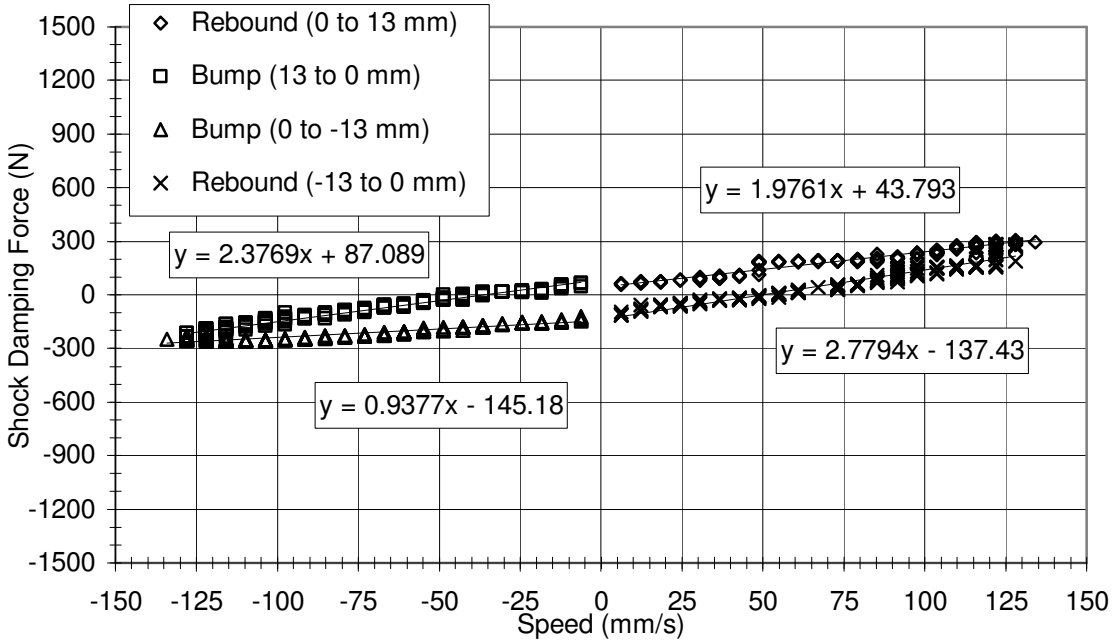

Figure 37: Risse Racing Jupiter-5 Shock #4 – Damping, MID Bump + LOW Rebound

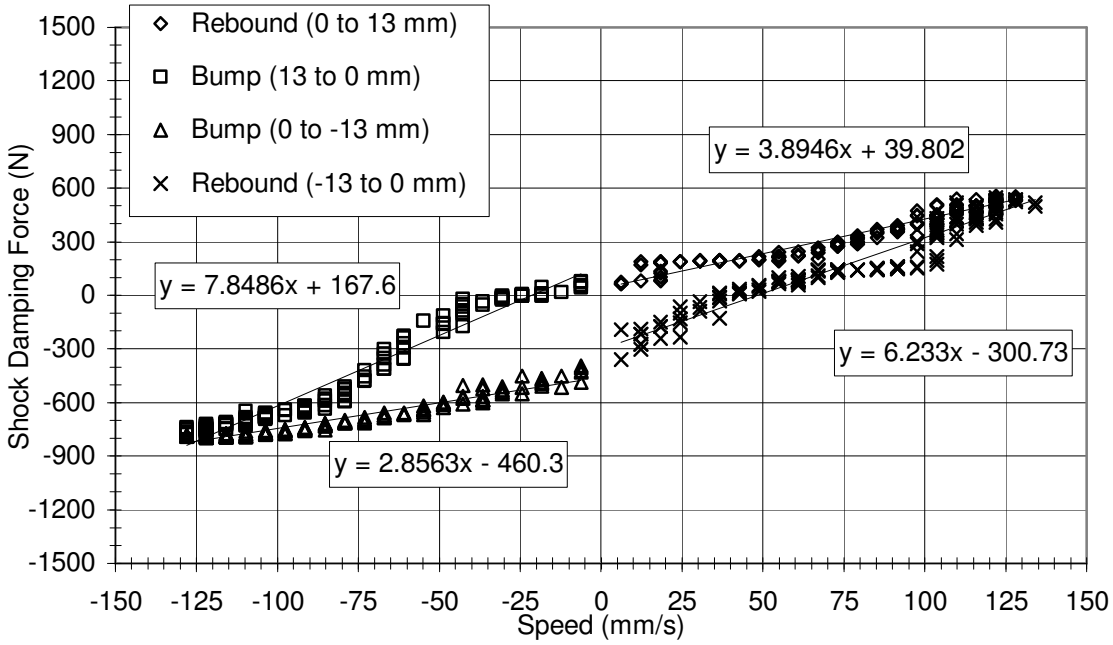

Figure 38: Risse Racing Jupiter-5 Shock #4 – Damping, HI Bump + MID Rebound

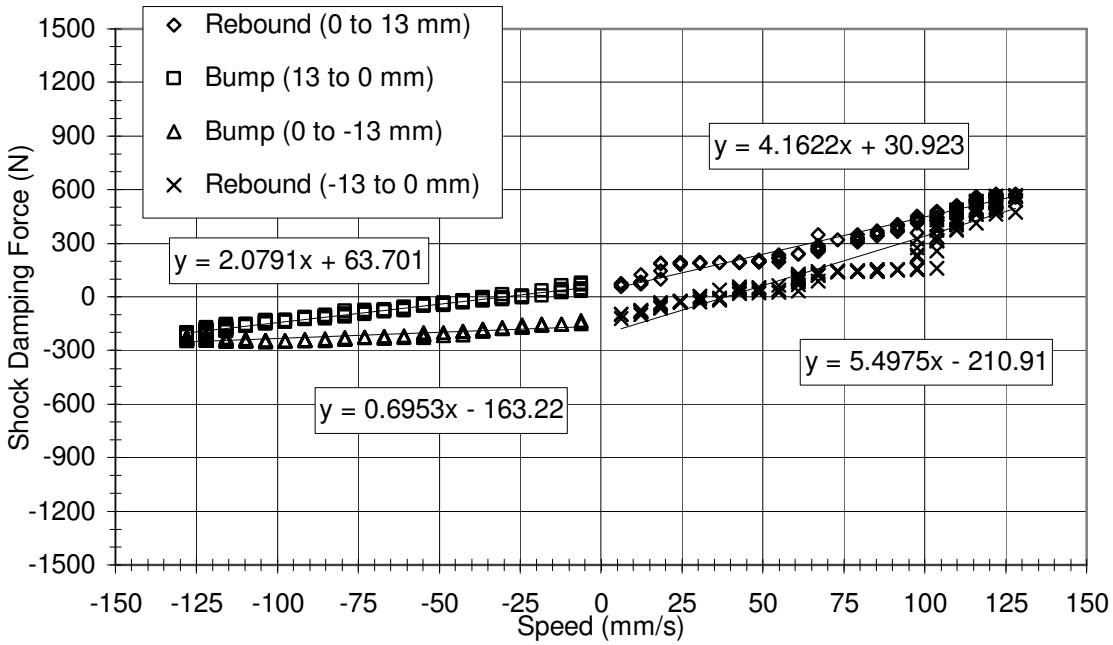

Figure 39: Risse Racing Jupiter-5 Shock #4 – Damping, LOW Bump + MID Rebound

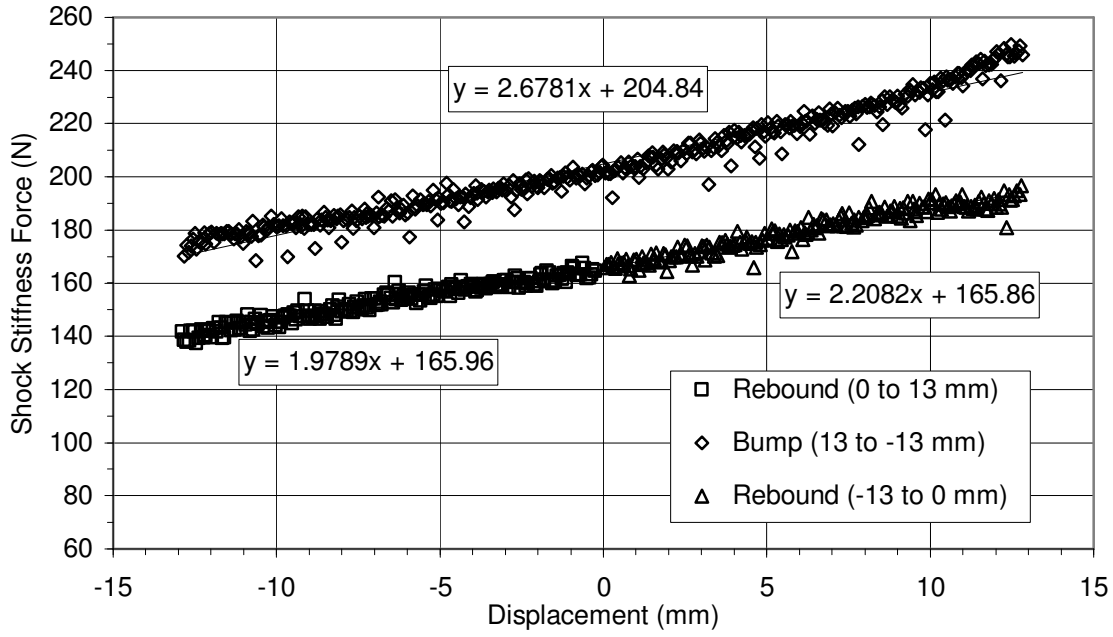

Figure 40: Risse Racing Jupiter-5 Shock #4 – Stiffness (Speed = 0.13 mm/s)

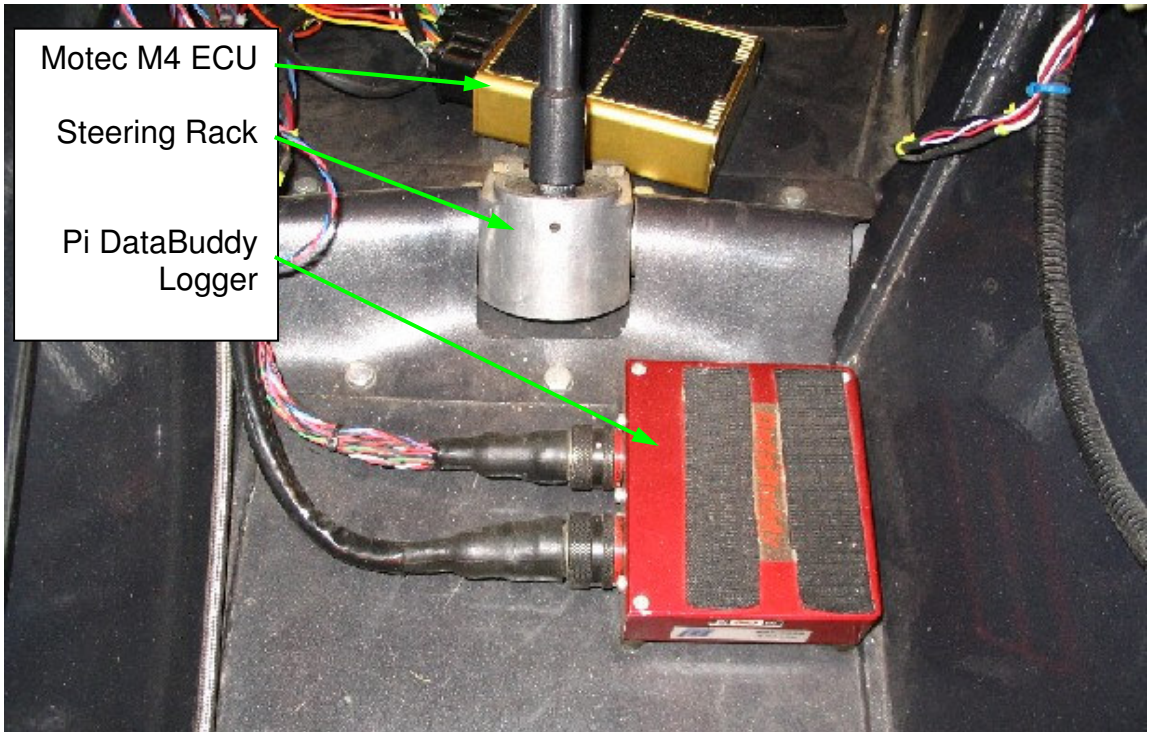

Figure 41: DAQ Installation – Pi DataBuddy Logger

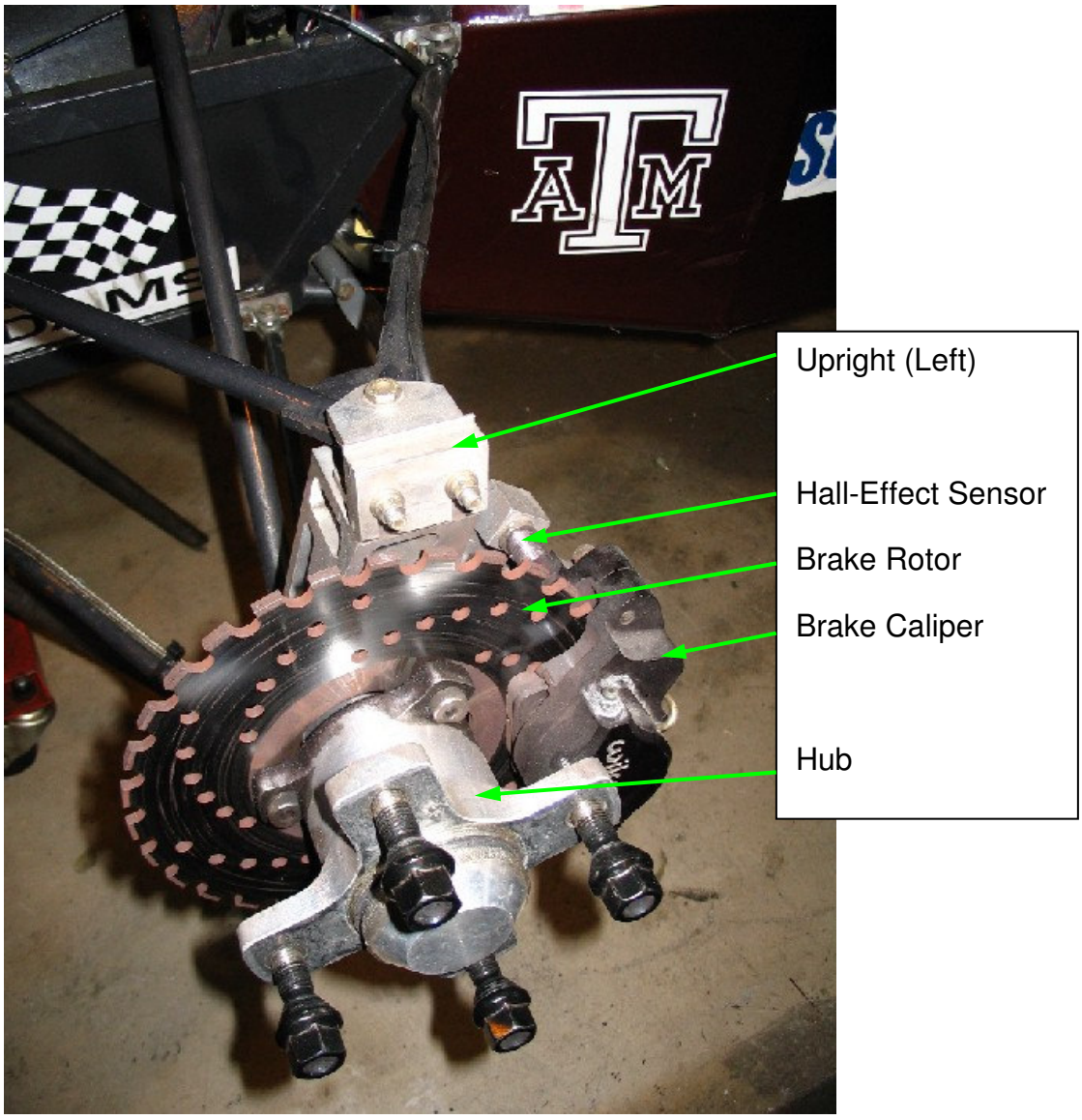

Figure 42: DAQ Installation – Front Wheel Speed Sensor

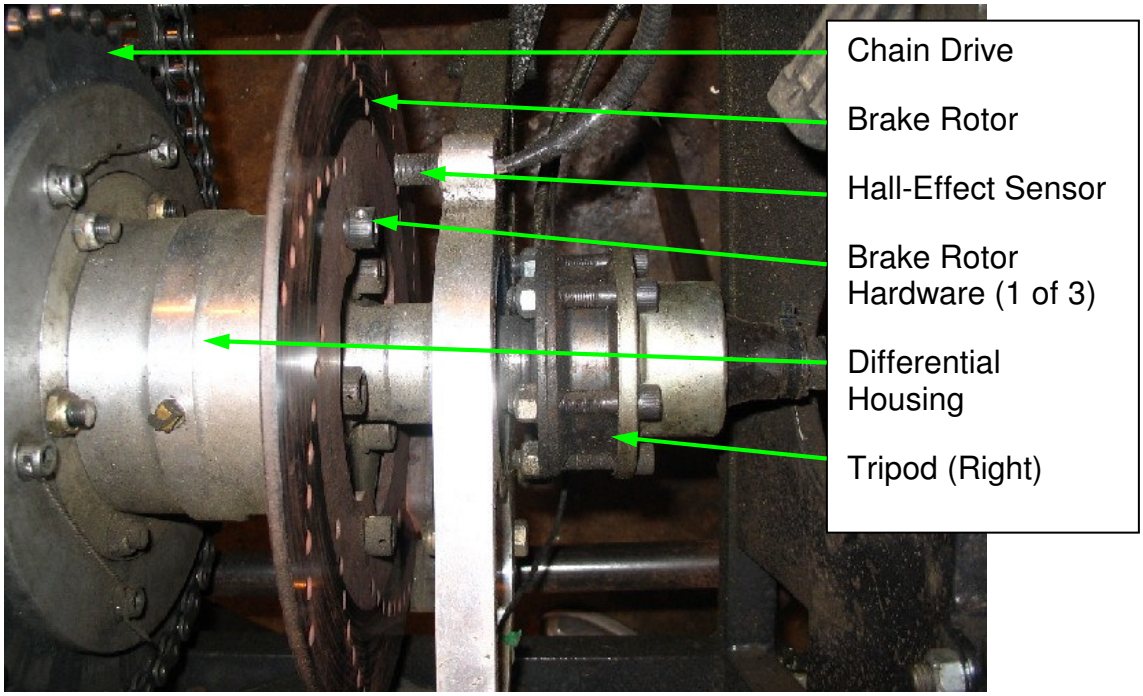

Figure 43: DAQ Installation – Rear Wheel Speed Sensor

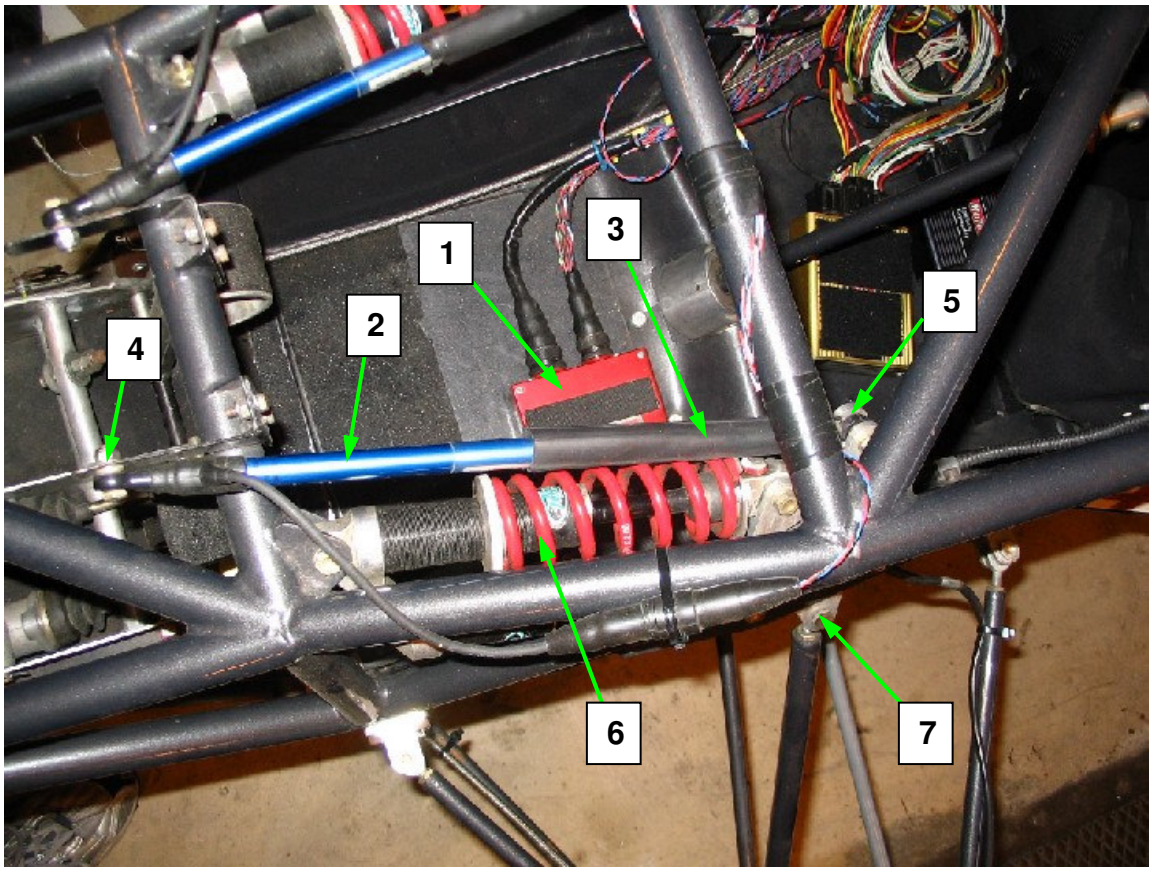

1. Pi DataBuddy Logger
2. Pi Research 100mm Suspension Potentiometer (Front Left)
3. Sensor Protective Sheath
4. Chassis Frame Mount Location
5. Bellcrank Mount Location
6. Risse Racing Jupiter-5 Coil-Over Shock
7. Pushrod Mount on Bellcrank

Figure 44: DAQ Installation – Front Suspension Travel

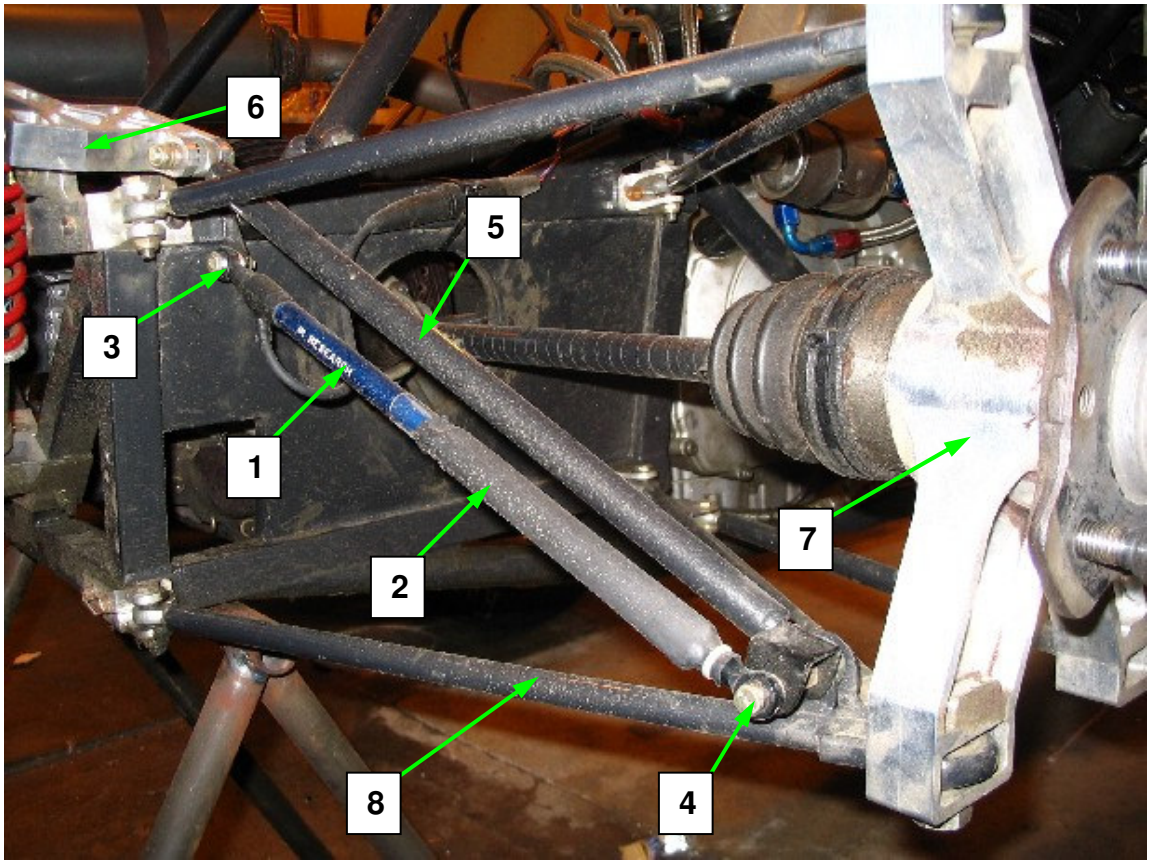

1. Pi Research 100mm Suspension Potentiometer (Rear Right)
2. Sensor Protective Sheath
3. Chassis Frame Mount Location
4. Lower Control Arm Mount Location
5. Pushrod
6. Bellcrank
7. Upright
8. Lower Control Arm

Figure 45: DAQ Installation – Rear Suspension Travel

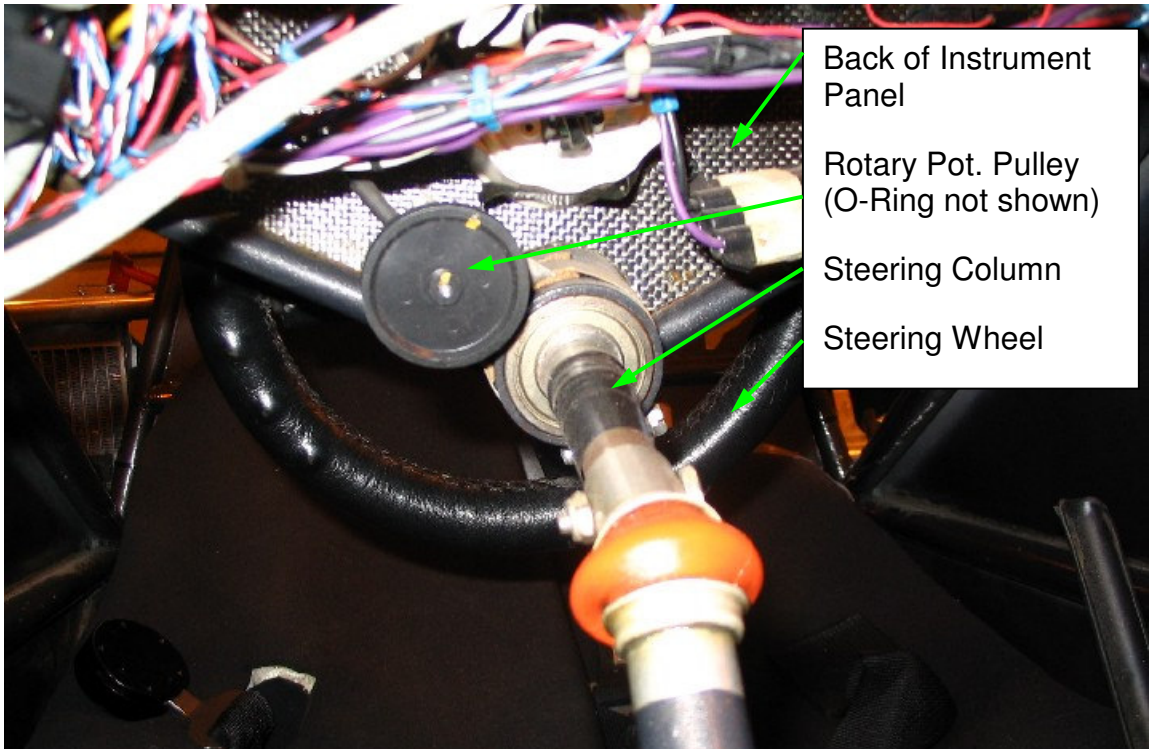

Figure 46: DAQ Installation – Steering Wheel Angle

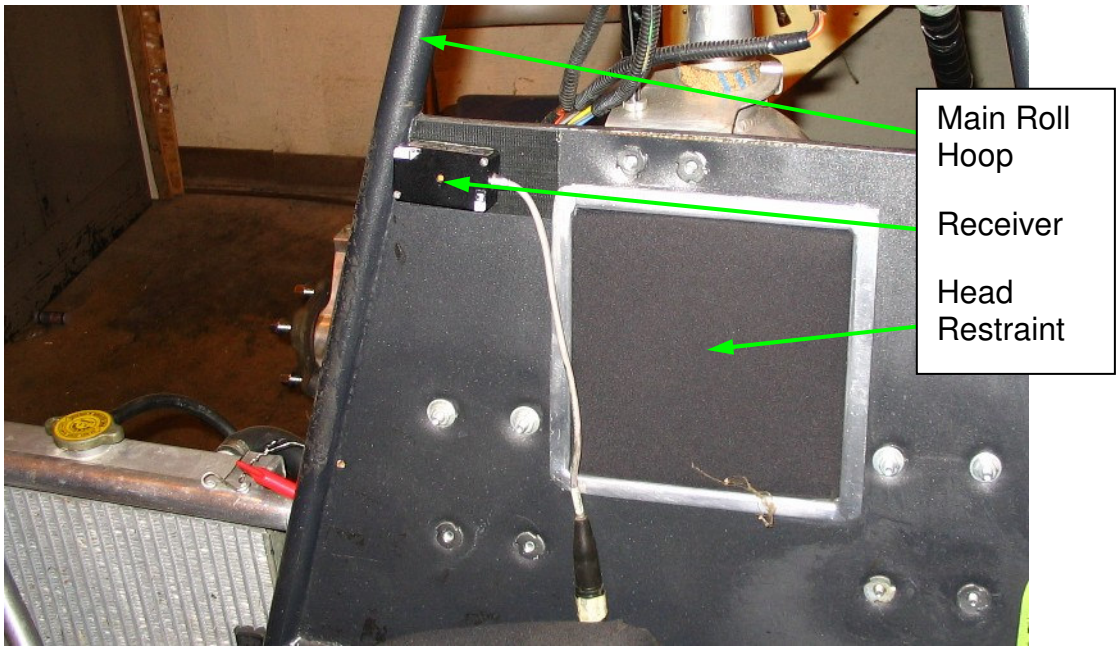

Figure 47: DAQ Installation – Beacon Receiver

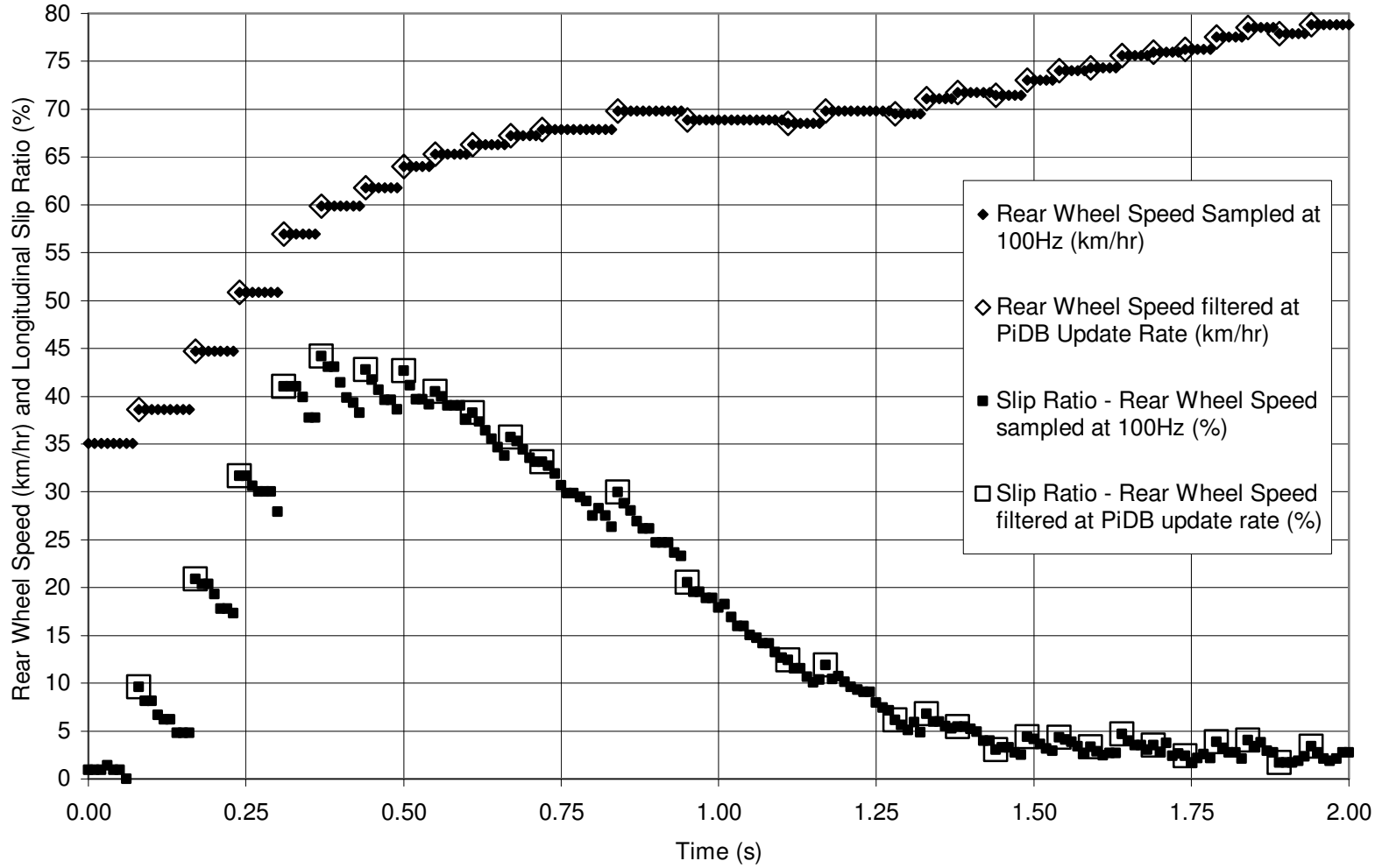

Figure 48: Configuration 1 – Filtered Rear Wheel Speed and Longitudinal Slip Ratio

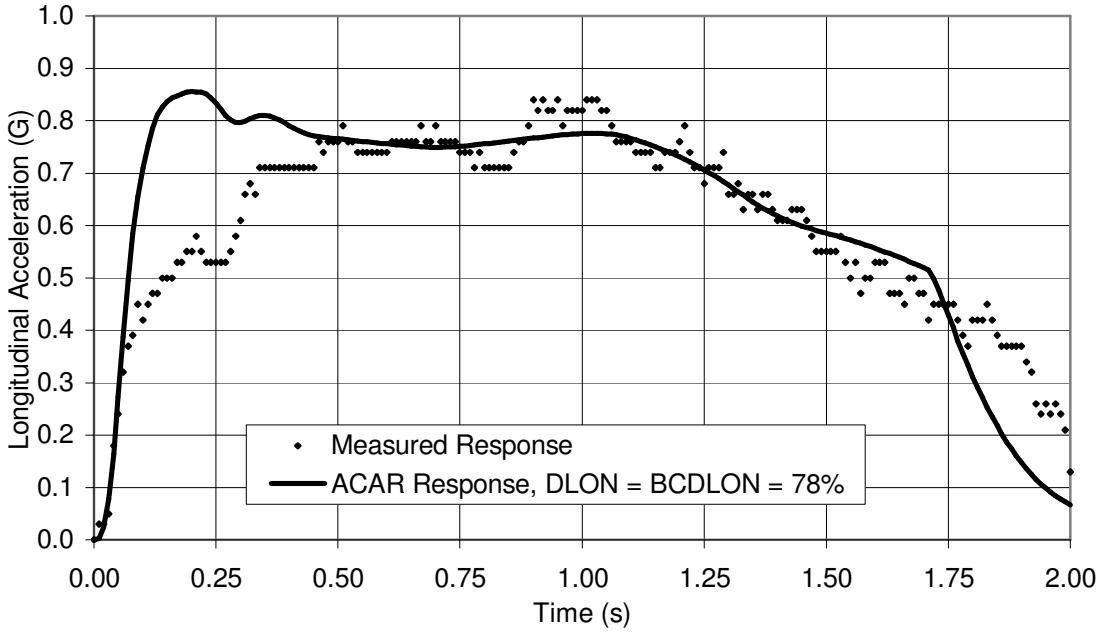

Figure 49: Configuration 1 – Longitudinal Chassis Acceleration

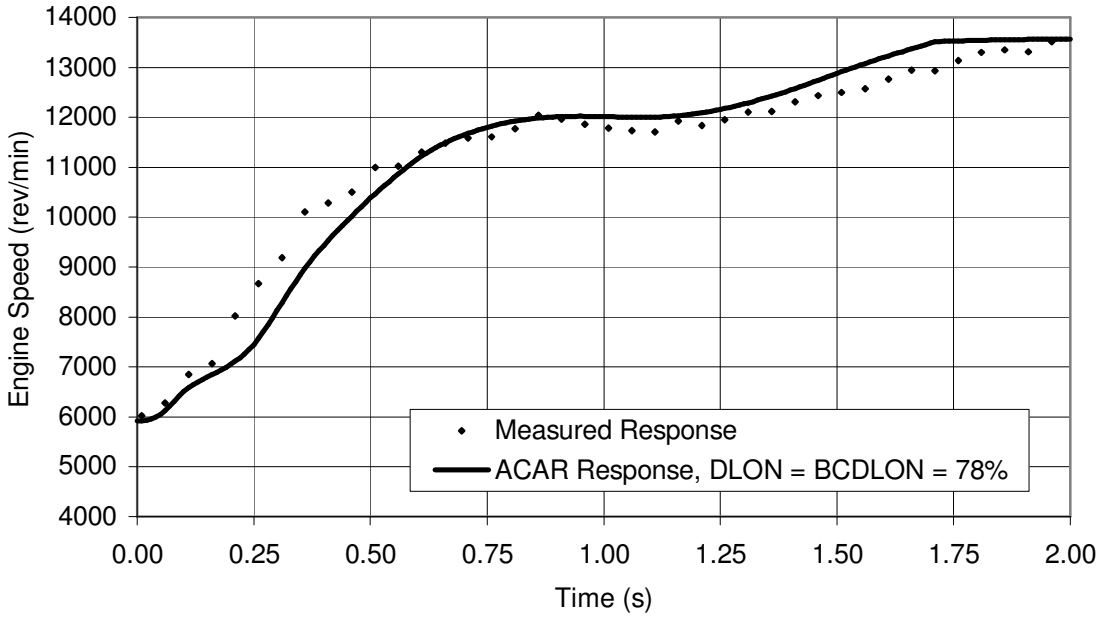

Figure 50: Configuration 1 – Engine Speed

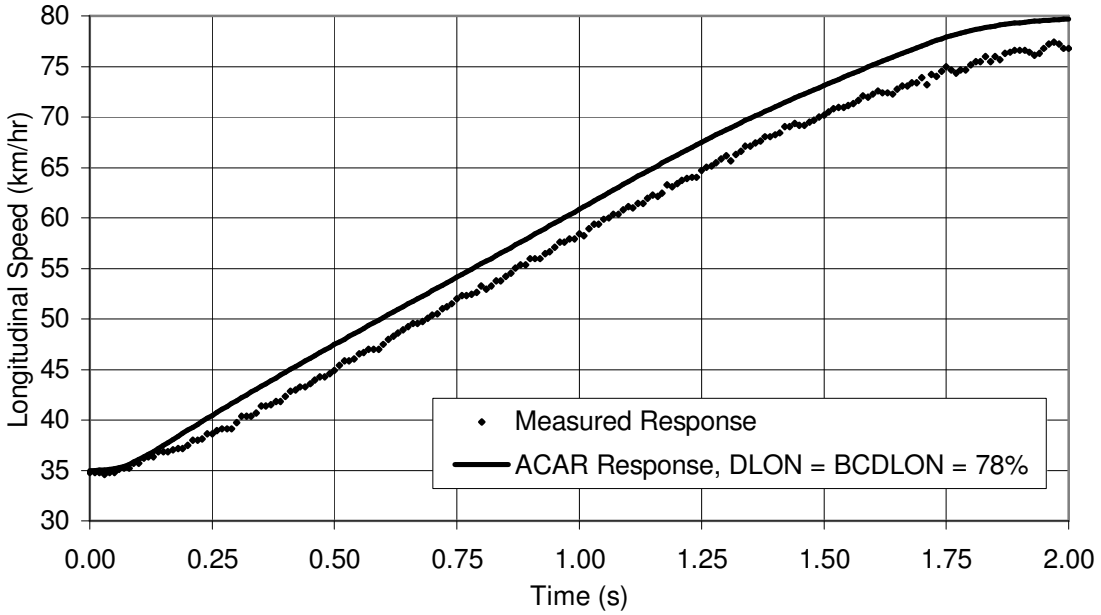

Figure 51: Configuration 1 – Longitudinal Chassis Speed

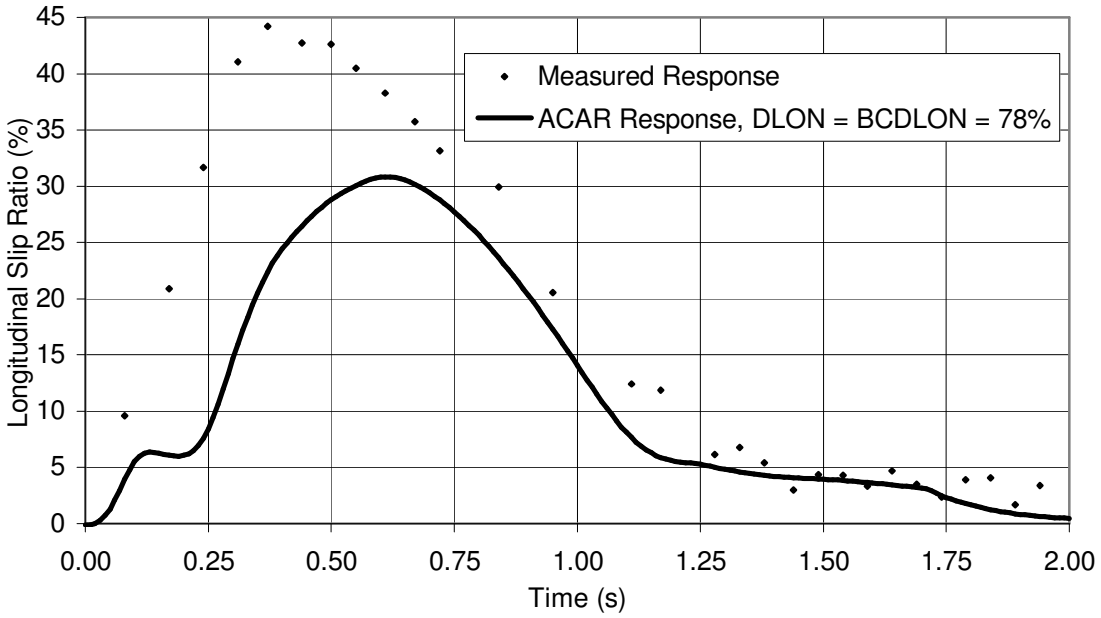

Figure 52: Configuration 1 – Longitudinal Slip Ratio

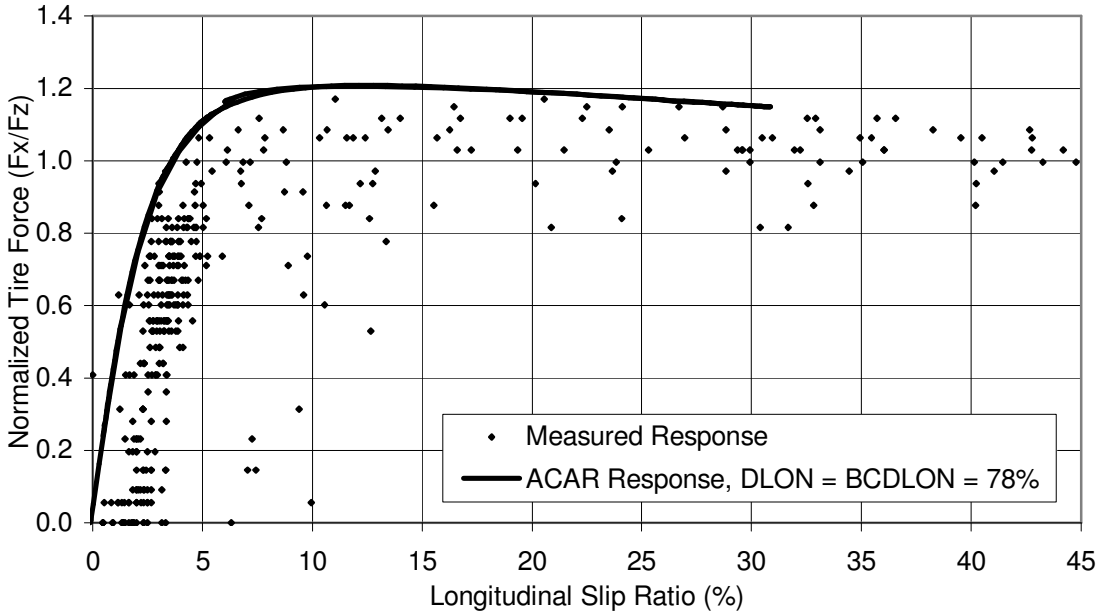

Figure 53: Configuration 1 – Normalized Tire Force vs. Longitudinal Slip Ratio

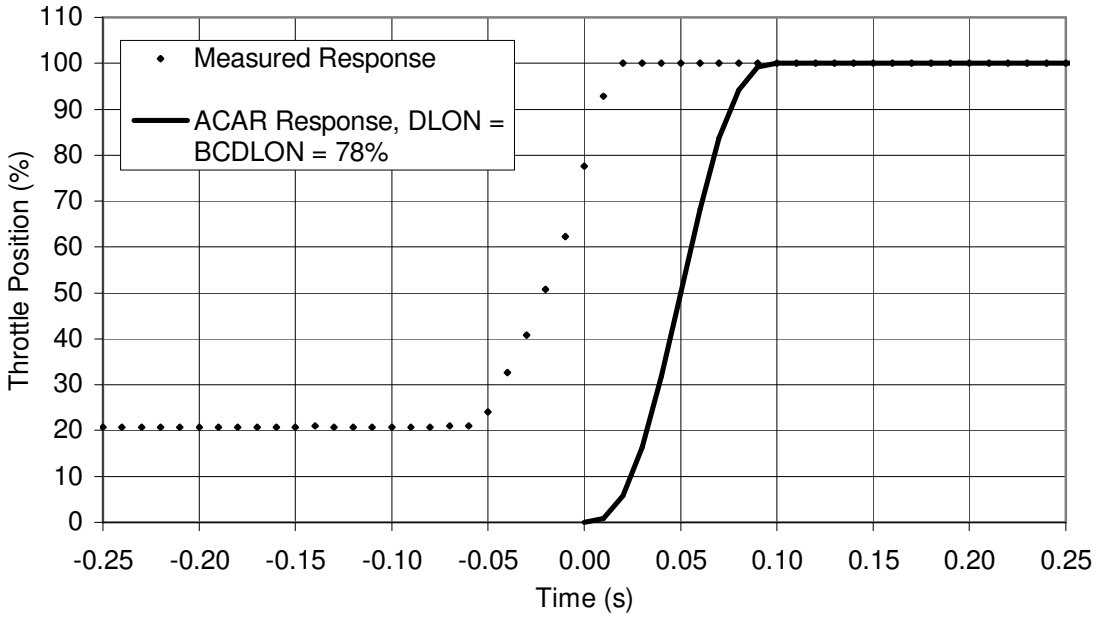

Figure 54: Configuration 1 – Throttle Position

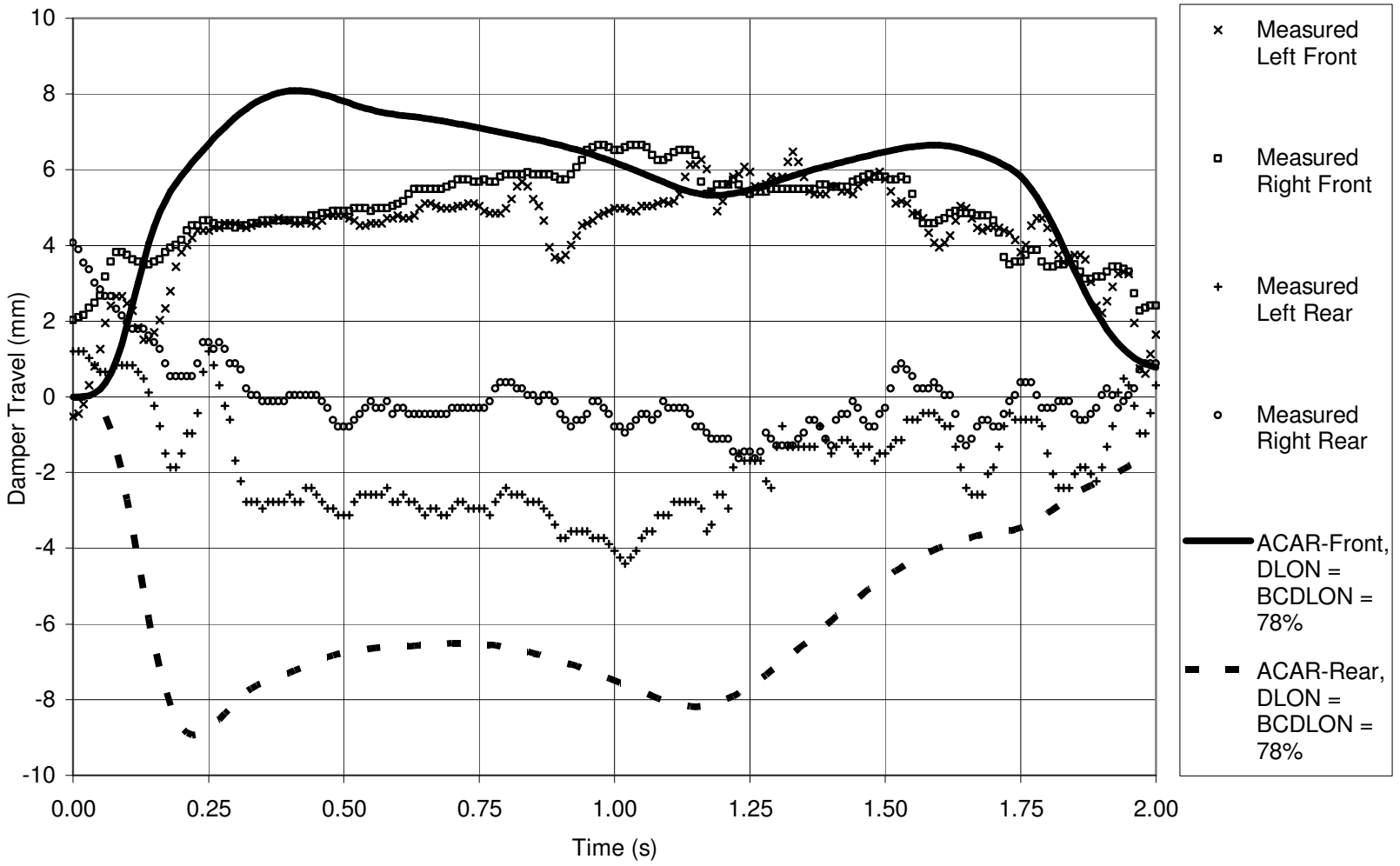

Figure 55: Configuration 1 – Damper Travel

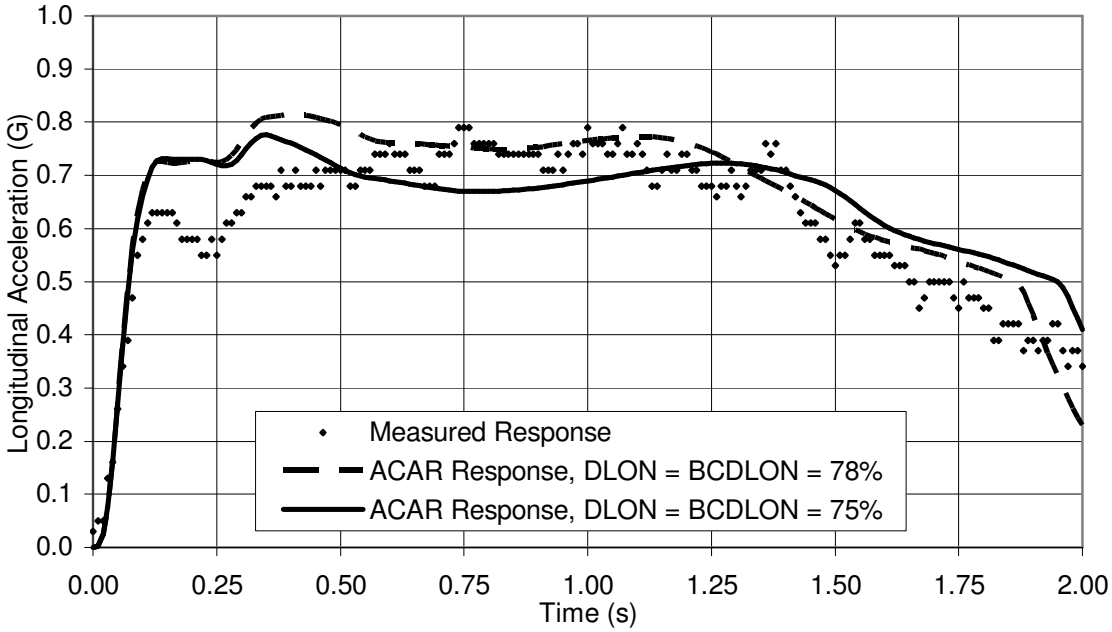

Figure 56: Configuration 2 – Longitudinal Chassis Acceleration

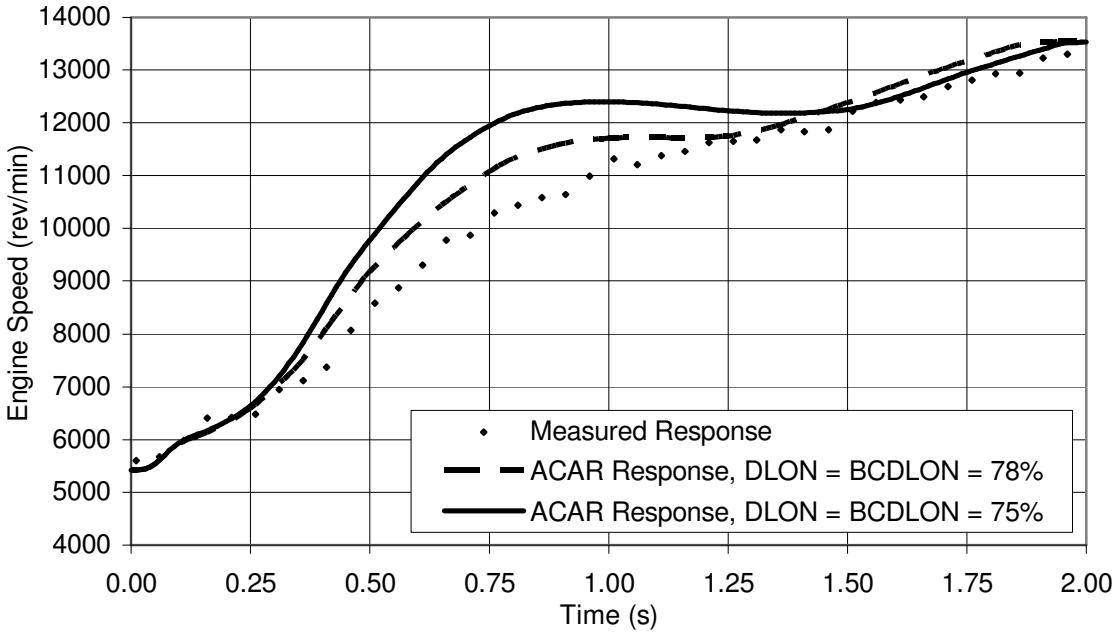

Figure 57: Configuration 2 – Engine Speed

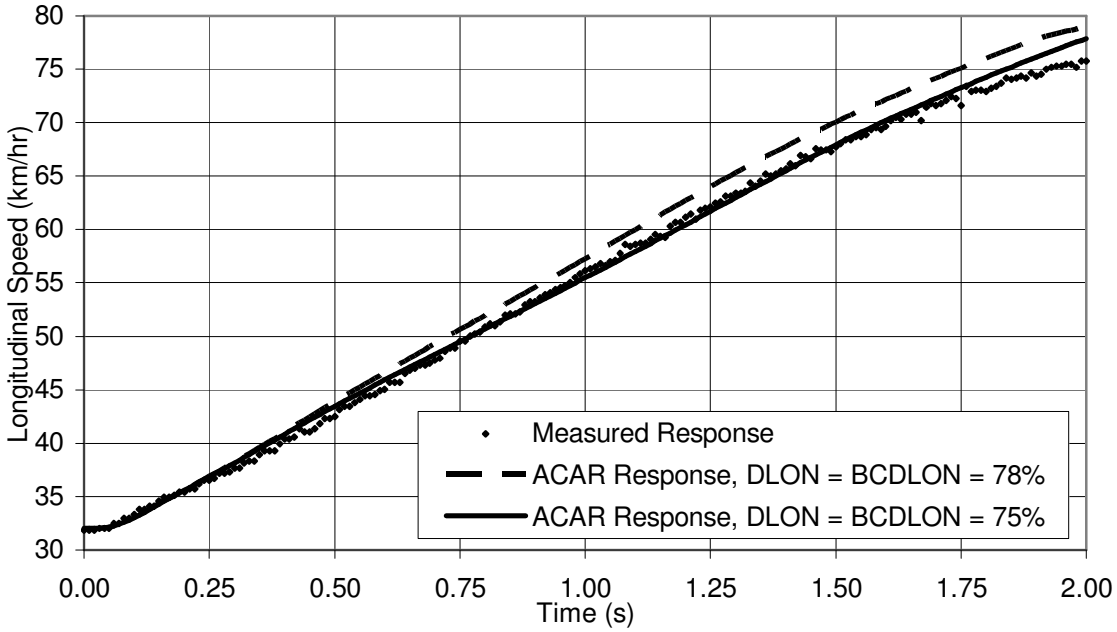

Figure 58: Configuration 2 – Longitudinal Chassis Speed

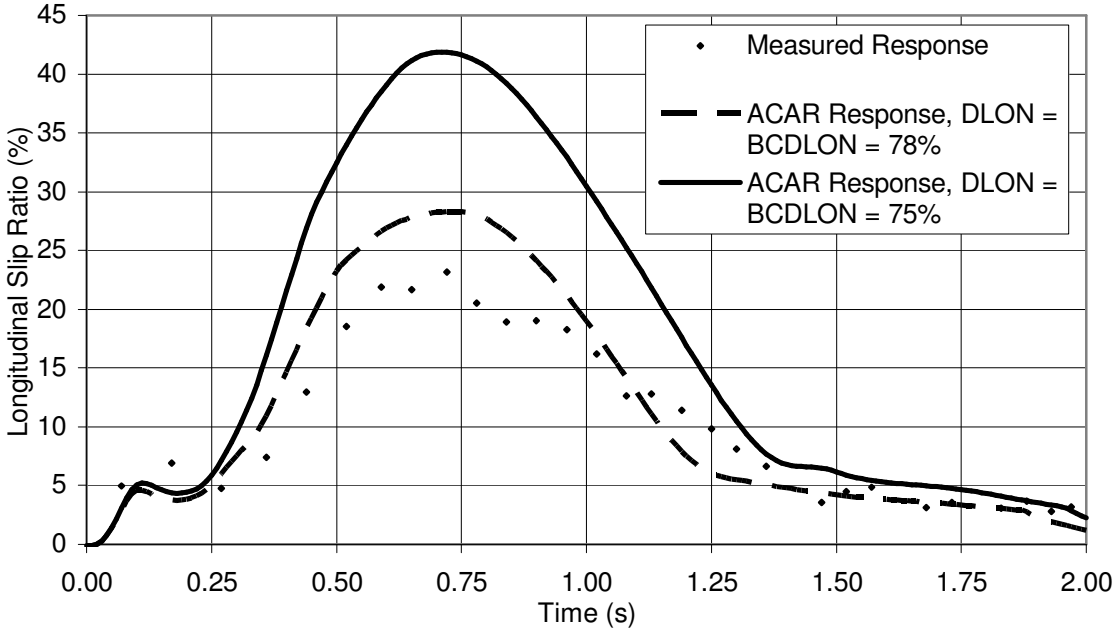

Figure 59: Configuration 2 – Longitudinal Slip Ratio

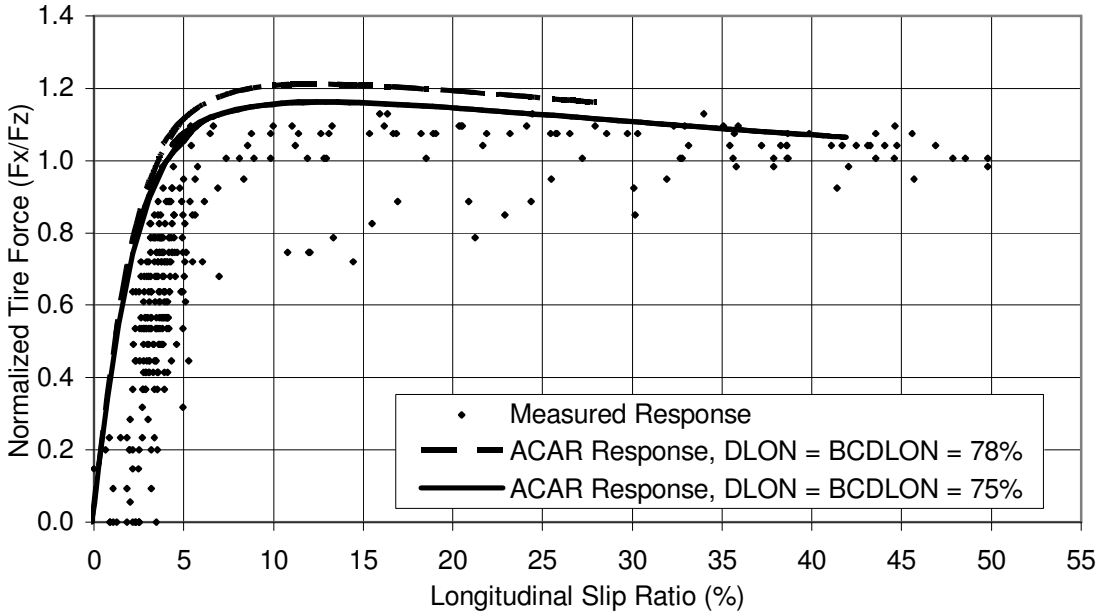

Figure 60: Configuration 2 – Normalized Tire Force vs. Longitudinal Slip Ratio

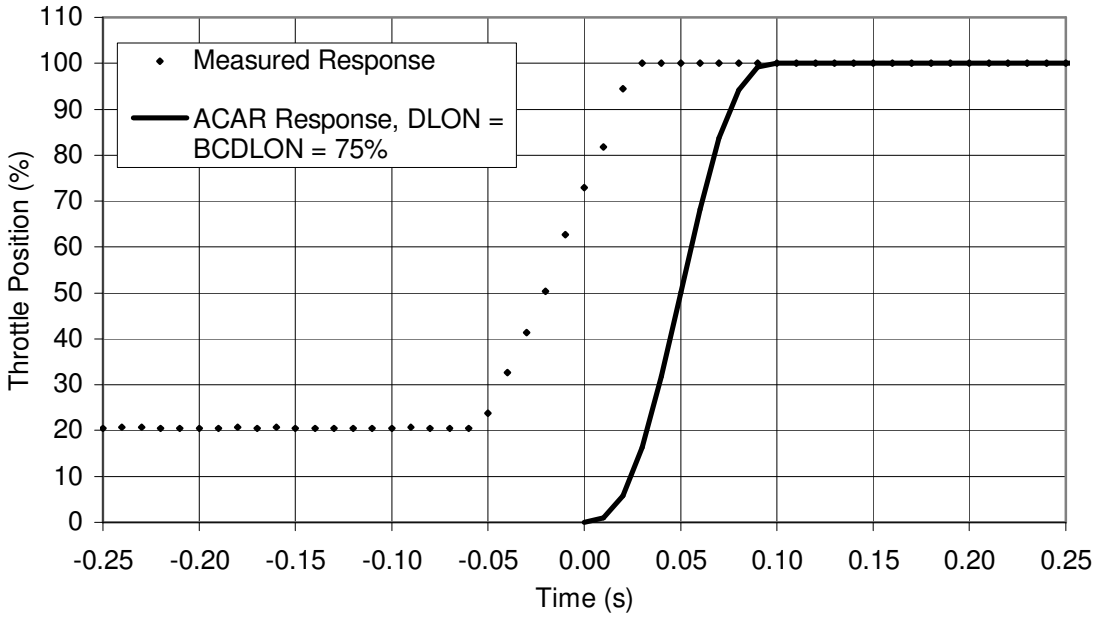

Figure 61: Configuration 2 – Throttle Position

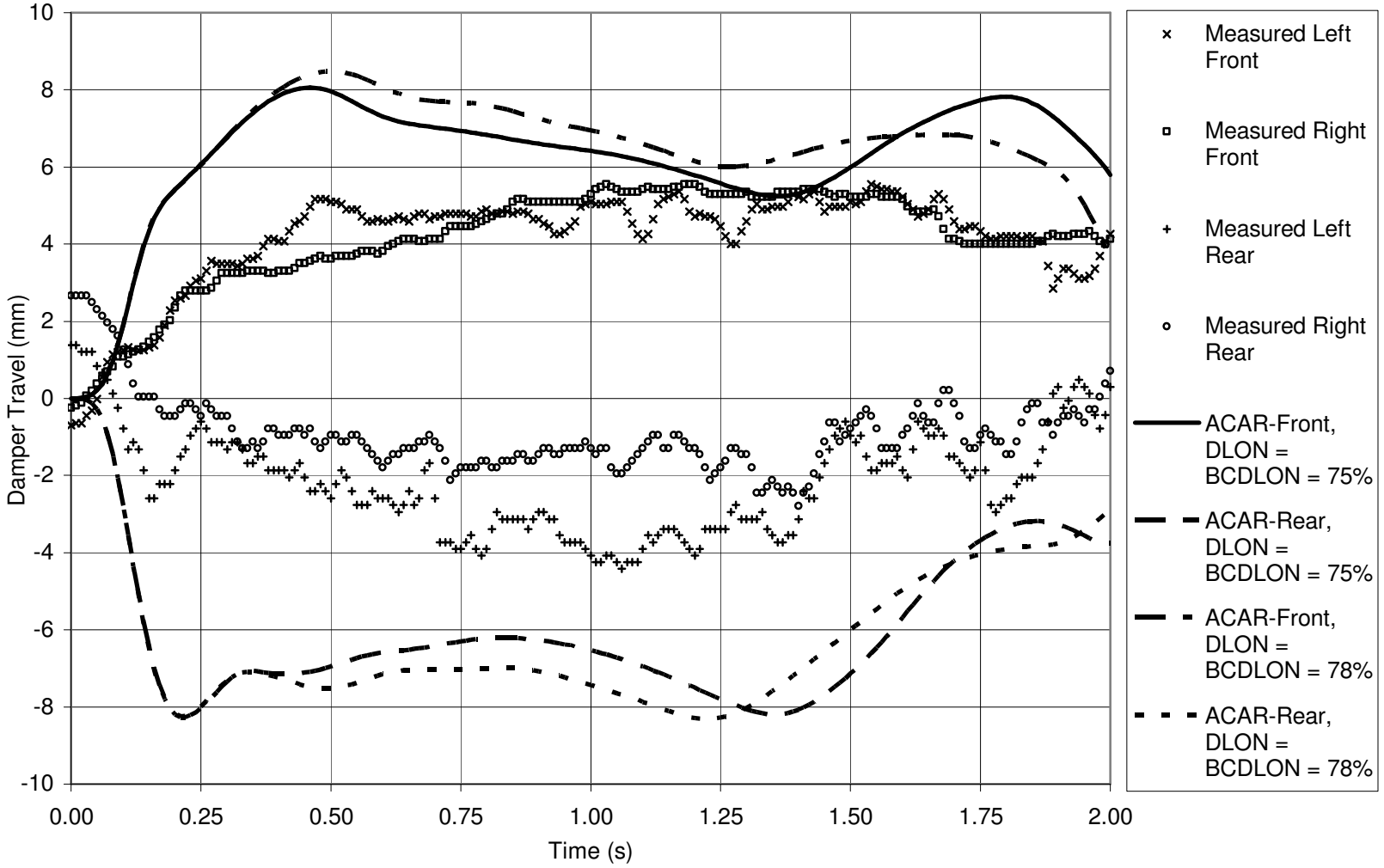

Figure 62: Configuration 2 – Damper Travel

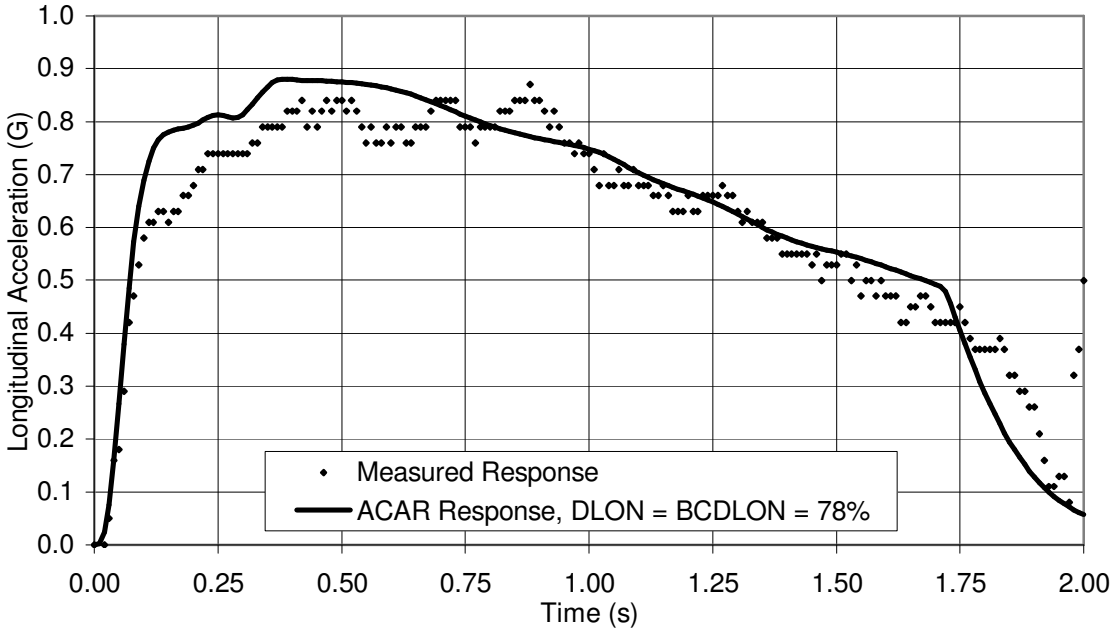

Figure 63: Configuration 3 – Longitudinal Chassis Acceleration

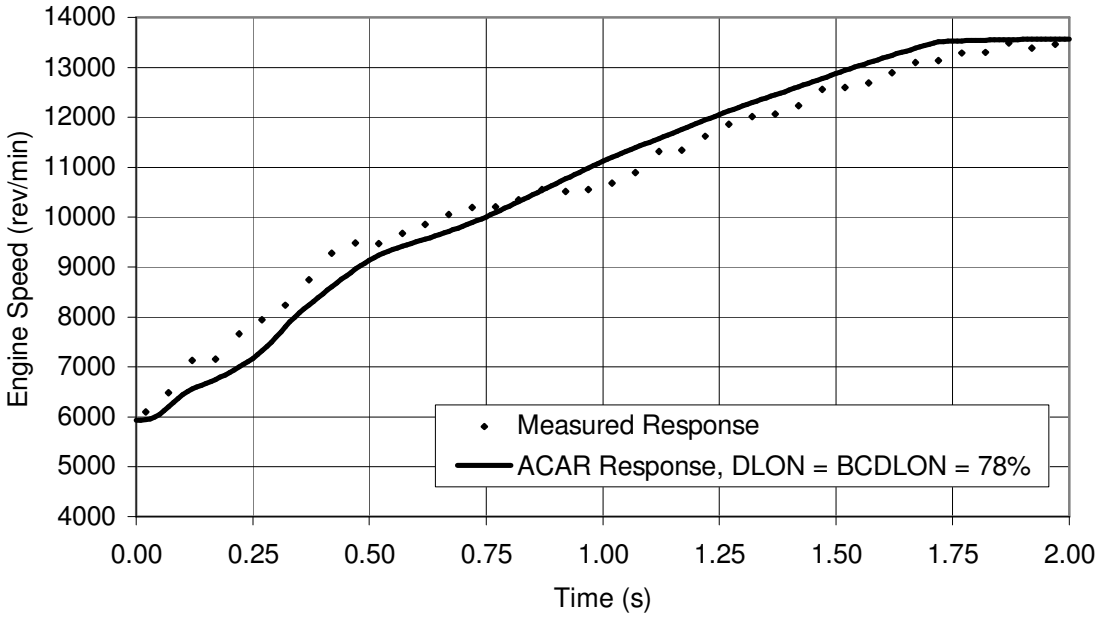

Figure 64: Configuration 3 – Engine Speed

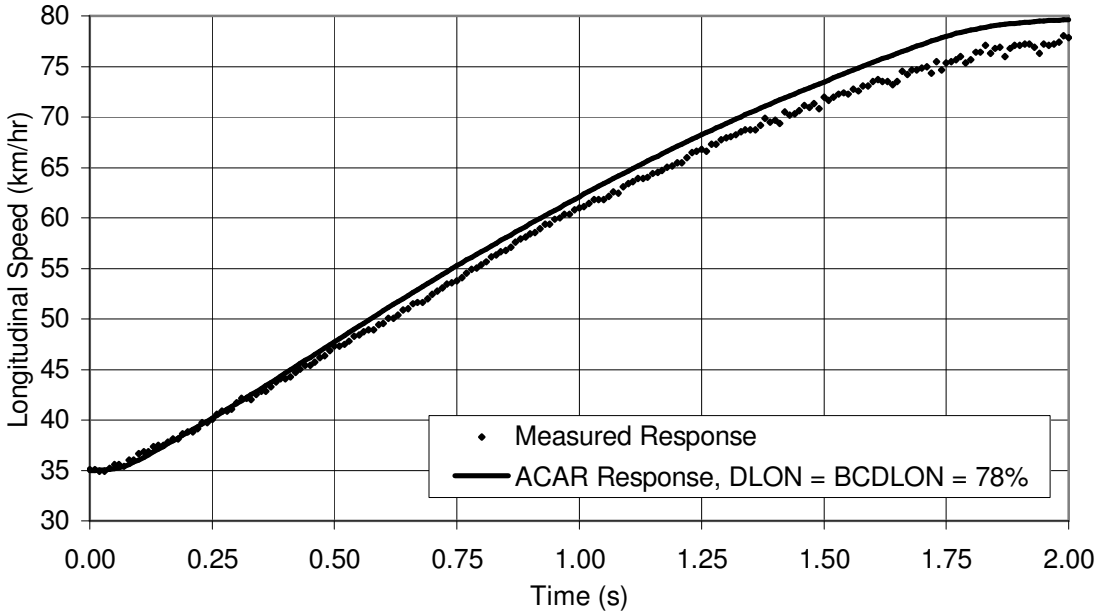

Figure 65: Configuration 3 – Longitudinal Chassis Speed

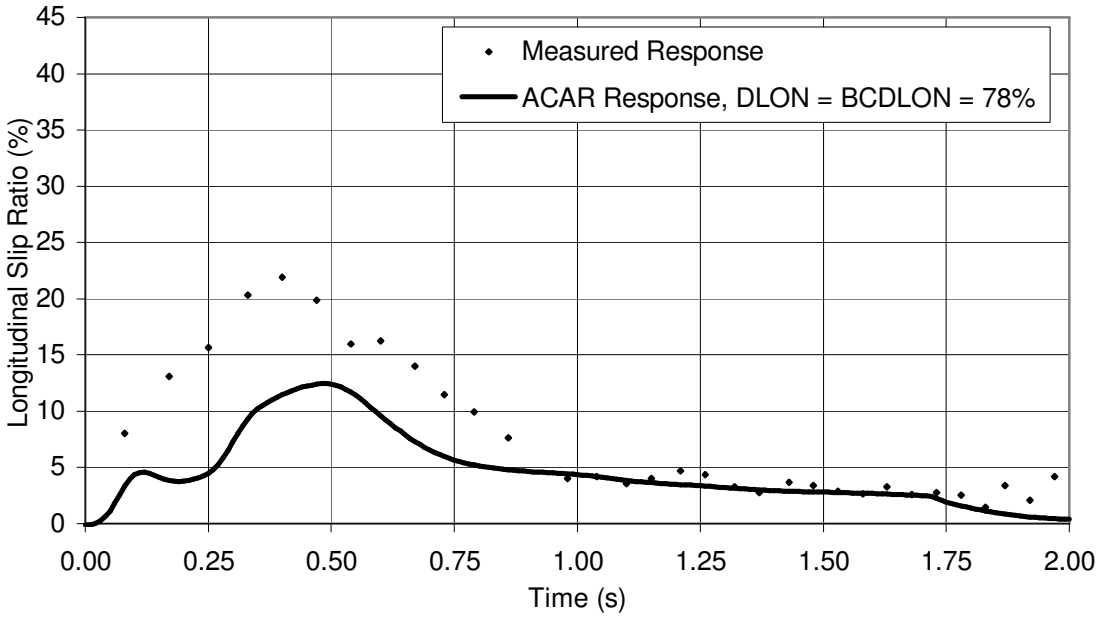

Figure 66: Configuration 3 – Longitudinal Slip Ratio

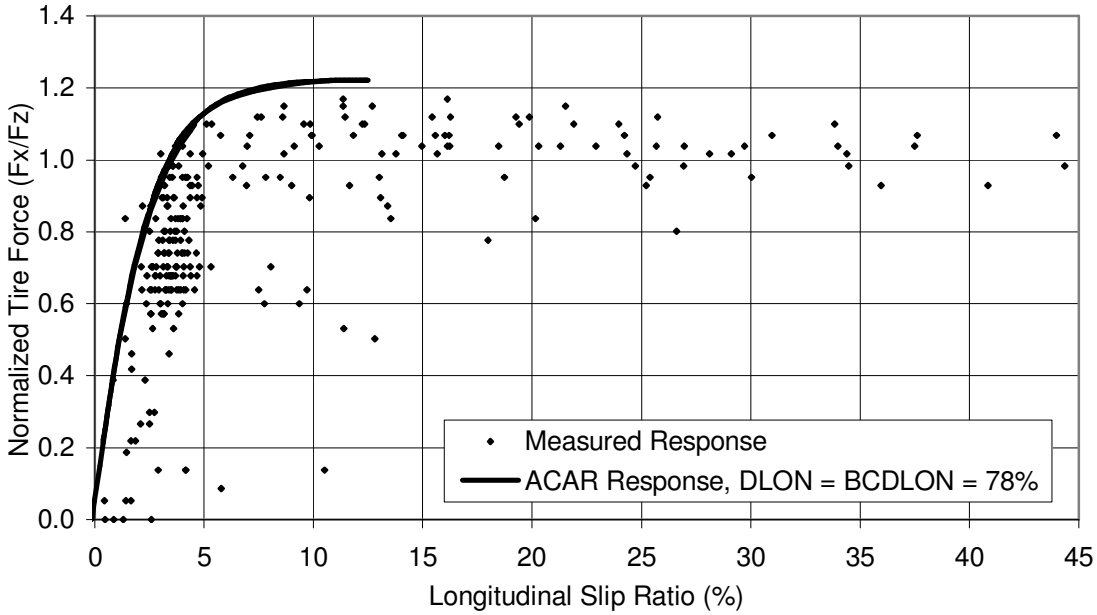

Figure 67: Configuration 3 – Normalized Tire Force vs. Longitudinal Slip Ratio

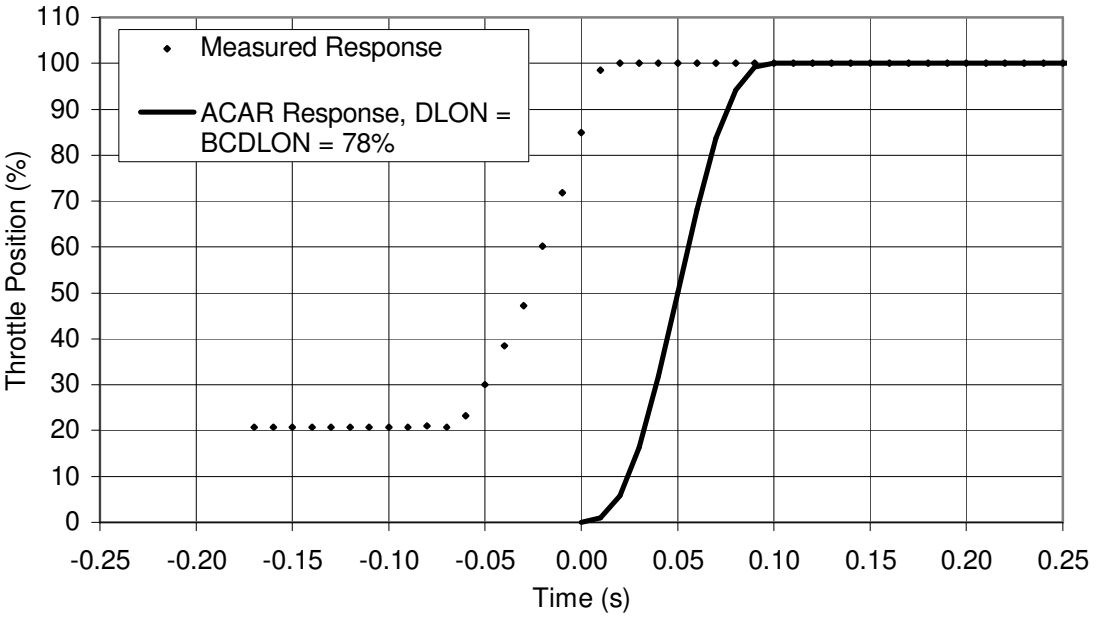

Figure 68: Configuration 3 – Throttle Position

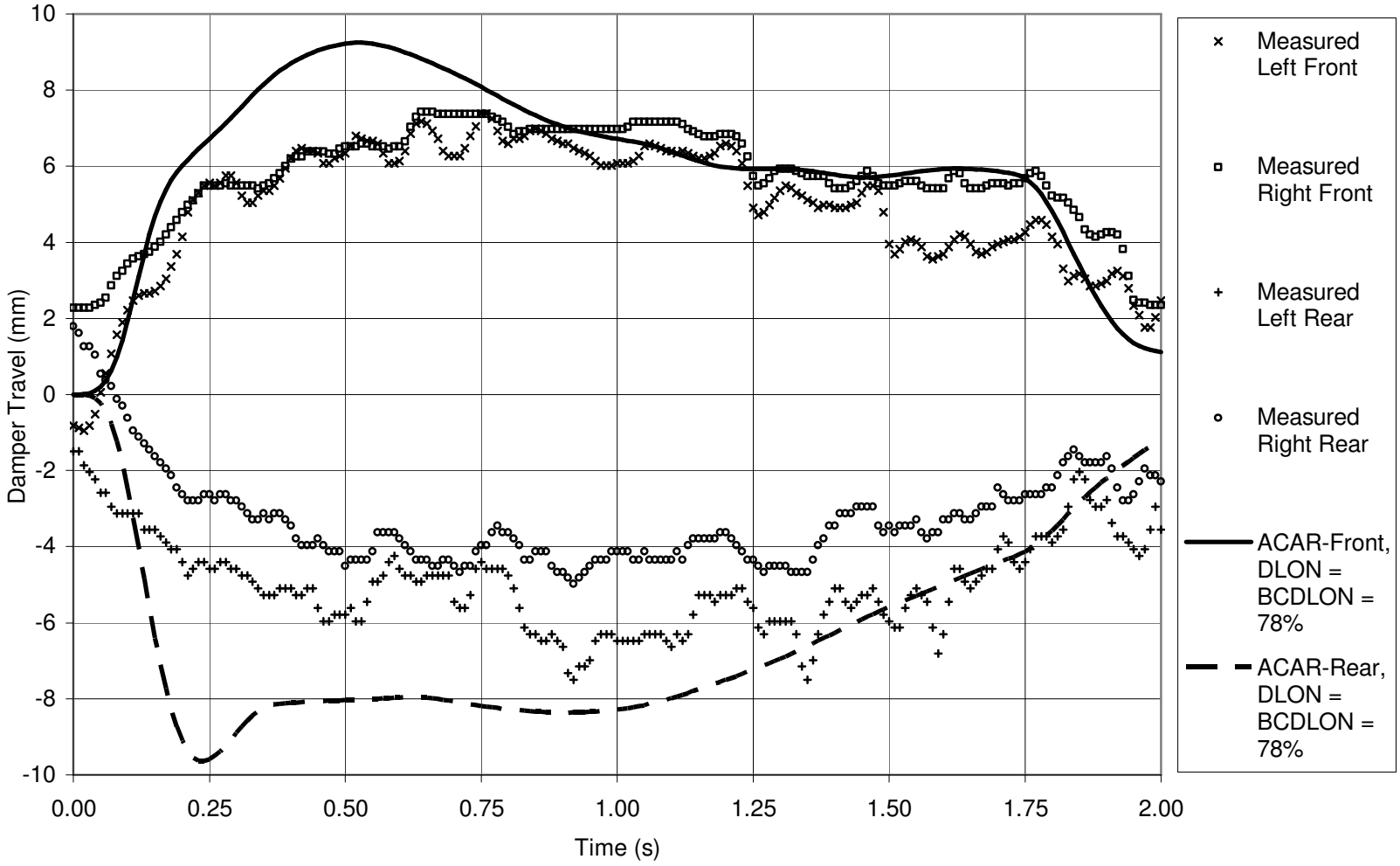

Figure 69: Configuration 3 – Damper Travel

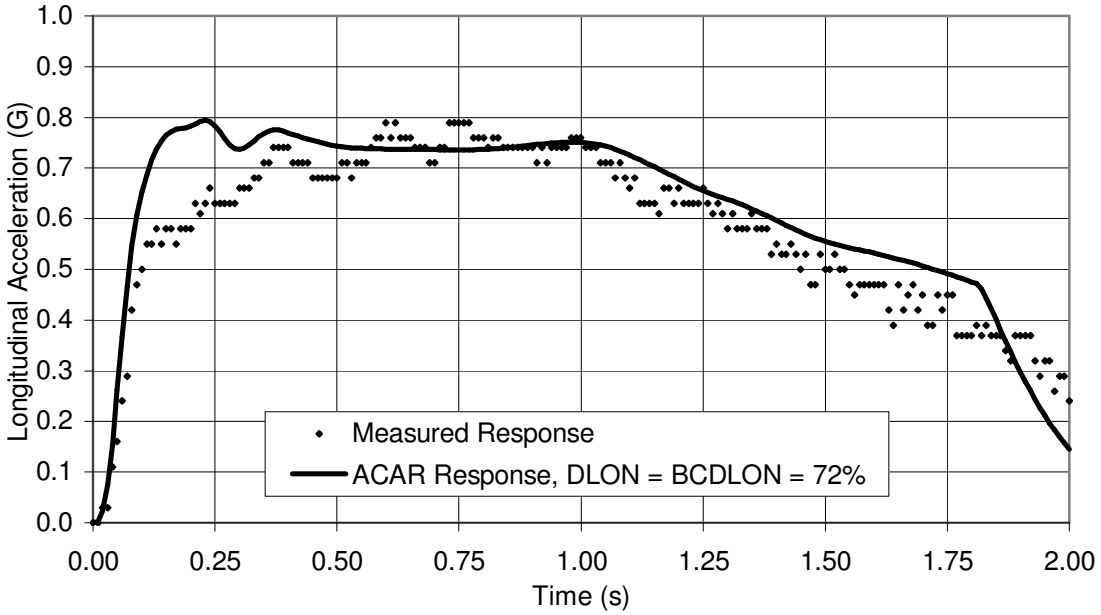

Figure 70: Configuration 4 – Longitudinal Chassis Acceleration

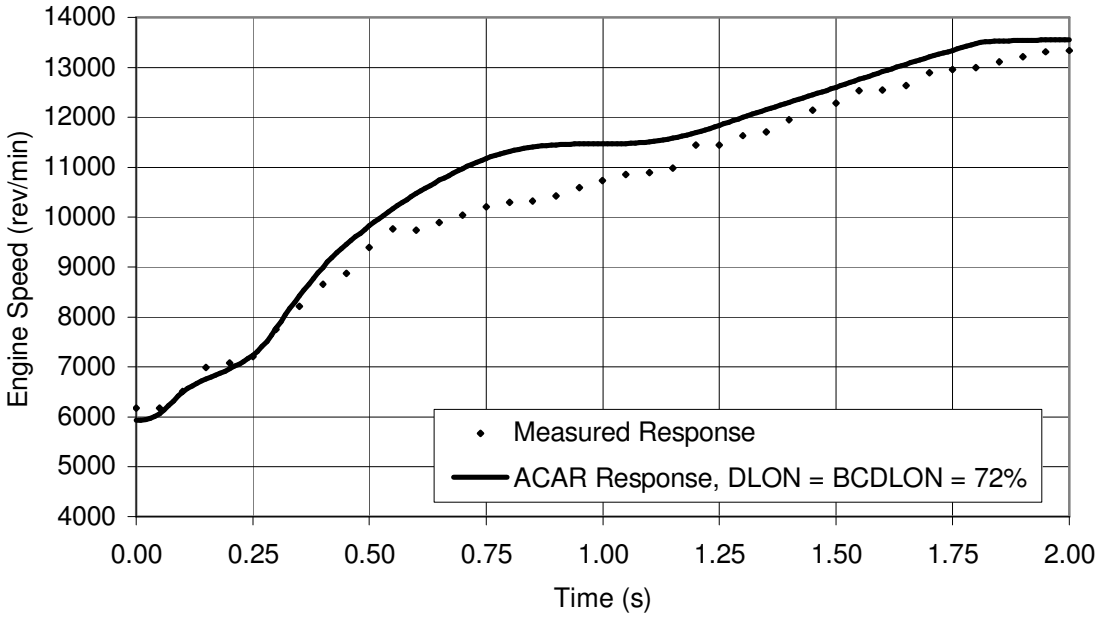

Figure 71: Configuration 4 – Engine Speed

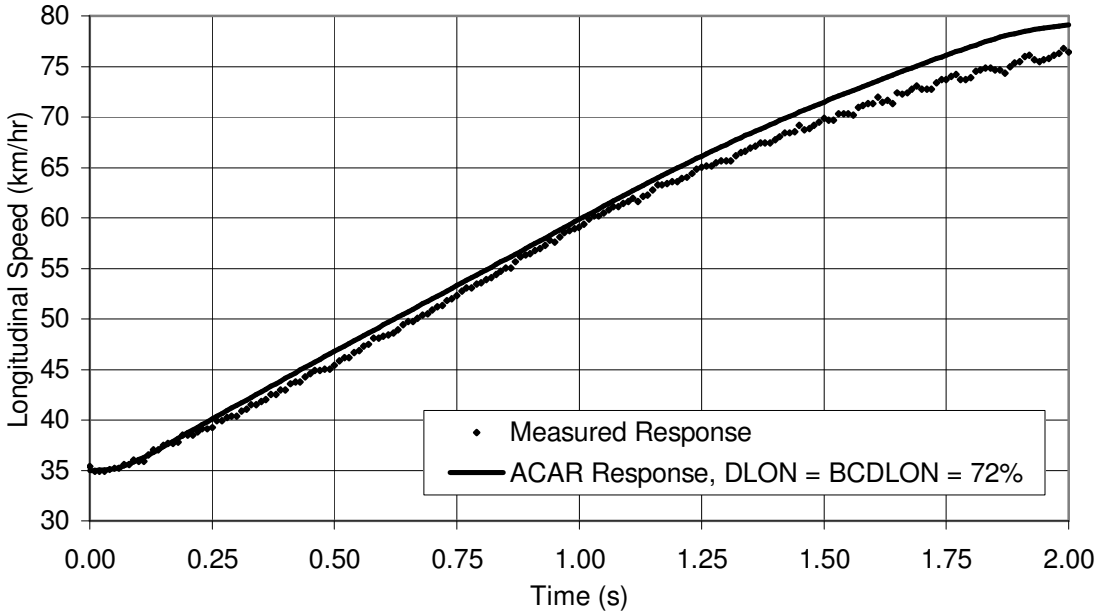

Figure 72: Configuration 4 – Longitudinal Chassis Speed

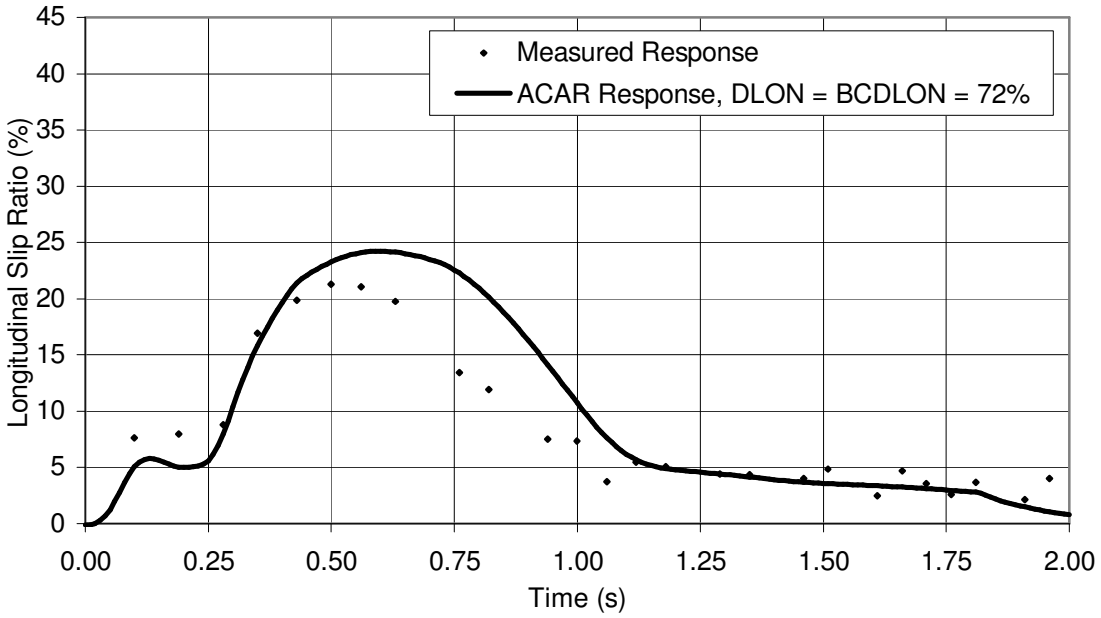

Figure 73: Configuration 4 – Longitudinal Slip Ratio

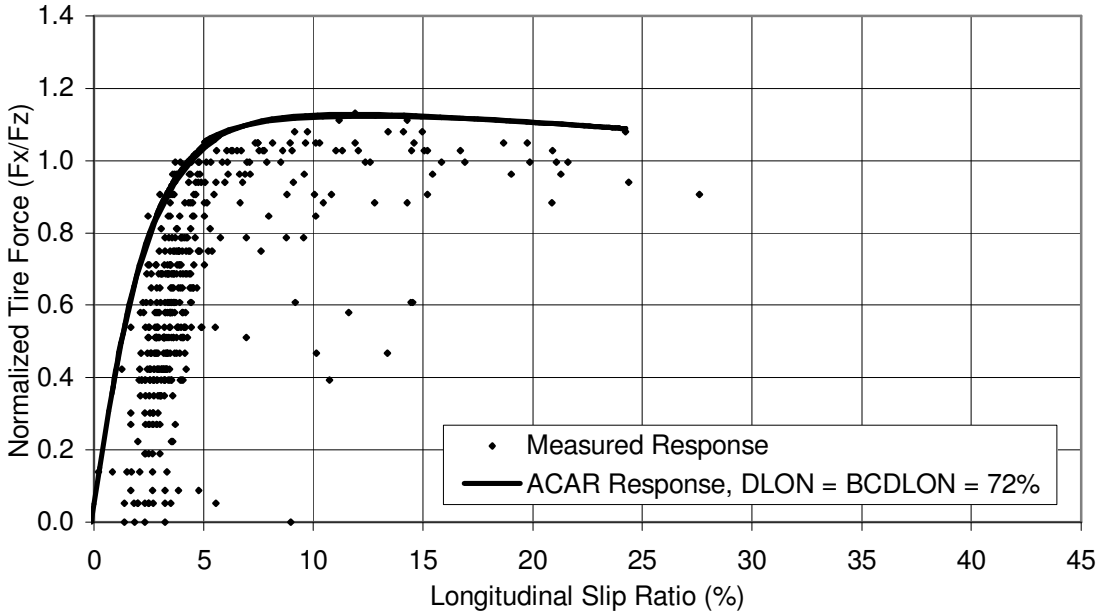

Figure 74: Configuration 4 – Normalized Tire Force vs. Longitudinal Slip Ratio

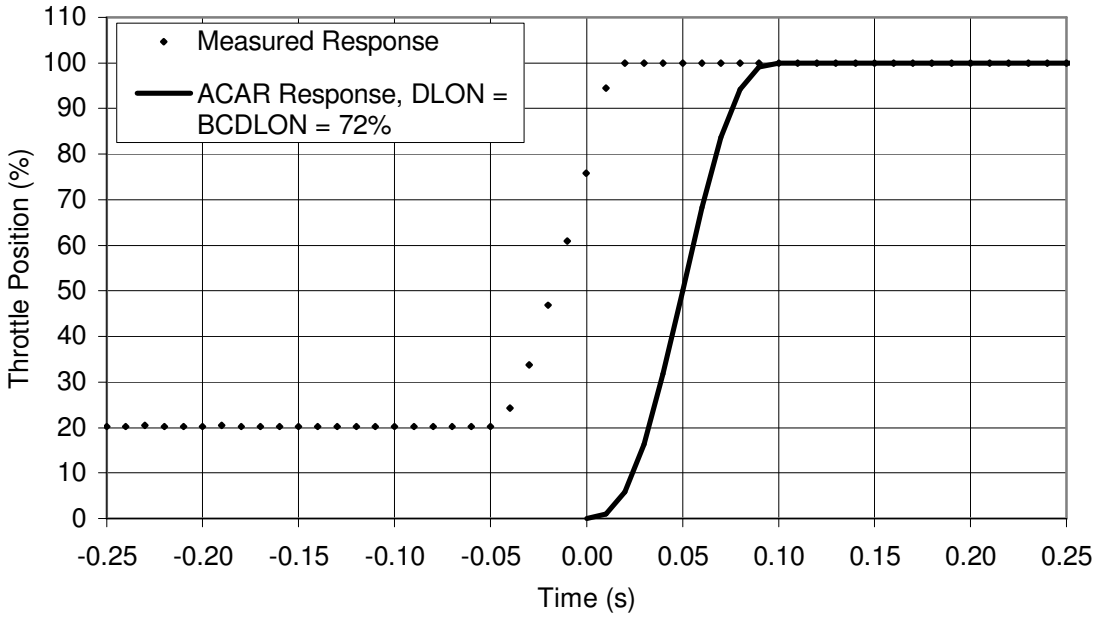

Figure 75: Configuration 4 – Throttle Position

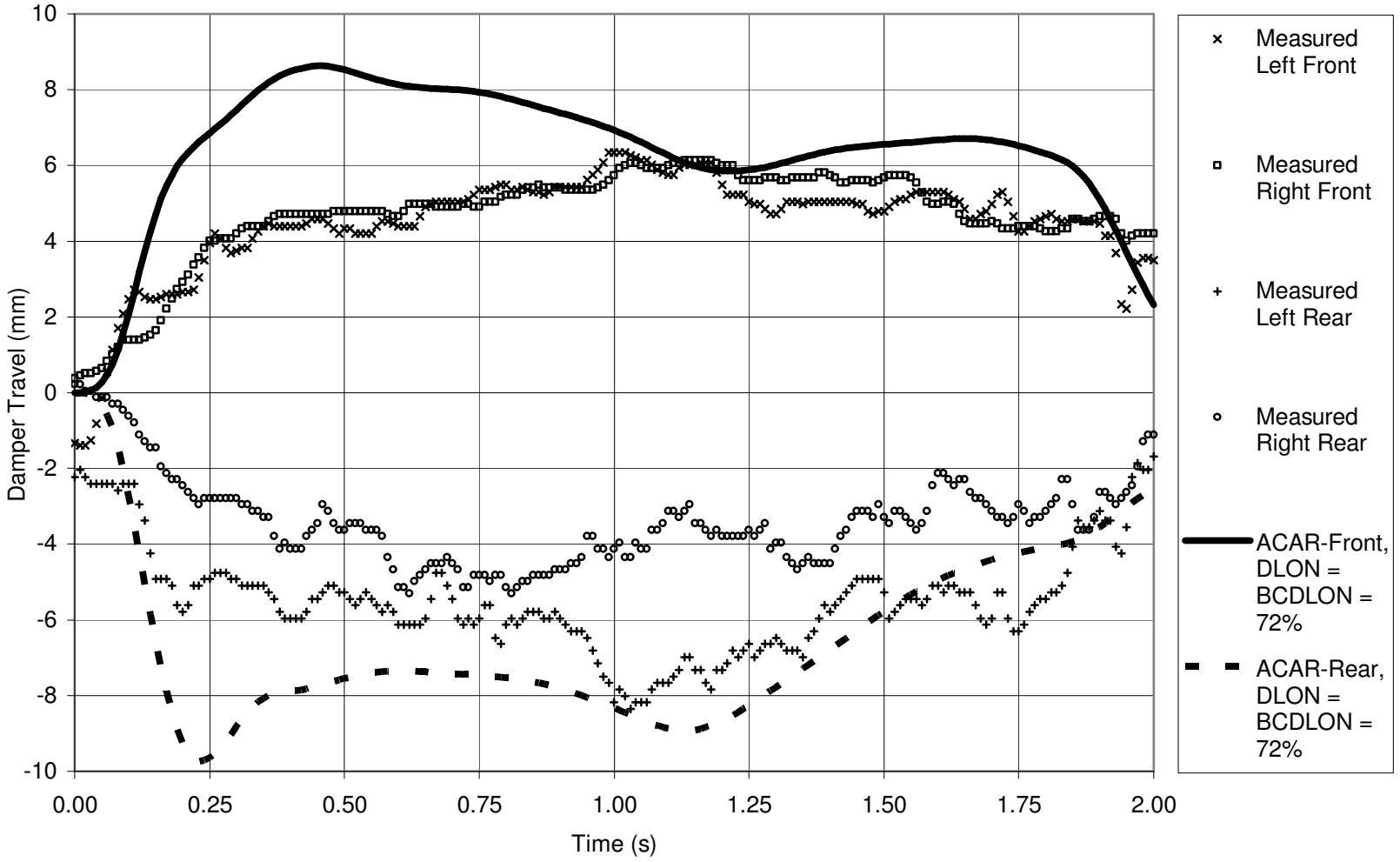

Figure 76: Configuration 4 – Damper Travel

APPENDIX B

TABLES

Table 1: Description of the Kinematic Joints in ADAMS/Car

Name	Abbr.	DOF	Type of motion DOF allow:
Translational	TRA	1	Translation of one part with respect to another while all axes are co-directed.
Revolute	REV	1	Rotation of one part with respect to another along a common axis.
Cylindrical	CYL	2	Translation and rotation of one part with respect to another.
Spherical	SPH	3	Three rotations of one part with respect to the other while keeping two points, one on each part, coincident.
Planar	PLA	3	The x-y plane of one part slides with respect to another.
Fixed	FIX	0	No motion of any part with respect to another.
Inline	INL	4	One translational and three rotational motions of one part with respect to another.
Inplane	INP	5	Two translational and three rotational motions of one part with respect to another.
Orientation	ORI	3	Constrains the orientation of one part with respect to the orientation of another one, leaving the translational degrees of freedom free.
Parallel_axes	PAX	4	Three translational and one rotational motions of one part with respect to another.
Perpendicular	PER	5	Three translational and two rotational motions of one part with respect to another.
Convel	CNV	2	Two rotations of one part with respect to the other while remaining coincident and maintaining a constant velocity through the spin axes.
Hooke	HOK	2	Two rotations of one part with respect to the other while remaining coincident.

Table 2: Hardpoint Definitions

Item No.	Hardpoint I.D.	Hardpoint Name	Joint Type	Part 1 Name	Part 2 Name
Front Suspension Subsystem					
1	A2	arblink_to_bellcrank	SPH	bellcrank	droplink (Front ARB Sub.)
2	A3	arb_bushing_mount	FIX	arb_bushing_mount	chassis (Chassis Sub.)
3	A4	bellcrank_pivot	REV	bellcrank	chassis (Chassis Sub.)
4	A5	bellcrank_pivot_orient	Defines bellcrank_pivot REV joint axis of rotation.		
5	A6	lca_front	BUS	lca	chassis (Chassis Sub.)
6	A7	lca_outer	SPH	lca	upright
7	A8	lca_rear	BUS	lca	chassis (Chassis Sub.)
8	A9	prod_outer	SPH	prod	lca
9	A10	prod_to_bellcrank	HOK	prod	bellcrank
10	A11	shock_to_bellcrank	HOK	damper_bellcrank	bellcrank
11	A11, A12	relative coordinates	CYL	damper_bellcrank	damper_chassis
12	A12	shock_to_chassis	HOK	damper_chassis	chassis (Chassis Sub.)
13	A13	tierod_inner	HOK	tierod	steering_rack (Steering Sub.)
14	A14	tierod_outer	SPH	tierod	lca
15	A15	uca_front	BUS	uca	chassis (Chassis Sub.)
16	A16	uca_outer	SPH	uca	upright
17	A17	uca_rear	BUS	uca	chassis (Chassis Sub.)
18	A18	wheel_center	REV	hub	upright

Table 2: Continued

Item No.	Hardpoint I.D.	Hardpoint Name	Joint Type	Part 1 Name	Part 2 Name
Rear Suspension Subsystem					
19	B2	arblink_to_bellcrank	SPH	bellcrank	droplink (Rear ARB Sub.)
20	B3	arb_bushing_mount	FIX	arb_bushing_mount	chassis (Chassis Sub.)
21	B4	bellcrank_pivot	REV	bellcrank	chassis (Chassis Sub.)
22	B5	bellcrank_pivot_orient	Defines bellcrank_pivot REV joint axis of rotation.		
23	B6	drive_shaft_inr	TRA	tripot	diff_output (Powertrain Sub.)
24			CNV	tripot	drive_shaft
25	B7	lca_front	BUS	lca	chassis (Chassis Sub.)
26	B8	lca_outer	SPH	lca	upright
27	B9	lca_rear	BUS	lca	chassis (Chassis Sub.)
28	B10	prod_outer	SPH	prod	lca
29	B11	prod_to_bellcrank	HOK	prod	bellcrank
30	B12	shock_to_bellcrank	HOK	damper_bellcrank	bellcrank
31	B12, B13	relative coordinates	CYL	damper_bellcrank	damper_chassis
32	B13	shock_to_chassis	HOK	damper_chassis	chassis (Chassis Sub.)
33	B14	tierod_inner	HOK	tierod	chassis (Chassis Sub.)
34	B15	tierod_outer	SPH	tierod	lca
35	B16	uca_front	BUS	uca	chassis (Chassis Sub.)
36	B17	uca_outer	SPH	uca	upright
37	B18	uca_rear	BUS	uca	chassis (Chassis Sub.)
38	B19	wheel_center	REV	spindle	upright
39			CNV	spindle	drive_shaft

Table 2: Continued

Item No.	Hardpoint I.D.	Hardpoint Name	Joint Type	Part 1 Name	Part 2 Name
Steering Subsystem					
40	C1	intermediate_shaft_forward	HOK	steering_shaft	intermediate_shaft
41	C2	intermediate_shaft_rear	HOK	intermediate_shaft	steering_column
42	C3	pinion_center_at_rack	REV	pinion	rack_housing
43			FIX	pinion	steering_shaft
44			CPL	pinion (rotation DOF)	steering_rack (translation DOF)
45	C4	steeringwheel_center	FIX	steering_column	steering_wheel
46	C2, C4	relative coordinates	CYL	steering_column	steering_column_support
47	C2, C4	relative coordinates	FIX	steering_column_support	chassis (Chassis Sub.)
48	A13	relative coordinates	TRA	steering_rack	rack_housing
49	A13	relative coordinates	FIX	rack_housing	chassis (Chassis Sub.)
Powertrain Subsystem					
50	D1	front_engine_mount	BUS	powertrain	chassis (Chassis Sub.)
51	D2	rear_engine_mount	BUS	powertrain	chassis (Chassis Sub.)
52	B6	relative coordinates	REV	powertrain	diff_output
Front ARB Subsystem					
53	E1	arb_middle	REV	arb (left)	arb (right)
54	E2	arb_bend	Defines location of bend in arb (connects "middle" to "droplink")		
55	E3	arb_bushing	BUS	arb	arb_bushing_mount (Front Susp. Sub.)
56	E4	droplink_to_arb	HOK	arb	droplink

Table 2: Continued

Item No.	Hardpoint I.D.	Hardpoint Name	Joint Type	Part 1 Name	Part 2 Name
Rear ARB Subsystem					
57	F1	arb_middle	REV	arb (left)	arb (right)
58	F2	arb_bend	Defines location of bend in arb (connects "middle" to "droplink")		
59	F3	arb_bushing	BUS	arb	arb_bushing_mount (Rear Susp. Sub.)
60	F4	droplink_to_arb	HOK	arb	droplink
Front Tires Subsystem					
61	A18	wheel_center	FIX	wheel	hub (Front Susp. Sub.)
Rear Tires Subsystem					
62	B19	wheel_center	FIX	wheel	spindle (Rear Susp. Sub.)

Table 3: Part Mass and Inertia

Item No.	Part Name	Symmetry	Mass (kg)	Inertia (kg-mm^2)		
				I_{XX}	I_{YY}	I_{ZZ}
Front Suspension Subsystem Total Mass =			1.06E+01			
1	arb_bushing_mount	left/right	4.50E-02	2.93E-01	2.93E-01	2.93E-01
2	bellcrank	left/right	2.55E-01	1.76E+02	1.29E+02	1.46E+02
3	damper_bellcrank	left/right	1.13E-01	2.93E+02	2.93E+02	1.76E+02
4	damper_chassis	left/right	2.27E-01	5.85E+02	5.85E+02	2.93E+02
5	hub	left/right	1.90E+00	5.85E+03	5.85E+03	8.78E+03
6	lca	left/right	4.54E-01	7.84E+03	3.69E+03	1.15E+04
7	prod	left/right	1.98E-01	3.19E+03	3.19E+03	4.39E+00
8	tierod	left/right	1.70E-01	1.46E+03	1.46E+03	3.80E+00
9	uca	left/right	3.69E-01	4.68E+03	5.12E+03	9.74E+03
10	upright	left/right	1.56E+00	5.36E+03	2.34E+03	5.56E+03

Table 3: Continued

Item No.	Part Name	Symmetry	Mass (kg)	Inertia (kg-mm^2)		
				I_{XX}	I_{YY}	I_{ZZ}
Rear Suspension Subsystem Total Mass =			1.68E+01			
11	arb_bushing_mount	left/right	4.50E-02	2.93E-01	2.93E-01	2.93E-01
12	bellcrank	left/right	1.98E-01	1.96E+02	1.96E+02	2.87E+02
13	damper_bellcrank	left/right	1.13E-01	2.93E+02	2.93E+02	1.76E+02
14	damper_chassis	left/right	2.27E-01	5.85E+02	5.85E+02	2.93E+02
15	drive_shaft	left/right	9.07E-01	1.42E+04	1.42E+04	1.46E+02
16	lca	left/right	4.82E-01	6.44E+03	5.09E+03	1.15E+04
17	prod	left/right	1.70E-01	1.93E+03	1.93E+03	3.80E+00
18	spindle	left/right	3.09E+00	9.95E+03	9.95E+03	7.90E+03
19	tierod	left/right	8.50E-02	1.08E+03	1.08E+03	2.05E+00
20	tripot	left/right	1.50E+00	3.22E+03	3.22E+03	2.19E+03
21	uca	left/right	3.12E-01	3.39E+03	3.13E+03	6.38E+03
22	upright	left/right	1.28E+00	4.04E+03	1.26E+03	4.68E+03
Steering Subsystem Total Mass =			2.38E+00			
23	intermediate_shaft	single	1.13E-01	1.76E+02	1.76E+02	2.93E+00
24	pinion	single	1.13E-01	1.17E+01	1.17E+01	8.78E+00
25	rack_housing	single	4.54E-01	2.78E+03	2.78E+03	6.73E+02
26	steering_column	single	2.27E-01	1.23E+03	1.23E+03	5.85E+00
27	steering_column_support	single	2.27E-01	8.78E+01	8.78E+01	1.46E+02
28	steering_rack	single	2.27E-01	3.13E+03	3.13E+03	1.76E+01
29	steering_shaft	single	1.13E-01	1.76E+02	1.76E+02	2.93E+00
30	steering_wheel	single	9.07E-01	7.32E+03	7.32E+03	1.46E+04

Table 3: Continued

Item No.	Part Name	Symmetry	Mass (kg)	Inertia (kg-mm^2)		
				I_{XX}	I_{YY}	I_{ZZ}
	Powertrain Subsystem Total Mass =		4.20E+01			
31	powertrain	single	3.40E+01	1.46E+06	1.46E+06	1.46E+06
32	diff_output	left/right	3.98E+00	2.05E+04	2.05E+04	1.17E+04
	Front ARB Subsystem Total Mass =		1.80E-01			
33	arb	left/right	4.50E-02	1.81E+02	9.36E+01	9.36E+01
34	droplink	left/right	4.50E-02	8.78E+01	8.78E+01	1.17E+00
	Rear ARB Subsystem Total Mass =		1.80E-01			
35	arb	left/right	4.50E-02	9.66E+01	3.80E+01	1.34E+02
36	droplink	left/right	4.50E-02	4.39E+02	4.39E+02	1.17E+00
	Front Tires Subsystem Total Mass =		1.51E+01			
37	wheel (including tire)	left/right	7.57E+00	2.34E+05	2.34E+05	3.51E+05
	Rear Tires Subsystem Total Mass =		1.51E+01			
38	wheel (including tire)	left/right	7.57E+00	2.34E+05	2.34E+05	3.51E+05
	4 Wheel Brakes Subsystem Total Mass =		0.00E+00			
	no parts defined.		0.00E+00	0.00E+00	0.00E+00	0.00E+00
	Total Mass (all parts except chassis) =		**1.02E+02**			

Table 4: Hardpoint Locations

Item	Hardpoint		ACAR Model (mm)			
No.	I.D.	Name	Sym.	z	y	z
Front Suspension Subsystem						
1	A1	global	single	0.00	0.00	0.00
2	A2	arblink_to_bellcrank	left/right	867.73	-144.96	439.29
3	A3	arb_bushing_mount	left/right	1000.00	-100.00	80.00
4	A4	bellcrank_pivot	left/right	851.29	-188.08	402.09
5	A5	bellcrank_pivot_orient	left/right	855.09	-255.09	478.21
6	A6	lca_front	left/right	639.73	-172.12	85.69
7	A7	lca_outer	left/right	852.61	-603.20	84.05
8	A8	lca_rear	left/right	933.62	-171.10	84.69
9	A9	prod_outer	left/right	846.36	-547.52	105.96
10	A10	prod_to_bellcrank	left/right	894.97	-209.72	381.00
11	A11	shock_to_bellcrank	left/right	867.73	-144.96	439.29
12	A12	shock_to_chassis	left/right	661.58	-111.67	450.59
13	A13	tierod_inner	left/right	989.92	-207.47	107.82
14	A14	tierod_outer	left/right	981.69	-526.01	97.41
15	A15	uca_front	left/right	662.90	-235.40	288.01
16	A16	uca_outer	left/right	885.46	-601.94	314.11
17	A17	uca_rear	left/right	1056.78	-234.31	284.50
18	A18	wheel_center	left/right	858.46	-665.06	200.00

Table 4: Continued

Item	Hardpoint		ACAR Model (mm)			
No.	I.D.	Name	Sym.	z	y	z
Rear Suspension Subsystem						
19	B1	global	single	0.00	0.00	0.00
20	B2	arblink_to_bellcrank	left/right	2984.50	-139.70	342.90
21	B3	arb_bushing_mount	left/right	2890.52	-114.30	127.00
22	B4	bellcrank_pivot	left/right	2929.92	-189.88	293.66
23	B5	bellcrank_pivot_orient	left/right	2877.32	-169.89	294.75
24	B6	drive_shaft_inr	left/right	2760.00	-150.00	198.00
25	B7	lca_front	left/right	2592.86	-208.62	77.36
26	B8	lca_outer	left/right	2806.91	-586.38	90.32
27	B9	lca_rear	left/right	2933.40	-211.47	73.28
28	B10	prod_outer	left/right	2807.38	-537.01	105.74
29	B11	prod_to_bellcrank	left/right	2890.99	-233.44	298.83
30	B12	shock_to_bellcrank	left/right	2968.07	-150.48	326.51
31	B13	shock_to_chassis	left/right	2972.25	-48.18	136.27
32	B14	tierod_inner	left/right	2592.86	-208.62	77.36
33	B15	tierod_outer	left/right	2692.51	-584.90	86.91
34	B16	uca_front	left/right	2599.53	-251.44	272.10
35	B17	uca_outer	left/right	2801.81	-585.27	320.03
36	B18	uca_rear	left/right	2927.46	-248.68	269.95
37	B19	wheel_center	left/right	2759.06	-582.41	198.04

Table 4: Continued

Item	Hardpoint		ACAR Model (mm)			
No.	I.D.	Name	Sym.	x	y	z
Steering Subsystem						
38	C1	intermediate_shaft_forward	single	1069.90	0.00	263.08
39	C2	intermediate_shaft_rear	single	1149.33	0.00	370.55
40	C3	pinion_center_at_rack	single	990.46	0.00	155.61
41	C4	steeringwheel_center	single	1390.48	0.00	450.62
Powertrain Subsystem						
42	D1	front_engine_mount	left/right	2032.00	-254.00	50.80
43	D2	rear_engine_mount	left/right	2540.00	-254.00	50.80
Front ARB Subsystem						
44	E1	arb_middle	single	1016.00	0.00	304.80
45	E2	arb_bend	left/right	1016.00	-139.70	304.80
46	E3	arb_bushing	left/right	1016.00	-114.30	304.80
47	E4	droplink_to_arb	left/right	1016.00	-139.70	444.50
Rear ARB Subsystem						
48	F1	arb_middle	single	2890.52	0.00	127.00
49	F2	arb_bend	left/right	2890.52	-139.70	127.00
50	F3	arb_bushing	left/right	2890.52	-114.30	127.00
51	F4	droplink_to_arb	left/right	2984.50	-139.70	127.00
Chassis Subsystem						
52	G1	ground_height_reference	single	0.00	0.00	0.00
53	G2	path_reference	single	0.00	0.00	0.00

Table 5: Subsystem Parameters

Subsystem	Parameter Name	Symmetry	Value	Units
Front Susp.	camber_angle	left	0.0	deg
	camber_angle	right	0.0	deg
	toe_angle	left	0.0	deg
	toe_angle	right	0.0	deg
Rear Susp.	camber_angle	left	0.0	deg
	camber_angle	right	0.0	deg
	drive_shaft_offset	left	75.0	mm
	drive_shaft_offset	right	75.0	mm
	toe_angle	left	0.0	deg
	toe_angle	right	0.0	deg
Steering	reduction_ratio[1]	single	0.0024	rev/mm
Powertrain	bevel_gear	single	1.0	gear ratio
	clutch_damping[2, 4]	single	1.00E+005	No units
	clutch_stiffness[2, 4]	single	1.00E+005	No units
	clutch_torque_threshold[2]	single	1.00E+008	N-mm
	drop_gear	single	1.708	gear ratio
	engine_idle_speed	single	1500	rev/min
	engine_rev_limit	single	13500	rev/min
	engine_rotational_inertia	single	5853	N-mm^2
	final_drive	single	4.909	gear ratio
	gear_1	single	2.846	gear ratio
	gear_2	single	1.947	gear ratio
	gear_3	single	1.545	gear ratio
	gear_4	single	1.333	gear ratio
	gear_5	single	1.190	gear ratio
	gear_6	single	1.074	gear ratio
	max_gears	single	6	integer
	max_throttle	single	100	%
Front ARB	torsional_spring_stiffness[3]	single	1.0	N-mm/deg
Rear ARB	torsional_spring_stiffness[3]	single	1.0	N-mm/deg
Chassis	aero_frontal_area[4]	single	1.275	No units
	air_density[4]	single	1.225	No units
	drag_coefficient[4]	single	0.5	No units

[1]ACAR defines a reduction ratio as a "gear assembly" and not as a parameter. The value is listed here for convenience.
[2]Arbitrary clutch parameters approximates a rigid connection between engine and transmission.
[3]Low stiffness assigned because 2002 racecar does not have anti-roll bars installed.
[4]Refer to ADAMS/Car Help Documentation > Templates > Rigid Chassis regarding unit convention.

Table 6: Bushing Stiffness and Damping Characteristics

	Units	Control Arm Bushings	Anti-Roll Bar Bushings
$\mathbf{F_X}$ Damping (force along x)	N-s/mm	1.8E-01	1.8E-01
$\mathbf{F_Y}$ Damping (force along y)	N-s/mm	1.8E-01	1.8E-01
$\mathbf{F_Z}$ Damping (force along z)	N-s/mm	1.8E-01	1.8E-01
$\mathbf{T_X}$ Damping (torque about x)	N-mm-s/deg	1.1E+01	1.1E+01
$\mathbf{T_Y}$ Damping (torque about y)	N-mm-s/deg	1.1E+01	1.1E+01
$\mathbf{T_Z}$ Damping (torque about z)	N-mm-s/deg	1.1E+01	1.1E+01
$\mathbf{F_X}$ Stiffness (force along x)	N/mm	4.4E+04	4.4E+04
Total Travel (along x)	mm	5.1E+00	5.1E+00
$\mathbf{F_Y}$ Stiffness (force along y)	N/mm	4.4E+04	4.4E+04
Total Travel (along y)	mm	5.1E+00	5.1E+00
$\mathbf{F_Z}$ Stiffness (force along z)	N/mm	4.4E+04	1.8E+01
Total Travel (along z)	mm	5.1E+00	2.5E+01
$\mathbf{T_X}$ Stiffness (torque about x)	N-mm/deg	1.5E+00	1.1E+04
Total Travel (about x)	deg	1.8E+02	1.2E+01
$\mathbf{T_Y}$ Stiffness (torque about y)	N-mm/deg	1.5E+00	1.1E+04
Total Travel (about y)	deg	1.8E+02	1.2E+01
$\mathbf{T_Z}$ Stiffness (torque about z)	N-mm/deg	1.5E+00	1.5E+00
Total Travel (about z)	deg	1.8E+02	1.8E+02

Table 7: Pacejka '94 Handling Force Model Tire Coefficients for Goodyear FSAE Tire
(20in outside diameter, 6.5in width, 13in diameter rim, 12psi inflation pressure)

Lateral Force		Longitudinal Force		Aligning Moment	
A0	1.5000000E+00	B0	1.6226000E+00	C0	2.3500000E+00
A1	4.4255739E+01	B1	0.0000000E+00	C1	9.7149319E+00
A2	1.5523042E+03	B2	-1.5735423E+03	C2	-1.6034520E+00
A3	-3.5002492E+03	B3	-3.2753698E+01	C3	4.5126096E+00
A4	-1.5215217E+01	B4	-5.6439577E+02	C4	-2.6719007E+00
A5	6.6089451E-02	B5	3.5889021E-02	C5	1.2675784E-01
A6	-1.0564438E-02	B6	5.4078991E-03	C6	1.2924694E-01
A7	2.9197666E-01	B7	1.6524269E-01	C7	-3.0000000E-01
A8	-3.7541013E-02	B8	9.9999995E-01	C8	-2.1668433E+00
A9	8.5183467E-02	B9	8.9513884E-02	C9	-3.4857569E+00
A10	-3.1927707E-02	B10	2.9988183E-01	C10	3.0903661E-01
A11	-4.7678765E+01	B11	-9.1505449E+01	C11	1.5247976E-01
A12	-1.4027698E+02	B12	-1.1503518E+02	C12	3.2791519E-01
A13	8.8456962E-01	B13	4.8984496E-08	C13	1.8419775E-01
A14	-2.0369299E+01			C14	6.4124756E-02
A15	-3.8214868E-03			C15	4.7139574E-01
A16	-2.8742850E-02			C16	1.5927502E+00
A17	2.0000000E-01			C17	-1.6572575E+00
				C18	-7.2889710E-02
				C19	-1.8056243E-01
				C20	-4.2424885E-01

Table 8: Pacejka '94 Handling Force Model Parameters for Goodyear FSAE Tire
(20in outside diameter, 6.5in width, 13in diameter rim, 12psi inflation pressure)

Parameter Name	Value	Units
UNLOADED_RADIUS	2.6000000E-01	m
WIDTH	1.6510000E-01	m
ASPECT_RATIO	3.0000000E-01	
VERTICAL_STIFFNESS	1.8018980E+05	N/m
VERTICAL_DAMPING	2.5000000E+02	N-s/m
LATERAL_STIFFNESS	9.0094900E+04	N/m
ROLLING_RESISTANCE	0.0000000E+00	

Table 9: CG Locations – 2002 TAMU FSAE Racecar

	Units	Vehicle Only	Vehicle with Driver	Driver Only	Ballast Only
Wheelbase	mm	1900			
Tire Radius (unloaded)	mm	260			
Mass	kg	225.9	310.3	84.4	20.4
Mass on front axle	kg	90.3	146.1	55.8	0
Mass on rear axle	kg	135.6	164.2	28.6	20.4
Incline (front end lifted)	deg	41.0	42.5		
Mass on front axle	kg	76.2	122.9		
Mass on rear axle	kg	149.7	187.3		
X_{CG} (behind front axle)	mm	1141	1006	644	1900
Z_{CG} (above ground)	mm	396	415	464	520

Table 10: Chassis Part CG – Configuration 1 (75kg Driver, No Ballast)

		Desired Total	All Parts but Chassis		
M	kg	3.012E+02	1.024E+02		
X_{CG}	mm	1016.46	1230.91		
Z_{CG}	mm	413.11	281.50		
		Driver	**Ballast**	**Frame**	**Chassis Part**
M	kg	7.530E+01	0.000E+00	1.235E+02	1.988E+02
X_{CG}	mm	643.55	1900.00	1066.00	905.98
Z_{CG}	mm	464.25	520.00	491.06	480.90
I_{XX}	kg-mm^2	2.533E+04	0.000E+00	1.253E+07	1.256E+07
I_{YY}	kg-mm^2	5.219E+06	0.000E+00	8.063E+07	8.585E+07
I_{ZZ}	kg-mm^2	5.197E+06	0.000E+00	7.859E+07	8.379E+07
I_{XY}	kg-mm^2	4.690E-04	0.000E+00	9.536E+03	9.536E+03
I_{ZX}	kg-mm^2	3.309E+05	0.000E+00	1.596E+06	1.927E+06
I_{YZ}	kg-mm^2	-4.690E-04	0.000E+00	-6.620E+03	-6.620E+03

Table 11: Chassis Part CG – Configuration 2 (88kg Driver, No Ballast)

		Desired Total	All Parts but Chassis		
M	kg	3.143E+02	1.024E+02		
X_{CG}	mm	1000.85	1230.91		
Z_{CG}	mm	415.25	281.50		
		Driver	**Ballast**	**Frame**	**Chassis Part**
M	kg	8.845E+01	0.000E+00	1.235E+02	2.119E+02
X_{CG}	mm	643.55	1900.00	1066.00	889.69
Z_{CG}	mm	464.25	520.00	491.06	479.87
I_{XX}	kg-mm^2	2.681E+04	0.000E+00	1.254E+07	1.256E+07
I_{YY}	kg-mm^2	5.395E+06	0.000E+00	8.131E+07	8.671E+07
I_{ZZ}	kg-mm^2	5.373E+06	0.000E+00	7.927E+07	8.464E+07
I_{XY}	kg-mm^2	5.510E-04	0.000E+00	9.536E+03	9.536E+03
I_{ZX}	kg-mm^2	3.422E+05	0.000E+00	1.639E+06	1.981E+06
I_{YZ}	kg-mm^2	-5.510E-04	0.000E+00	-6.620E+03	-6.620E+03

Table 12: Chassis Part CG – Configuration 3 (75kg Driver, 20kg Ballast)

		Desired Total	All Parts but Chassis		
M	kg	3.216E+02	1.024E+02		
X_{CG}	mm	1072.54	1230.91		
Z_{CG}	mm	419.89	281.50		
		Driver	**Ballast**	**Frame**	**Chassis Part**
M	kg	7.530E+01	2.041E+01	1.235E+02	2.192E+02
X_{CG}	mm	643.55	1900.00	1066.00	998.55
Z_{CG}	mm	464.25	520.00	491.06	484.54
I_{XX}	kg-mm^2	3.546E+04	2.643E+04	1.253E+07	1.259E+07
I_{YY}	kg-mm^2	9.532E+06	1.661E+07	7.803E+07	1.042E+08
I_{ZZ}	kg-mm^2	9.501E+06	1.659E+07	7.599E+07	1.021E+08
I_{XY}	kg-mm^2	4.690E-04	0.000E+00	9.536E+03	9.536E+03
I_{ZX}	kg-mm^2	5.443E+05	6.521E+05	1.449E+06	2.646E+06
I_{YZ}	kg-mm^2	-4.690E-04	0.000E+00	-6.620E+03	-6.620E+03

Table 13: Chassis Part CG – Configuration 4 (88kg Driver, 20kg Ballast)

		Desired Total	All Parts but Chassis		
M	kg	3.348E+02	1.024E+02		
X_{CG}	mm	1055.68	1230.91		
Z_{CG}	mm	421.63	281.50		
		Driver	**Ballast**	**Frame**	**Chassis Part**
M	kg	8.845E+01	2.041E+01	1.235E+02	2.323E+02
X_{CG}	mm	643.55	1900.00	1066.00	978.45
Z_{CG}	mm	464.25	520.00	491.06	483.40
I_{XX}	kg-mm^2	3.765E+04	2.812E+04	1.253E+07	1.259E+07
I_{YY}	kg-mm^2	9.967E+06	1.736E+07	7.841E+07	1.057E+08
I_{ZZ}	kg-mm^2	9.934E+06	1.734E+07	7.638E+07	1.036E+08
I_{XY}	kg-mm^2	5.510E-04	0.000E+00	9.536E+03	9.536E+03
I_{ZX}	kg-mm^2	5.692E+05	6.883E+05	1.478E+06	2.736E+06
I_{YZ}	kg-mm^2	-5.510E-04	0.000E+00	-6.620E+03	-6.620E+03

Table 14: DAQ System – Recorded Channels

Ch.	Sensor (Part No.)	Vehicle Parameter	Source	Sampling Rate (Hz)	Resolution
1	Pi DataBuddy internal accelerometer	Longitudinal Acceleration	n/a	100	0.03G estimated
2	Pi DataBuddy internal accelerometer	Lateral Acceleration	n/a	100	0.03G estimated
3	Pi Research (01G-233035) 100mm Suspension Potentiometer	Suspension Travel FL	Pi Xpress, www.pixpress.com	100	50mV per mm
4	Pi Research (01G-233035) 100mm Suspension Potentiometer	Suspension Travel FR	Pi Xpress, www.pixpress.com	100	50mV per mm
5	Pi Research (01G-233035) 100mm Suspension Potentiometer	Suspension Travel RL	Pi Xpress, www.pixpress.com	100	50mV per mm
6	Pi Research (01G-233035) 100mm Suspension Potentiometer	Suspension Travel RR	Pi Xpress, www.pixpress.com	100	50mV per mm
7	MoTec M4 ECU RPM signal	Engine Speed	n/a	100	n/a
8	MoTec M4 ECU TPS signal	Throttle Position	n/a	100	50mV per 1% throttle
9	Pi Research (30K-162085) Rotary Potentiometer	Steering Wheel Angle	Included with Pi DataBuddy kit	100	15mV per degree
10	Cherry (GS100701) Commerical Hall Effect Gear Tooth Speed Sensor	Front Wheel Speed	Mouser Electronics, www.mouser.com	100	30 triggers per revolution, averaged over 3 triggers
11	Cherry (GS100701) Commerical Hall Effect Gear Tooth Speed Sensor	Differential Speed	Mouser Electronics, www.mouser.com	100	3 triggers per revolution, averaged over 3 triggers
12	Pi DataBuddy internal box temperature	n/a	n/a	1	0.1deg F
13	Pi DataBuddy internal box voltage	n/a	n/a	1	10mV
14	Pi DataBuddy internal clock	Elapsed Time/Lap Time	n/a	n/a	n/a
15	Pi Research 10-Channel Beacon Transmitter (01F-152033) and Receiver (01F-034110)	Lap number	Included with Pi DataBuddy kit	n/a	n/a

VITA

Name: Russell Lee Mueller

Address: Bell Helicopter Textron, P.O. Box 482, Mail Drop 38-1, Machining Center of Excellence (Plant 5), Fort Worth, TX 76101

Education: B.S., Mechanical Engineering, Texas A&M University, 2000
M.S., Mechanical Engineering, Texas A&M University, 2005